INVESTIGATION OF CHEMICAL ANCHORING OF NICKEL CATALYST NETWORKS BY ALUMINUM TITANATE ADDITIVES

by

Cameron Hunter Law

A thesis submitted in partial fulfillment
of the requirements for the degree

of

Master of Science

in

Mechanical Engineering

MONTANA STATE UNIVERSITY
Bozeman, Montana

July 2011

APPROVAL

of a thesis submitted by

Cameron Hunter Law

This thesis has been read by each member of the thesis committee and has been found to be satisfactory regarding content, English usage, format, citation, bibliographic style, and consistency, and is ready for submission to The Graduate School.

Dr. Stephen W. Sofie

Approved for the Department of Mechanical & Industrial Engineering

Dr. Chris Jenkins

Approved for The Graduate School

Dr. Carl A. Fox

STATEMENT OF PERMISSION TO USE

In presenting this thesis in partial fulfillment of the requirements for a master's degree at Montana State University, I agree that the Library shall make it available to borrowers under rules of the Library.

If I have indicated my intention to copyright this thesis by including a copyright notice page, copying is allowable only for scholarly purposes, consistent with "fair use" as prescribed in the U.S. Copyright Law. Requests for permission for extended quotation from or reproduction of this thesis in whole or in parts may be granted only by the copyright holder.

Cameron Hunter Law

July 2011

ACKNOWLEDGEMENTS

I would like to express gratitude to Dr. Stephen Sofie for his extensive guidance and support throughout my research; and Dr. David Miller, Dr. Paul Gannon, and Dr. Chris Jenkins for their support as committee members. I would also like to thank Cameron Kennedy, Grant Wheeler, Chi-Long Tsai, and Casey James for their creative ideas, feedback, and assistance. Finally, I would like to thank Montana State University's Imaging and Chemical Analysis Laboratory and the Department of Mechanical and Industrial Engineering for all of their support.

Financial support was provided by the United States Department of Defense, under FA8650-08-D-2806-0002, the National Aeronautics and Space Administration under Award No. NNX09AP73A, and a portion of the research was performed using EMSL, a national scientific user facility sponsored by the Department of Energy's Office of Biological and Environmental Research and located at Pacific Northwest National Laboratory under the rapid access Award No. 43791

TABLE OF CONTENTS

TABLE OF CONTENTS – CONTINUED

TABLE OF CONTENTS - CONTINUED

LIST OF TABLES

LIST OF FIGURES

LIST OF FIGURES - CONTINUED

LIST OF FIGURES - CONTINUED

LIST OF FIGURES - CONTINUED

LIST OF FIGURES - CONTINUED

LIST OF FIGURES - CONTINUED

Figure Page

ABSTRACT

Electrocatalysts are incorporated into a plethora of technologies and material systems such as catalytic converters, reforming systems, multilayer ceramic capacitors, and solid oxide fuel cells (SOFCs). In SOFCs, nickel is commonly the catalyst of choice due to its chemical stability, high catalytic activity, and lower cost. While traditional SOFCs have a bulk mixture of nickel and yttria stabilized zirconia (YSZ) with at least 33 vol% nickel, solution infiltrated anode SOFCs have several benefits including lower nickel vol% to satisfy percolation, better mechanical strength and CTE matching that can improve redox cycling. Coarsening of the fine nickel metal catalyst with microstructures below 1 micrometer have shown a strong propensity to coarsen from thermal migration at temperatures above 700°C. This migration induced degradation by decreasing particle surface area and nickel network connectivity for electrical conduction. Utilizing meta-stable oxide additives as a minor dopant in the anode cermet system, novel methods of anchoring the metal phase to porous YSZ ceramic scaffolds have been identified as a means to engineer infiltrated anodes for improved performance. Less than 10 wt% aluminum titanate (ALT-Al_2TiO_5), added to YSZ by mechanical mixing, has shown a stepwise process in the formation of $NiAl_2O_4$ at 1100°C and $ZrTiO_4$ at 1205°C for chemically binding the nickel phase to YSZ. XRD, SEM, TEM, and EDS characterization coupled with FIB sample preparation has been utilized to identify the size, morphology, composition and temperature at which the anchoring phases form. Area specific resistance tests of component anodes indicate a decrease in degradation of at least 521%/1000 hr compared to infiltrated specimens without the ALT additive. Electrochemical tests of electrolyte supported cells (ESC) show higher initial performance of cells doped with ALT and at least a 1400%/1000 hr reduction in performance degradation at the same nickel loading content.

CHAPTER ONE

INTRODUCTION TO THESIS

Catalysis Background

Catalysis occurs as a process in a multitude of systems where the rate of a chemical reaction changes due to the participation of a catalyst. Automobiles and power plants use catalysts in catalytic converters and post-combustion scrubbers. Fuel production applications, such as methane reforming and carbon dioxide reforming, use catalysts to clean exhaust gases and produce hydrogen. Energy conversion systems, such as solid oxide fuel cells, use catalysts for the electrodes including the anode and cathode which require specific catalytic activity to reduce or oxidize the gas inlets. Systems which incorporate catalysts also require a degree of optimization for a more environmentally friendly, energy conscience society to minimize quantity of catalyst necessary. Improving the catalyst, in material and structure, will reduce the necessary quantities and limit materials and energy necessary.

Precious metals such as the platinum family (osmium, iridium, ruthenium, rhodium, palladium, and platinum) provide incredible catalytic activity for many systems. A multitude of research has been conducted on the emissions related to internal combustion engines. Emissions of polycyclic aromatic hydrocarbons (PAH) and oxygenated polycyclic aromatic hydrocarbons (OXY-PAH) are 21 times higher for automobiles without catalytic converters than automobiles with sufficient catalysis of the exhaust [1]. One issue with catalytic converters is the emission of the catalysts particles.

Initial break-in of the catalytic converters emits far greater amounts of platinum group metals than an aged catalytic converter. Catalytic converters perform three tasks; oxidize carbon monoxide (CO) to carbon dioxide, oxidize hydrocarbons to water and carbon, and reduce nitrous oxides (NO_x) to diatomic nitrogen (N_2) [2] as exemplified in Figure 1.1.

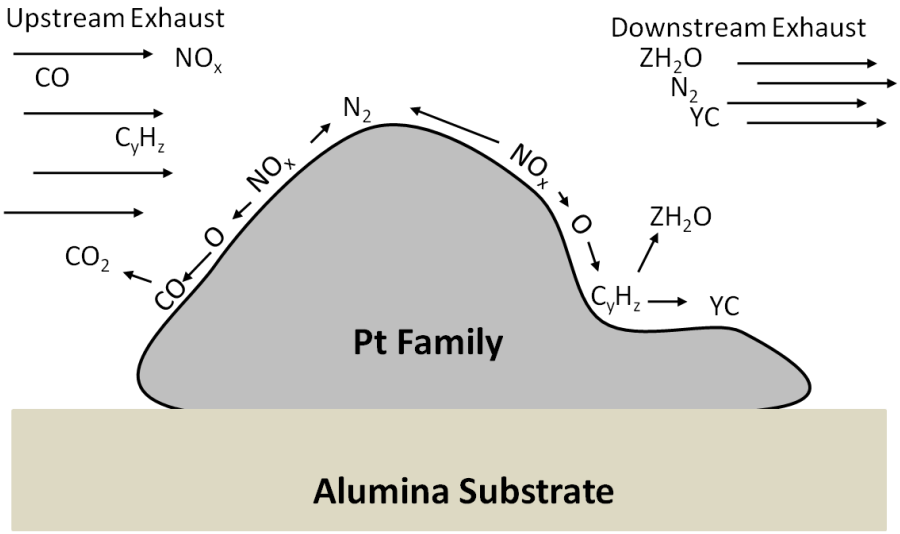

Figure 1.1: Catalytic converter schematic and the oxidation of CO and hydrocarbons and the reduction of NO_x.

Silver is another metal that has performed well in many systems both as a catalyst and as an electrical conductor. The use of silver as current collectors in solid oxide fuel cell (SOFC) systems is extensive due to its low cost and eases of incorporation [3]. Silver has also been used for contacts in microelectronics such as multilayer ceramic capacitors [4], providing an excellent history of current carrying in similar fields. Similar to platinum, silver is known to have significant catalytic activity and excellent electron conductivity [5] which may also allow for silver to be used as a cathode in certain electrochemical systems. Silver is also much less expensive than platinum (Pt: ~ $1714/troy oz, Ag: ~ $34/troy oz [6]). However, silver has a low melting temperature

compared to the other catalysts of interest, as shown in Table 1.1 [7], which limits many of its high temperature application potential.

Table 1.1: Listing of the melting temperatures for silver, nickel, and platinum.

Catalyst	Melting Temperature (^{o}C)
Silver	960
Nickel	1435
Platinum	1753

The least expensive of these catalysts is nickel metal (Ni: ~ $1.10 /troy oz [8]). Nickel has shown very high catalytic activity accompanied by stable electron conductivity and high melting temperature. Catalytic conversion of para-hydrogen has been studied using nickel, alongside platinum and palladium, which shows the exceptional catalytic activity of nickel [9]. Using a chemical combustion looping process, nickel was evaluated as a catalyst for reduction and oxidation processes in a fluidized bed [10]. Reforming methane to a synthesis gas, or a combination of carbon monoxide (CO) and hydrogen (H_2), has traditionally been accomplished by steam reformation as described in Equations 1.1-1.2. This method is extremely energy intensive and has poor carbon monoxide selectivity due to the reversibility of the reactions. Exiting gas mixtures at equilibrium depend on the molar steam to carbon ratio with higher temperatures resulting in less methane and more carbon monoxide. The first step in the steam reformation process occurs at 750 -800^{o}C with a second step at 350^{o}C followed by 200^{o}C. When steam reformation occurs in the anode of an SOFC, the steam in the anode can decompose and increase the concentration of H_2 over the CO. This

yields a higher open circuit voltage with better anode diffusion characteristics and thus an increase in performance.

$$CH_4 + H_2O \leftrightarrow CO + 3H_2 \qquad \text{Equation 1.1}$$

$$CO + H_2O \leftrightarrow CO_2 + H_2 \qquad \text{Equations 1.2}$$

Provendier et al. worked with partial oxidation of methane into synthesis gas using nickel metal as the catalyst. When compared to steam reforming, oxy-reforming had a 13 fold higher activity, giving a more efficient way to produce synthesis gas [11]. In a study performed by Ruckenstein, the nickel catalyst outperformed copper and iron based catalysts yielding better selectivity and lower degradation rates. While nickel did not perform as well as the noble metal catalysts, its cost and labor benefits were preferred and was recommended as a methane reforming catalyst [12]. Nickel also has been shown to resist coking to various degrees based on particle size and strength of the bond to the support [11].

Metal nanoparticles have unique properties when compared to normal metals. Gold, for instance, exhibits total oxidation of carbon monoxide when its size is approximately 2 nanometers. Nanoparticles are difficult to create and introduce to a sample, especially by infiltration, due to Van der Waals forces agglomerating the particles in fluids [13]. Some methods of metal particle preparation, such as synthesis by COD (cycloocta-1,5-diene) organometallic precursors, can produce agglomerates of metals 20 to 30 nanometers in diameter with the actual particles on the order of 3 to 4

nanometers [14]. Other methods have been investigated, such as thin film ablation, but all exhibit equally challenging tasks of producing fine nanoparticle networks [15].

Migration and Coarsening of Catalysts

Since catalytic reactions are highly dependent upon surface area, a fine, evenly distributed nano-network of catalyst is preferential for increased catalytic activity. Unfortunately, a high tendency towards agglomeration of the nano-particles causes reduced surface area and can cause inconsistencies in an electrochemical system. Particle size and surface area are intimately linked, but not directly correlated due to the particle shape. While some particles can have extremely high surface area compared to the same approximate particle size due to variations in morphology, comparing spherical particles of different size can show just how significant of a change occurs in the surface area, as shown in Figure 1.2. Thus, to maximize surface area of the catalyst while minimizing the volume of material required, maintaining the smallest particle size possible is a necessity. Smaller particle size also has a greater radius of curvature, which has been shown to increase the catalytic activity in catalysts [16]. Minimizing the quantity of material is also economically desirable, especially when using the precious metals.

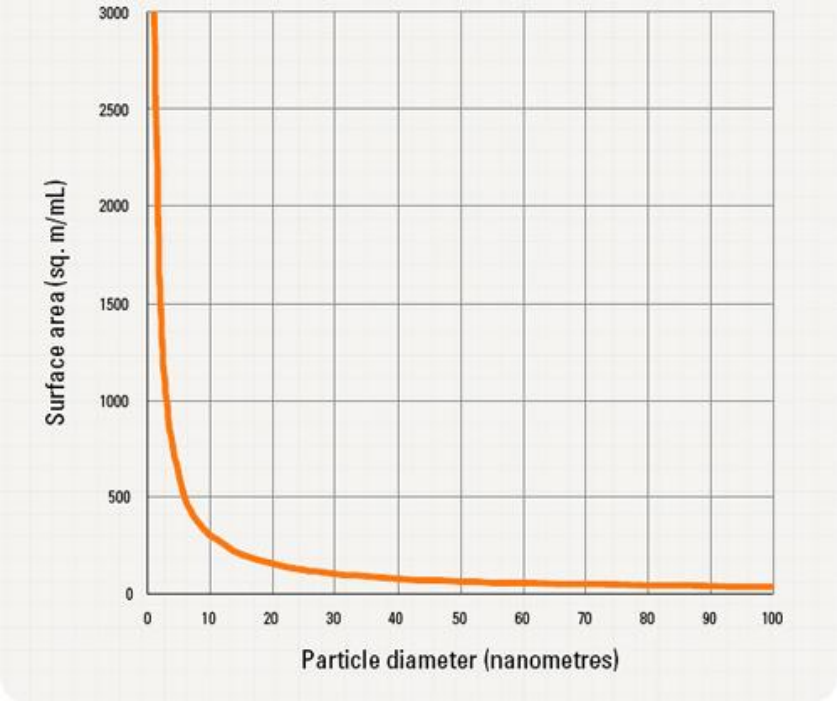

Figure 1.2: Particle diameter vs surface area (http://www.choice.com.au/reviews-and-tests/food-and-health/food-and-drink/safety/nanotechnology-and-food/page/risks%20-%20the%20new%20asbestos.aspx)

This agglomeration of nanoparticles can be due to many environmental factors. First, agglomeration can be caused by the imbalance of surface free energy and volume free energy. If a particle has a significantly higher surface free energy than volume free energy, such as nanoparticles, they will agglomerate with neighboring nanoparticles to form a shape that minimizes the large surface free energy of the system, often assuming shapes that resemble spheres after prolonged coarsening. A second cause for agglomeration is electromigration. This is the phenomena where a current traveling through the catalyst network will force atoms to migrate and separate, in which electrons slowly push host ions analogous to fast moving ping pong balls pushing a resting bowling ball. Electromigration is very problematic in situations where the catalyst is part of an

electrical path, such as with many electrochemical systems. The prior catalysts mentioned (nickel, silver, and platinum) all have had evidence of migration due to agglomeration and/or electromigration [1-5, 9, 11-17, 19, 24-25].

Platinum migration has been most readily observed in catalytic converters, a scenario where electromigration is absent. Automobile exhaust is currently a 'hot' topic in climate stability discussions at this time. Better catalysts to reduce or oxidize the exhaust are necessary to limit poisons and greenhouse gases (CO, NO_x, SO_x, etc.) emitted from internal combustion engines. The catalytic converters are used in the common engine of automobiles, both gasoline and diesel, as well as larger combustion processes such as industrial or residential power production. A very common catalyst in these systems is platinum or platinum group elements. Platinum reduces nitrous oxides to nitrogen and oxidizes carbon monoxide and hydrocarbons to carbon dioxide and water. The substrates, often a cordierite honeycomb structure, and the coatings, a highly porous alumina, are used to provide mechanical and chemical stability to the platinum catalyst. Unfortunately, the platinum has a tendency to migrate and eventually become physically unattached to the substrates, and expelled with the semi-treated exhaust. This presents two problems. First, the platinum is now an exhausted particulate and gas, which adds to the waste emitted. The acute toxicity of platinum is highly dependent on solubility, which varies with the environmental conditions. Second, the loss of catalyst reduces the effectiveness at oxidizing and reducing the exhaust stream. This causes more pollutants to be released and gives rise to greater health risks [2]. The work by Rogge et al. exemplifies the need for these catalysts as mentioned previously.

Electromigration of silver has been an important topic of research since silver is used on wiring boards, silicon dioxide, tin-lead alloys, and lead borosilicate for electrical connections and catalysts on these substrates. One specific use of silver was also investigated in multilayer ceramic capacitors. Low voltage failure in these capacitors was attributed to the electromigration of palladium, while normal voltage failure was attributed to the electromigration of silver. The silver was observed to migrate up to 700 microns causing a short circuit in the capacitor [5].

Electromigration of silver has also been reported in SOFC environments. Simner et al. produced a composite cathode consisting of a perovskite-coated silver particle prepared via mechanofusion. This system exhibited noticeable degradation due to silver migrating across the SDC interlayer on the air electrode side. Instead of the common migration problem of agglomeration, silver migrated to fill in pores necessary for oxygen gas transfer [17]. Simner also reported on studies of silver in a SOFC as a current collector on the cathode. Silver from the current collector had a tendency to migrate to the interface of the electrode and electrolyte [5]. Platinum also exhibited migration from the current collector onto the electrode, but did not penetrate the pores to the degree that silver did. While the platinum did not degrade the cell output as significantly as the silver did, it still showed large migration of distances up to 50 microns over a time frame of up to 500 hours. The method for migration of the platinum could be by formation of platinum oxide vapors as determined by partial pressure modeling. However, this same modeling reported that silver might migrate through both vapor and solid state diffusion

mechanisms. Both of these catalysts gave increased performance for short durations, but eventually led to a degraded output [3,18].

Nickel migration was observed when the anode of a SOFC was poisoned by hydrogen sulfide (H_2S). This migration on the anode caused a decreased catalytic activity area and degraded the electron network, similar to the degradation of silver in the cathode. Power losses varied from seconds for short periods of poisoning, to minutes with longer periods of poisoning. Since H_2S is a common electrode contaminant from the coal gasification process and natural gas fuels, developing a sulfur tolerant anode would reduce costs of scrubbers and simplify the overall system [19]. In the systems of methane reforming, nickel has also been shown to migrate. The mobility of nickel lead to more sophisticated methods where metal was initially inserted into the structure in an attempt to physically limit the migration [11].

As witnessed in prior sections, electromigration and agglomeration of particles plagues multiple fields of catalysts and electrochemistry. While a multitude of literature and research highlights these issues, very little research has been conducted to investigate the methods to engineer metal based anodes for the mitigation of coarsening related degradation.

Solid Oxide Fuel Cells

Solid oxide fuel cells (SOFCs) were briefly mentioned previously in regards to the catalysts incorporated in the electrodes such as silver and nickel. However, to fully understand the difficulties related to nickel catalysts in anodes (fuel electrodes), further

explanation of SOFCs is required. There are at least three key parts to any SOFC; the anode, electrolyte, and cathode, however, in practice additional interlayers are often added to increase performance and decrease degradation induced by chemical interaction. The electrolyte is a hermetic layer that does not allow gas to permeate, is not electronically conductive, and conducts oxygen ions. The cathode reduces oxygen gases to oxygen ions and must be electronically conductive. The anode, the focus of this work, completes the reaction by combining the H_2 fuel fed to the system and the oxygen ions traversing the electrolyte. Anodes must also be electronically conductive to extract the electrons given off from the oxygen ion. In the simplest terms, the reactions related to the SOFC system are shown in Equations 1.3-5 and are represented graphically in Figure 1.3.

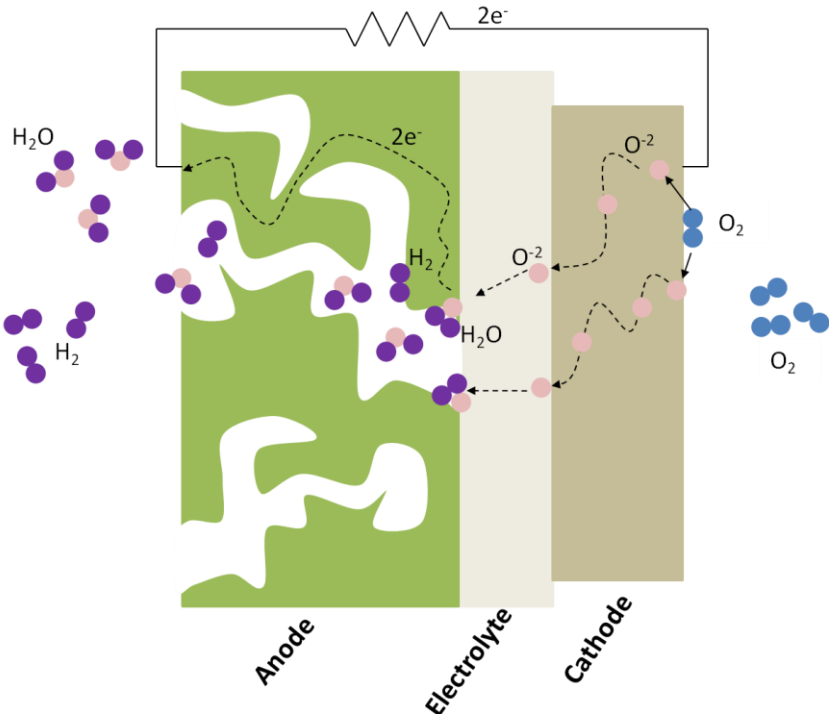

Figure 1.3: Schematic of reactions in an SOFC with the cathode (right), electrolyte (middle), and anode (left).

Cathode: $\frac{1}{2} O_2 + 2e^- = O^{2-}$ Equation 1.3

Anode: $H_2 + O^{2-} = H_2O + 2e^-$ Equation 1.4

Overall: $H_2 + \frac{1}{2} O_2 = H_2O$ Equation 1.5

From Equations 1.3-5, it is apparent that when pure hydrogen is used, SOFCs are a clean power production system because no hazardous emissions are created. SOFCs can handle several fuels directly minimizing the external reforming necessary but the emissions will change and reflect the input gases, such as in Equation 1.6 when CO was an additional fuel source. The addition of CO causes an emission of CO_2, which is a green house gas but much more benign than emitting CO, which is an EPA criteria pollutant.

$$H_2 + CO + 2O^{2-} = H_2O + CO_2 + 2e^- \qquad \text{Equation 1.6}$$

The theoretical limit for the potential produced by SOFCs is dictated by the Nernst Equation, developed by the German physical chemist, Walther Hermann Nernst [20]. The Nernst Equation considers the equilibrium potential, partial pressures, the temperature, and a number of constants to indicate the voltage of an electrochemical cell in operation. The equation itself is listed in Equation 1.7:

$$E = E_o + (RT/2F) \ln [P_{H_2}/P_{H_2O}] + (RT/2F) \ln [P^{1/2}{}_{O_2}] \qquad \text{Equation 1.7}$$

where R is the universal gas constant, P is the gas pressure, F is Faraday's constant (96485.3365 C/mol), T is the absolute temperature and E_o=1.18V for cells with

gaseous H_2O produced [21]. The potential is then used to calculate the theoretical maximum electrical work (W_{el}) as shown in Equation 1.8:

$$W_{el} = \Delta G = \Delta H - T\Delta S = -nFE \qquad \text{Equation 1.8}$$

where ΔG is the change in Gibbs free energy of the electrochemical reaction, ΔH is the change in enthalpy, $T\Delta S$ is the unavailable energy resulting from the entropy change, n is the number of electrons in the reaction, F is again Faraday's constant, and E is the ideal potential dictated by the Nernst Equation.

SOFCs have several advantages over other processes for producing power. For example, the Carnot cycle has a maximum theoretical efficiency dictated by the difference in temperature, as shown in Equation 1.9. If the lower temperature were to reach absolute zero, or 0^o Kelvin, then the Carnot cycle could have 100% efficiency. This is the maximum efficiency possible before the mechanical losses are accounted for. After mechanical losses are considered, the range of efficiencies of heat engines are 15 percent for automotive engines [22] up to 60 percent for a combined cycle gas turbine [23]. The maximum theoretical efficiency for SOFCs is given by the ratio of change in Gibbs free energy to the change in enthalpy as in Equation 1.10 [21]. From these equations, it is evident that the Carnot cycle can outperform the efficiency of an SOFC theoretically, but it requires extreme temperature differences, which are often limited by the environment or the materials used, or reference absolute zero as $T_{c,}$ which is not physically possible. Still, if high efficiencies were calculated, it again must go through

the process of converting the chemical energy (fuel) to electrical energy which has significant losses from the several intermediate steps as illustrated in Figure 1.4.

$$\eta = (T_h - T_c) / T_h \qquad \text{Equation 1.9}$$

$$\eta = \Delta G/\Delta H = 0.83 \qquad \text{Equation 1.10}$$

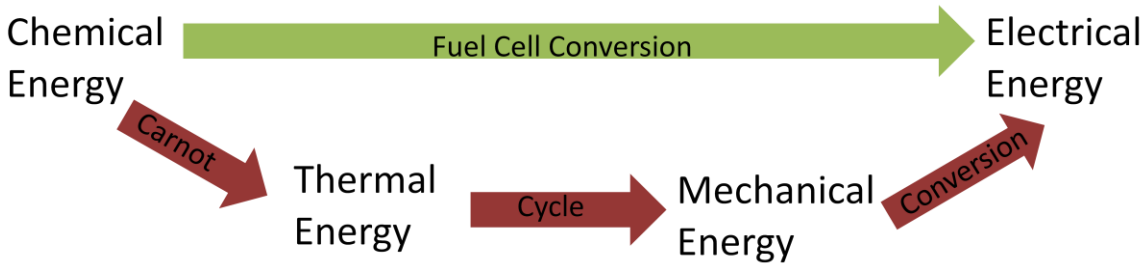

Figure 1.4: Graphical representation of the conversion processes for SOFCs and the Carnot Cycle

Traditional anodes of SOFCs are processed as a mixture of nickel oxide (NiO), yttria-stabilized zirconia (YSZ), and a pyrolyzable thermal fugitive. The constituents are usually mixed such that a 33 vol% of each constituent will be present and the slurry will be homogenous[24-28]. The 33 vol% requirement is a stipulation to maintain percolated networks of nickel catalyst, YSZ, and pores in the anode as displayed in Figure 1.5. This percolation is paramount to operation of the SOFC. The nickel acts as a catalyst as well as an electron conduction path throughout the anode and must be present and fully connected throughout the layer. The YSZ can act to extend the triple phase boundary (TPB) beyond the planar interface of the electrolyte and the anode. The pores must also extend throughout the layer to allow gas fuel to penetrate to the TPB and exhaust gases to

exit. The TPB is the interface where oxygen ions can meet the nickel catalyst and the H_2 fuel to react and expel H_2O gas and the electrons as depicted in Figure 1.6. The NiO is reduced in-situ and provides additional porosity from the volume change. The homogeneous powder can then be pressed, tape cast, or formed in one of several other methods to provide an anode layer [28].

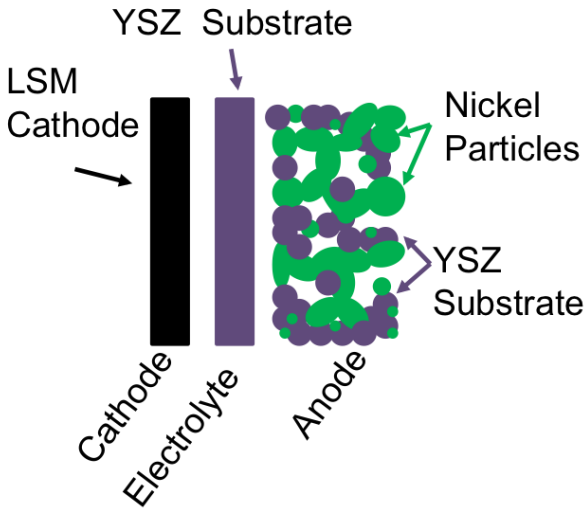

Figure 1.5: Traditionally processed anode-supported SOFC with nickel shown in green, YSZ shown in purple, and the cathode shown in black.

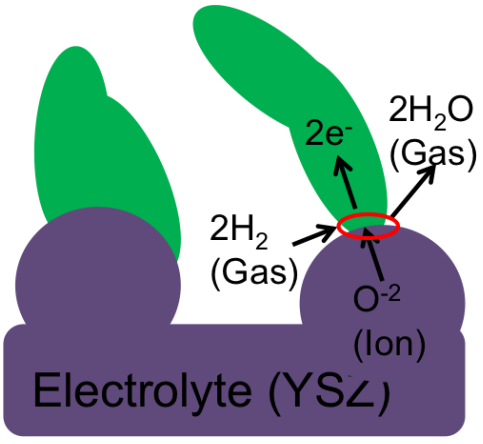

Figure 1.6: Triple Phase Boundary (in red) is the point of activity for SOFC anode.

Another method of processing an SOFC anode is to infiltrate the nickel in the form of a nickel nitrate. Mixing the YSZ and pyrolyzable thermal fugitive as mentioned previously would produce a porous YSZ disk. The disk would be sintered to provide porosity and mechanical strength which the nickel nitrate would then be infiltrated into as displayed in Figure 1.7. Gorte et al. has contributed greatly to this method and helped to identify the strengths and weaknesses of infiltrated anodes [25,29]. Infiltrated anodes use much less catalyst (~15 wt%) than traditional anodes, and have a perfect coefficient of thermal expansion (CTE) match to the electrolyte since the bulk of the anode is the same material as the electrolyte. This perfect match allows greater resistance to thermal shock and a stronger cell overall. However, multiple infiltrations may be necessary to reach the requisite nickel loading and at SOFC operating temperatures (650-1000^{o}C) the nickel has a tendency to coarsen as mentioned in previous sections.

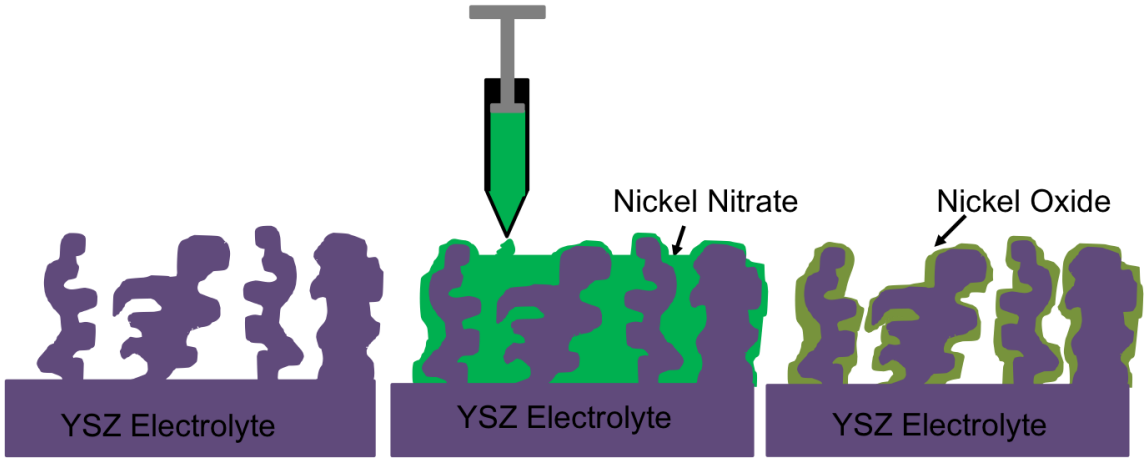

Figure 1.7: Infiltration process of porous anode on a dense electrolyte.

Research Objectives

The work for this Master's Thesis is based on the coarsening of the nickel in an infiltrated anode of an SOFC. As described throughout the introduction, several other catalyst systems and metallic networks suffer from similar migration and could benefit from materials engineering solutions to mitigate the effect of coarsening. To date, the most heavily pursued route of reducing thermally induced degradation is to reduce the temperature of the SOFC. This temperature reduction is the basis of the push toward intermediate temperature solid oxide fuel cells (IT-SOFCs) and coincides with the capability to use low cost ferritic stainless steel interconnects. This however yields substantial decreases in performance where the power output of SOFCs nearly doubles every 100^{o}C [30]. The only other current field of study that provides an opportunity to diminish the effects of high temperature anode coarsening is mixed ionic and electronic conducting (MIEC) ceramics. These materials can achieve sufficient conductivity but rarely reach the level of catalysis available through metals such as nickel [31-33]. This research study uses the novel concept of a chemical anchor as a secondary phase, which decomposes to bond with both the substrate (YSZ) and the catalyst (nickel) to directly inhibit nickel migration. The research objectives in engineering an improved nickel based anode were to: 1) develop a physical understanding of the nickel migration and methodology of forming chemical bonds between a metal and ceramic phase; 2) perform chemical analysis of the anchoring additive (Al_2TiO_5) via XRD, EDX, and microscopy to identify the evolution of phases formed; and 3) perform electrical conductivity and

electrochemical testing to quantify the improvement achieved by the addition of the anchoring dopant.

Reporting of Research Findings

Three independent manuscripts and one expansion on a proceedings paper address the previously mentioned research interests. The first manuscript has been published in the Electrochemical Society Transactions, a peer reviewed conference publication, and the second manuscript was an expansion on this proceedings paper submitted to the Journal of the Electrochemical Society. The third manuscript will be submitted to the Journal of Power Sources. One additional manuscript was completed as a co-author and was listed in the appendices as Appendix A. Appendix A was a manuscript published to TMS in 2010 as a supplemental proceeding. Appendix B was the data from a series of validating experiments for a model provided by another department. This work may be used to develop another co-authored manuscript in the future. A brief summary of these manuscripts was listed below, offering connections between the publications and the research goals.

Anchoring of Nickel Electro-Catalyst by the Addition of Aluminum Titanate

The first and second manuscripts share the same title but the second, a submission to a peer reviewed journal manuscript, is an expansion upon the first, a published peer reviewed proceedings manuscript. These publications were the first investigations into chemical anchoring of nickel catalyst by aluminum titanate and were aimed at a broader

audience than the SOFC community. The Electrochemical Society Transactions manuscript was published after the 2010 ECS international conference in Vancouver B.C. in which the data was presented as a poster. Samples with and without ALT incorporated were infiltrated with nickel and imaged at high magnification with a FE-SEM. These images illustrated the effects of coarsening and that ALT mitigated the metal migration. Powders of NiO, YSZ, ALT, alumina (Al_2O_3), and titania (TiO_2) were combined in several mixtures to provide an XRD analysis of the anchoring reactions and constituents. Finally, applying a porous YSZ anode to a dense electrolyte and infiltrating the nickel catalyst evaluated the catalytic activity. A standard lanthanum strontium manganate cathode was applied, providing an electrolyte-supported cell. Some cells had ALT incorporated as well into the anode prior to infiltration. These cells clearly indicated that ALT increased performance and decreased the degradation rate.

Investigation of Aluminum Titanate for
Chemical Anchoring of Infiltrated Nickel
Catalyst in Solid Oxide Fuel Cell Anode Systems

The final manuscript was a deeper analysis on the concept of chemical anchoring nickel catalyst to a YSZ substrate in a SOFC. Similar to the previous manuscripts, this took an imaging, chemical composition, and catalytic activity approach to the analysis of the anchors. The thermal coarsening was first analyze by FE-SEM by applying a surface treatment of nickel to dense YSZ pellets and heat treating them between 650^{o}C and 900^{o}C for 100 hours. Some pellets also included a 10wt% ALT in the bulk, while some included a surface coating of ALT of negligible mass. Then chemical analysis was performed on powders of NiO, YSZ, ALT, Al_2O_3, and TiO_2 between 1100^{o}C and 1400^{o}C

to identify the reaction temperatures required. Some of the characterization tools needed to complete this study were not available at Montana State University (MSU) and different options were explored to achieve the means to characterize the anchors. Through a rapid access proposal written primarily by the candidate and granted by the Environmental Molecular Science Laboratory (EMSL) at the Pacific Northwest National Laboratory (PNNL), use of scanning electron microscopes with a focused ion beam attachment (FIB-SEM) and high resolution transmission electron microscopes (HRTEM) were used to perform elemental mapping on anchored particles and investigate the interface between nickel catalyst, YSZ substrates, and ALT anchors. Finally, porous electrode materials were processed by tape casting and infiltrated with conductivity monitored over the course of 100 hours.

Sintering Performance of YSZ Ceramics With Transition Metal Oxide Sintering Aid

The first manuscript in the appendices did not directly relate to the anchoring of nickel metal catalyst, but exemplifies the candidate's knowledge and expertise relating to SOFCs and doping of the relevant material systems. The merits of this study while not directly related to the above papers, provides a framework that demonstrates the capability to process and test functional oxide ceramics. Due to the high sintering temperature of YSZ, advances in the co-sintering process, which reduces cost and time for manufacturing, have been somewhat limited. Fully stabilized YSZ (8Y) and partially stabilized YSZ (3Y) were doped with up to 1 mol% cobalt, nickel, chromium, and copper oxides and sintered between 1300^{o}C and 1400^{o}C with a 1 hour dwell. The particle sizes

and porosity were analyzed to determine effects on sintering. All of these studies were similar to those initially performed on anchoring dopants to isolate the best options.

Critical Current In Nickel Filaments Analogous To Nickel Networks In SOFC Anodes

Appendix B was a set of validating experiments for a collaborative effort between the Mechanical Engineering Departments and the Physics Department at MSU. A graduate student in the physics department had developed a model in an attempt to predict SOFC degradation based on nickel network failure. His hypothesis was that the nickel failed due to joule heating and the melting of the wire. To corroborate the model, nickel filaments ranging from 10μm to 250μm in diameter were connected to a power supply set to constant voltage and a multimeter measuring the current through the circuit. The nickel filaments were tested in a variety of atmospheres and temperatures to simulate SOFC conditions. The resulting data was that the nickel filaments, at similar scale to the filaments in an anode, could handle much more than the model predicted.

The fact that the model would show ever increasing degradation through the method of failure described indicates that nickel filament failure would not be a good match for the degradation of SOFCs in a controlled testing environment. While this cannot clearly identify all of degradation as coarsening, it certainly strengthens the argument by ruling out other possible methods of failure. This work is in the process of being formulated into a manuscript in the future.

References

1. *Sources of Fine Organic Aerosol. 2. Noncatalyst and Catalyst-Equipped Automobiles and Heavy-Duty Diesel Trucks.* Rogge, Wolfgange F., et al. 1993, Environ. Sci. Technol., Vol. 27, pp. 636-651.

2. *Environmental Risk of Particulate and Soluble Platinum Group Elements Released From Gasoline and Diesel Engine Catalytic Converters.* Moldovan, M., Palaios, M.A. and Gomer, M.M. 2002, The Science of the Total Environmental, Vol. 296, pp. 199-208.

3. *Performance Variability of La(Sr)FeO3 SOFC Cathode with Pt, Ag, Au Current Collectors.* Simner, S.P., et al. 9, 2005, Journal ofthe Electrochemical Society, Vol. 152, pp. A1851-A1859.

4. *Silver (Ag) as Anode and Cathode Current Collectors in High temperature Planar Solid Oxide Fuel Cells.* Channa, K, et al. 2010, International Journal of Hydrogen Energy, pp. 1-8.

5. *Correlation of Silver Migration with Temperature-Humidity-Bias (THB) Failures in Multilayer Ceramic Capacitor.* Ling, Hung C and Jackson, Anna M. 1, 1989, IEEE Transactions on Component, Hybrids, and Manufacturing Technology, Vol. 12.

6. Monex Precious Metals. *Live Current Prices.* [Online] [Cited: 06 29, 2011.] http://www.monex.com/liveprices.

7. *The Temperature Work of the Bureau of Standards.* Waidner, C. W. 1, 1910, The Journal of Industrial and Engieneering Chemistry, Vol. 2.

8. Metal Prices. *London Metal Exchange.* [Online] [Cited: 06 28, 2011.] http://www.metalprices.com/freesite/metals/nickelalloy/nickelalloy.asp.

9. *The Mechanism of the Catalytic Conversion of Para-Hydrogen on Nickel, Platinum, and Palladium.* Farkas, A. and Farkas, L.

10. *Comparison of Iron-, Nickel-, Copper- and Manganese-Based Oxygen Carriers For Chemical-Looping Combustion.* Cho, Paul, Mattisson, Tobias and Lyngfelt, Anders. 2004, Fuel, Vol. 83, pp.1215-1225.

11. *Stabilisation of Active Nickel Catalysts in Partial Oxidation of Methane to Synthesis Gas by Iron Addition.* Provendier, H., et al. 1999, Applied Catalysis A: General, Vol. 180, pp. 163-173.

12. *Carbon Dioxide Reforming of Methane Over NIckel/Alkaline Earth Metal Oxide Catalysts.*Ruckenstein, Eli and Hu, Yun Hang. 1995, Applied Catalysis A: General, Vol. 133, pp. 149-161.

13. *Growth of Pd, Pt, Ag and Au nanoparticles on carbon nanotubes.* Xue, Bin, et al. 2001, Journal of Materials Chemsitry, Vol. 11, pp. 2378-2381.

14. *Synthesis of Nickel Nanoparticles. Influence of Aggregation Induced By Modification of Poly(Vinylpyrrolidone) Chain Length On Their Magnetic Properties.* Ely, Teyeb Ould, et al. 1999, Chem. Mater., Vol. 11, pp. 526-59.

15. *Formation of silver nanoparticles by through thin film ablation.* Murray, P.T. and Shin, E. 2008, Materials Letters, pp. 4336-4338.

16. *Radius of curvature effect of V-MCM-41 probed by methanol oxidation.* Yang, Yanhui, et al. 2005, Journal of Catalysis, Vol. 234, pp. 318-327.

17. *Silver-Perovskite Composite SOFC Cathodes Processed Via Mechanofusion.* Simner, Steven P, Anderson, Michael D and Templeton, Jared W. 2007, Journal of Power Sources, Vol. 168, pp. 236-239.

18. *Development of Fabrication Techniques and Electrodes for Solid Oxide Fuel Cells.* Simner, S.P., et al. [ed.] H. Yokokawa and S.C. Singhal. Tsukuba, Japan : s.n., 2001. International Symposia on Solid Oxide Fuel Cells. Vol. 16, p. 1051.

19. *Mechanism for SOFC Anode Degradation From Hydrogen Sulfide Exposure.* Lussier, A, et al. 2008, International Journal of Hydrogen Energy, Vol. 33, pp. 3945-3951.

20. Coffey, Patrick. *Cathedrals of Science, The Personalities and Rivalries That Made Modern Chemistry.* Oxford, New York : Oxford University Press, 2008. 978-0-19-532134-0.

21. EG&G Technical Services, Inc. *Fuel Cell Handbook (Seventh Edition).* Morgantown, West Virginia : U.S. Department of Energy, Office of Fossil Energy, National Energy Technology Laboratory, 2004.

22. *Automobile engine tribology - design considerations for efficiency and durability.* Taylor, C.M. s.l. : Elsevier, 1998, Wear, Vol. 221, pp. 1-8.

23. Langston, Lee S. Efficiency by the Numbers. *Mechanical Engineering.* [Online] [Cited: 06 29, 2011.] http://memagazine.asme.org/web/efficiency_by_numbers.cfm.

24. *Processing and properties of the ceramic conductive multilayer device solid oxide fuel cell (SOFC).* Stover, D., Buchkremer, H.P. and Uhlenbruck, S. 2004, Ceramics International , Vol. 30, pp. 1107-1113.

25. *Nanostructured anodes for solid oxide fuel cells.* Gorte, R.J. and Vohs, J.M. 2009, Current Opinion in Colloid & Interface Science, Vol. 14, pp. 236-244.

26. *Influence of porous composite microsctructure on the processing and properties of solid oxide fuel cell anodes.* Clemmer, R.M.C. and Corbin, S.F. 2004, Solid State Ionics, Vol. 166, pp. 251-259.

27. *Mechanical properties of tape cast nickel-based anode materials for solid oxide fuel cells before and after reduction in hydrogen.* Radovic, M. and Lara-Curzio, E. 2004, Acta Materialia, Vol. 52, pp. 5747-5756.

28. *Processing Microstructure Property Correlation of Porous Ni-YSZ Cermets Anode for SOFC Application.* Pratihar, S.K., Dassharma, A. and Maiti, H.S. 2005, Materials Research Bulletin.

29. Atkinson, A., et al. 2004, Nat. Mater., Vol. 3.

30. *A symmetrical, planar SOFC design for NASA's high specific power density requirements.* Cable, T.L. and Sofie, S.W. 1, 2007, Journal of Power Sources, Vol. 174, pp. 221-227.

31. *Structure, thermal stability and electrical properties of Ca(V0.5Mo0.5)O3 as solid oxide fuel cell anode.* Aguadero, A., et al. 2009, Journal of Power Sources, Vol. 192, pp. 78-83.

32. *Double-Perovskite Anode Materials Sr2MMoO6 (M=Co, Ni) for Solid Oxide Fuel Cells.* Yun-Hui Huang, Gan Liang, Mark Croft, Matti Lehtimaki, Maarit Karppinen, John B. Goodenough. 2009, Chemical Materials, Vol. 21, pp. 2319-2326.

33. *Activation and Ripening of Impregnated Manganese Containing Perovskite SOFC Electrodes under Redox Cycling.* Corre, G., et al. 2009, Chemical Materials, Vol. 21, pp. 1077-1084.

CHAPTER TWO

ANCHORING OF INFILTRATED NICKEL ELECTRO-CATALYST BY ADDITION OF ALUMINUM TITANATE

Contribution of Authors and Co-Authors

Chapter 2:

Author: Cameron H. Law

Contributions: Processed samples and performed the experiments, collected and analyzed output data, and primarily wrote the manuscript.

Co-Author: Dr. Stephen W. Sofie

Contributions: Discussed the results and implications of data and commented on the manuscript at all stages.

Manuscript Information Page

Cameron H. Law and Stephen W. Sofie
Journal Name: Journal of the Electrochemical Society
Status of Manuscript:
_____Prepared for submission to a peer-reviewed journal
_____Officially submitted to a peer-reviewed journal
_____Accepted by a peer-reviewed journal
_____Published in a peer-reviewed journal
__X__Published in a peer-reviewed conference proceedings

Published by The American Institute of Physics

Abstract

Solid oxide fuel cell electrodes based on catalyst coatings offer substantial potential for creating more effective anode and cathode structures. Infiltrated anodes based on nickel metal can yield finer catalyst phase distribution at volumetric concentrations well below percolation for traditional cermets. The coarsening of nickel after high temperature thermal treatment poses substantial degradation to the deposited structure, therefore, methods of anchoring the nickel metal to the yttria-stabilized zirconia (YSZ) scaffold have been evaluated to stabilize fine scale electro-catalyst particles. Aluminum titanate was introduced into the porous YSZ anode scaffold to facilitate a step-wise chemical reaction to anchor the nickel metal catalyst as determined by XRD. SEM observation of thermally treated nickel infiltrated scaffolds indicates excellent preservation of the nickel network at 800°C for 72 hrs. Electrochemical tests show not only decreased degradation rates, but also increased initial performance levels due to the additive.

Introduction

Anode supported solid oxide fuel cells (SOFCs) have shown the best potential for high power densities due largely to the thin electrolytes, but also due to the catalytic characteristics of nickel as well as the excellent conductivity (2,3,4,7,12). The implementation of traditional nickel oxide processed anodes, however, requires in excess of 35vol% reduced nickel metal to satisfy full percolation of the catalyst network and hence current collection conduits (4-6,12-14). Infiltration of electro-catalysts offers substantial potential in creating finer metal networks to enhance triple phase boundary length, while requiring substantially less metal content. In addition to finer catalytic structures, benefits in weight and cost can be attained through infiltration in which more exotic catalysts can become viable given the substantially decreased loading. This methodology has several advantages, the first in that the coefficient of thermal expansion (CTE) of an infiltrated anode is dictated by the support scaffold, most notably yittria stabilized zirconia (YSZ), and the fabrication of tailored pore structures in the single phase scaffold can reduce diffusion limitations which has been shown to yield lag in redox cycling and concentration polarization (7-14). In this manner, a porous substrate can be infiltrated with a metal salt or other solution precursor to coat the walls of the pores thus creating a 3-D catalyst network and allowing an electron path to the interconnect (5,6,11). Infiltration can also yield better mechanical performance by allowing more YSZ to remain in the anode (12,14). However, the nickel metal coarsens rapidly at operational temperatures causing a discontinuous path and decreased triple phase boundary length (13). For this reason, most metal catalysts, in addition to nickel,

are currently poor choices for infiltrated anode catalysts. While this current study is focused on SOFC electrodes, this novel concept in metal catalyst thermal stabilization can be applied broadly to many high temperature electro-chemical applications as well as reformation.

The objective of this study was to evaluate the use of aluminum titanate to chemically anchor the nickel catalyst on the porous YSZ scaffold. Aluminum titanate anchoring additives were introduced to the anode substrate and thermally treated to facilitate chemical interactions with both the substrate and the infiltrated nickel to reduce the effects of thermally-induced nickel coarsening thus mitigating rapid degradation of fine infiltrated catalysts. The chemical interactions between the metastable aluminum titanate additive in addition to the nickel and YSZ were evaluated by x-ray diffraction (XRD) as a function of temperature. Further, microscopy and electrochemical testing were performed to characterize the effects of the chemical anchors.

Experimental Procedure

Chemical Reactivity

To evaluate the feasibility of anchors, the chemical interactions of forming secondary phases with regard to the YSZ scaffold and infiltrated catalyst were analyzed by XRD as a function of thermal treatment. The chemical reactivity of aluminum titanate powder (ALT) (Al_2TiO_5, AlfaAesar #14484) as well as ALT decomposition products including Al_2O_3 (Inframat 26R-0801) and TiO_2 (Inframat 22N-0801A) were investigated by mixing with traditional anode cermet precursors including NiO (AlfaAesar #12359)

and YSZ (Tosoh TZ-8YS) powers. Interactions with Al_2O_3 were investigated independently with NiO and reactions of TiO_2 independently with YSZ. All pellets had equal weights of all the constituent materials. Each combination of powders was homogenized in ethanol with an ultrasonic mixer. The solution was then set in a drying oven to allow the ethanol to evaporate. Several pellets from each batch were pressed in a 2.5 cm diameter stainless steel die at 138 MPa weighing 2 grams each. These pellets were then sintered to temperatures up to 1400°C at 10°C per minute, held for one hour, and returned to room temperature at 15°C per minute. After sintering, the dense pellets were ground in an aluminum oxide mortar and pestle and analyzed via XRD (Scintag Inc XGEN-4000). XRD scans were performed from 15 – 70° 2-theta at room temperature. After the initial runs were completed to evaluate the chemical interaction, NiO/ALT/YSZ pellets were sintered at 1400°C and thermally treated at 800°C for 150 hours under 250 ml/min of 5% H_2/N_2 gas (forming gas).

Infiltration

To analyze the effectiveness of anchoring systems, porous YSZ powders were prepared with the addition of thermal fugitives. YSZ powder, used as received, was mixed with 45 wt% cornstarch. Ammonium polymethacrylate (Darvan C-N, RT Vanderbilt) was added as a dispersant at 1 wt% to ensure proper homogenization of the powder mixture. An identical powder mixture also contained 5 wt% ALT so that both the baseline and doped mixture were prepared in the same manner for direct comparison. Both slurries were placed in a centrifugal mixing device (ARE-250, Thinky Corporation) for 5 minutes at 1500 revolutions per minute for homogenization. The powders were

prepared by freeze-drying to eliminate settling of the minor dopant phase and/or thermal fugitive. The slurries were poured directly into liquid nitrogen and flash frozen. The frozen slurry was then placed in a freeze-dryer and the solvent sublimed under a 0.00532 MPa vacuum. Pellets approximately 2 grams in mass were uni-axially pressed in a 1.9 cm die lubricated with pressing lubricant at 195 MPa. These pellets were then sintered in a furnace up to 1450°C, held at temperature for 2 hours, and allowed to cool to room temperature.

The pellets then underwent a two-step infiltration process involving an intermediate low temperature heat treatment. After weighing the porous specimens, fully saturated nickel nitrate solution was dripped onto the surface of the porous pellets and allowed to infiltrate until it pooled on the sample's surface. The pellet was then placed in a vacuum chamber for 5 minutes to assist nickel nitrate penetration into the substrate voids. The pellet was then placed in a furnace at 500°C for 15 minutes to decompose the nickel nitrate into nickel oxide prior to additional infiltration steps. After the pellets were infiltrated they were heated in a furnace up to 1400^{o}C to activate the chemical anchors. The furnace ramped up to 1400°C at 10°C per minute, held at 1400°C for 1 hour, and then returned to room temperature at a rate of 15°C per minute. The infiltrated pellets, with and without the ALT dopant, were then subjected to thermal treatment to mimic fuel cell and reformation processes. The specimens were thermally treated at 800°C for 72 hours to mimic SOFC operation under 250 ml/min of forming gas flow. Finally, the thermally treated pellets were examined using a Field Emission Scanning Electron

Microscope (FE-SEM, Zeiss Supra 55VP) to examine any changes in microstructure of the nickel network.

Cell Testing

In addition to the fundamental studies of anchoring dopants, electrochemical tests were performed to show the anchoring effects in operation. An electrolyte supported SOFC was fabricated with a 125 μm thick 8YSZ electrolyte (ESL Electro-Science, Tape 42401). The YSZ anode scaffold was applied by aerosol spraying of the slurry with and without dopant onto the anode side and the electrolyte and anode were then co-sintered to 1450°C. The nickel nitrate solution from the prior infiltrations was added uniformly to the anode substrates. Nickel nitrate infiltration was performed as before with only 1 or 2 infiltration steps. The cells were placed in a furnace and re-heated to 1450°C for one hour to activate the chemical anchors. A standard lanthanum strontium manganate cathode was then aerosol sprayed onto the cathode side and the entire cell was sintered to 1150°C for 1 hour. These cells were then tested in a solid oxide fuel cell testing apparatus at 800°C under 250 ml/min air on the cathode, and 125 ml/min H_2 and 125 ml/min N_2 on the anode side. The cells were left running under a 0.7 volt constant voltage condition for 72 hours. After testing, the cells current outputs were compared against time to show the degradation.

Results and Discussion

Chemical Reactivity

Initial studies using ALT were evaluated in traditional Ni/YSZ cermets with the intention of reducing the coefficient of thermal expansion of the anode given the low CTE, approx. 0.5 ppm/°C, for the ALT (15). While this previous study indicated the formation of major secondary phases including $ZrTiO_4$ and $NiAl_2O_4$, the order of formation of these phases from an anchoring perspective was unknown. All the powder diffraction cards used for identification of the peaks are listed in Table 2.1. From the XRD analysis, the NiO/YSZ/ALT powder mixture showed retention of YSZ and NiO compounds as expected.

Table 2.1: Compounds identified and their respective JCPDS Card Numbers.

Compound	**JCPDS Card Number**
Al_2O_3	88-0826
$Al_2Ti_7O_{15}$	39-0052
$AlZr_9O_{19.5}$	53-0559
NiO	89-7131
$NiAl_2O_4$	71-0965
TiO	89-3076
TiO_2	89-6975
YSZ	48-0224
$ZrTiO_4$	34-0415
$Zr_{.62}Y_{.2}Ti_{.18}O_{1.9}$	52-1493

Further, Figure 2.1 indicates that the ALT dopant reacted almost completely with the YSZ and NiO yielding several additional new phases including: $NiAl_2O_4$ and $ZrTiO_4$ as major secondary phases with $AlZr_9O_{19.5}$, $Zr_{0.62}Y_{0.2}Ti_{0.18}O_{1.9}$, and TiO as trace

secondary phases. The $ZrTiO_4$ has the highest intensity peak at 30.4 degrees, which made it difficult to identify due to overlap with a YSZ peak, however additional $ZrTiO_4$ peaks indicate that this is a major reaction phase. The presence of $ZrTiO_4$ and $NiAl_2O_4$ indicated the breakdown of ALT into its constituents of Al_2O_3 and TiO_2 followed by subsequent reaction with NiO and YSZ.

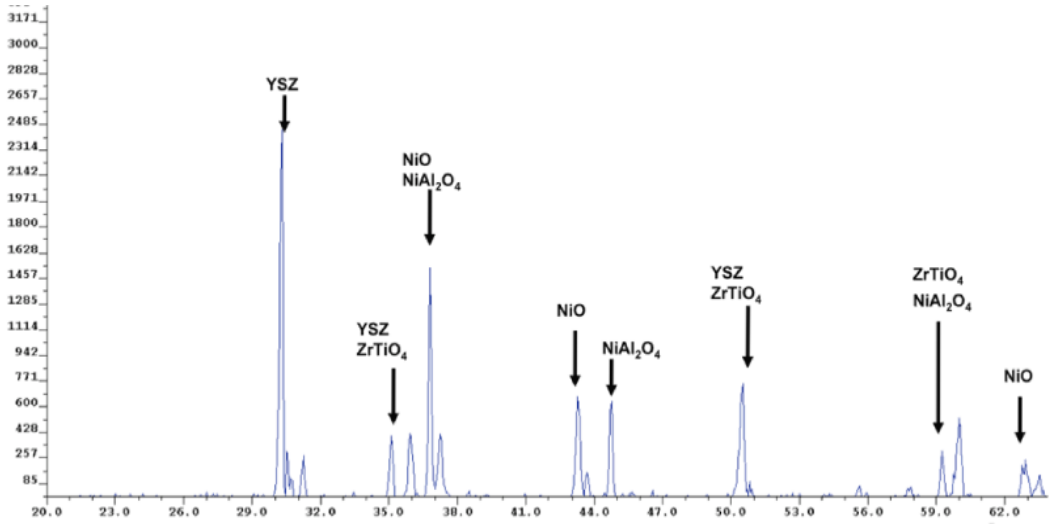

Figure 2.1: XRD plot for the NiO/YSZ/ALT powder, indicating unreacted quantities of NiO and YSZ.

XRD scans of the NiO/ALT pellets indicated peaks of NiO and $NiAl_2O_4$, shown in Figure 2.2, in addition to TiO. Further, the NiO/Al_2O_3 pellet also shown in Figure 2 indicates peaks of $NiAl_2O_4$ and NiO. By isolating the nickel constituent and the anchoring dopant, the half reaction of the anchoring process was tested. The multiple temperatures showed that the ALT readily decomposed to facilitate reaction with NiO in formation of $NiAl_2O_4$ at less than 1200°C, mimicking the reaction products of the pure

NiO and Al_2O_3 powder mixture. The NiO/Al_2O_3 pellet retained some alumina for which was completely consume din the NiO/ALT powder.

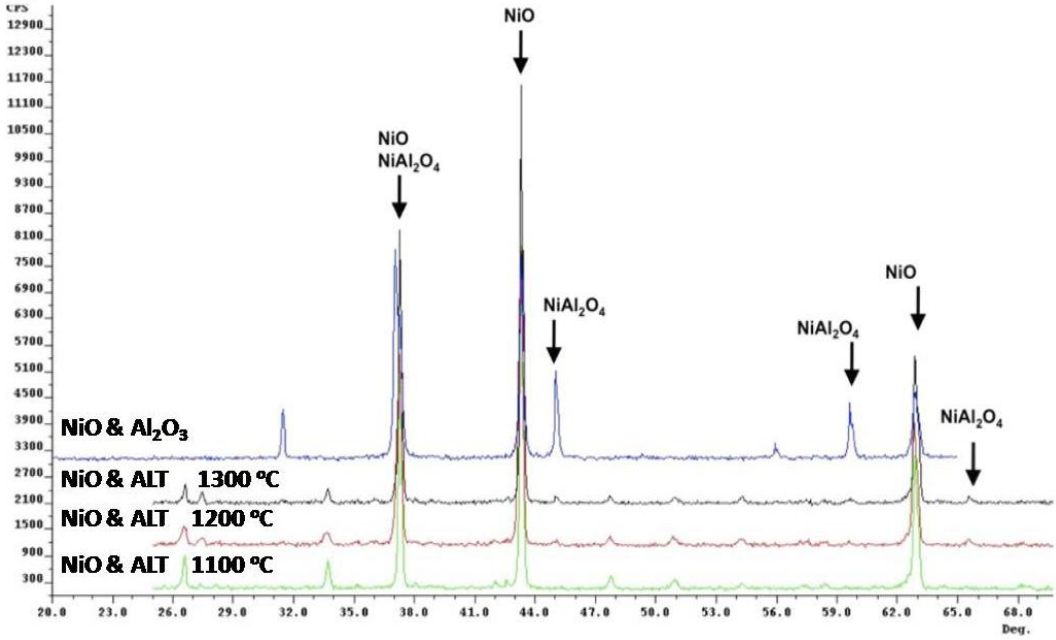

Figure 2.2: XRD plots of NiO/ALT powders for 1100°C, 1200°C, and 1300°C sintering temperatures compared to NiO/Al_2O_3 powder.

The XRD scan of the YSZ/ALT powder mixture, shown in Figure 2.3, yielded primary phases of YSZ, Al_2O_3 and $ZrTiO_4$ with additional minor phases of $Al_2Ti_7O_{15}$ and $AlZr_9O_{19.5}$. The YSZ/TiO_2 pellet indicated the presence of YSZ, TiO_2, and $ZrTiO_4$ phases. The half reaction involving the YSZ cermet component indicated a higher activation energy for chemical interaction such that ZrTiO4 was not formed until 1300°C in addition to other aluminum containing compounds. Using the ALT in minor dopant quantities respectively to the anode constituents in application of this concept, however, is anticipated to reduce the number of additional secondary phases due to limited quantity of Al_2O_3 and TiO_2 available for chemical interactions.

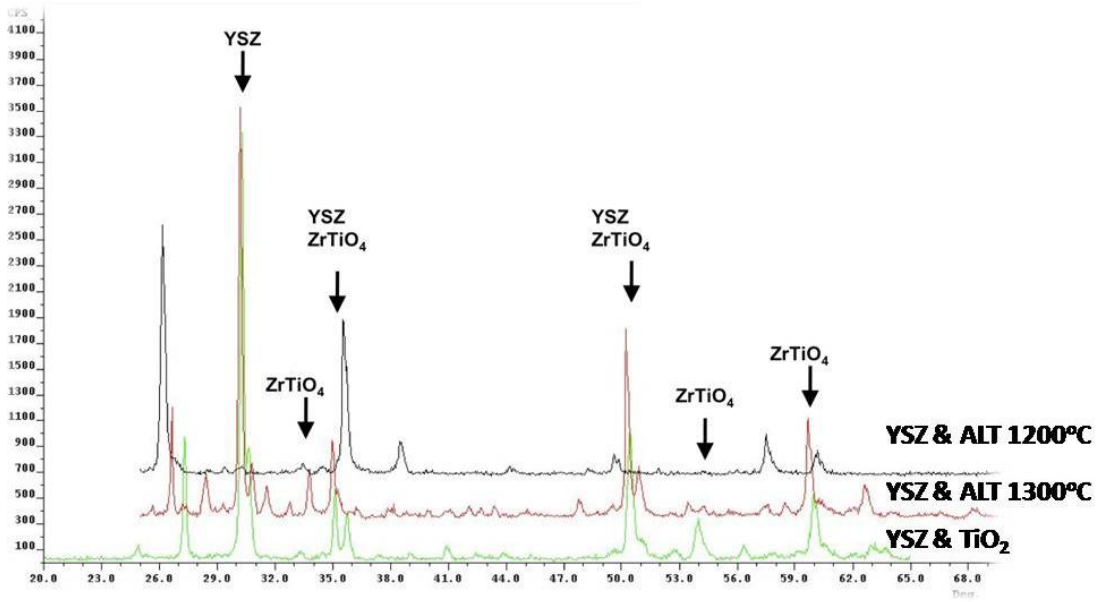

Figure 2.3: XRD plots of YSZ/ALT powders sintered at 1200°C and 1300°C compared to YSZ/TiO_2 powder.

From the XRD study, it is apparent that the reaction occurred sequentially to form all anchoring phases given that ALT is well understood to spontaneously decompose to its constituents in the 850 – 1200°C temperature range (16-19). Al_2O_3 as decomposed from ALT initially reacts with NiO after temperatures of 1100°C are achieved in the formation of the half-anchor $NiAl_2O_4$. Upon exposure to reducing gases at operating temperatures, the NiO will decompose to nickel metal, while the $NiAl_2O_4$ anchor will remain unaffected. Further, the TiO_2 as decomposed from the ALT reacts with YSZ, or more specifically ZrO_2, at temperatures above 1300°C to form the other half-anchor $ZrTiO_4$. In this manner, the use of ALT as opposed to simply adding discrete alumina and titania is of key importance with regard to the concept of anchoring. To successfully bond the YSZ with the NiO phase, the TiO_2 and Al_2O_3 must be sufficiently close in

proximity to facilitate mutual chemical interactions that are bound in between by trace host phase, thus yielding the chemical anchoring concept as depicted in Figure 2.4.

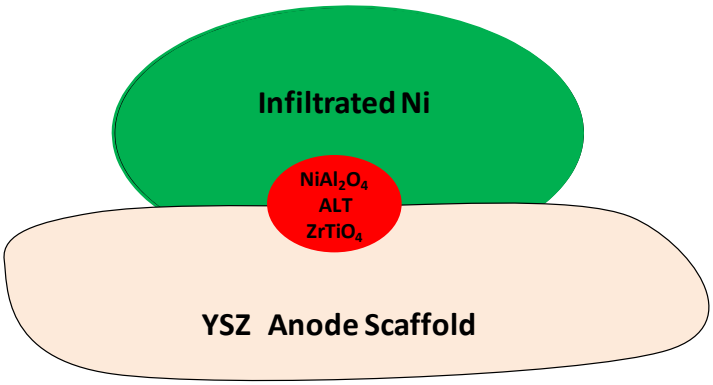

Figure 2.4: Illustration of Infiltrated nickel on a YSZ substrate with ALT anchoring mechanism.

While $NiAl_2O_4$ and $ZrTiO_4$ compounds, however, have negligible electronic and ionic conductivity, it is hypothesized that the majority of nickel remains in metallic form and in contact with pure YSZ, thus preserving the triple phase boundary length required for electrochemical operation. If excessive quantities of $NiAl_2O_4$ or $ZrTiO_4$ compounds were formed at sufficiently high ALT doping levels, the entire layer of nickel/YSZ interface would be replaced by secondary phases that would not support electrochemical function, thus degrading anode performance.

Infiltration

The infiltrated samples' fractured surfaces were examined under the SEM to determine the microstructural evolution of the nickel catalyst after exposure to elevated temperatures in a reducing atmosphere. An electron micrograph of the reduced nickel on a doped and baseline sample is shown in Figure 2.5, in which a region near the upper

surface and lower surface of each individual sample was examined to determine potential variation from the infiltration process. The vacuum assisted infiltration appears to yield very uniform nickel nitrate coverage through the pellet and no appreciable variation is noted indicating that in capillarity of the interconnected porosity was effective in homogenously distributing the precursor solution. Based on electron microscopy the continuity and size scale of the nickel network was directly compared between undoped and ALT doped YSZ to evaluate the effectiveness of the anchors to inhibit nickel migration and coarsening. The effects of coarsening are exaggerated in the baseline sample for which the nickel network is deteriorated on a 2-D surface with discrete nickel clusters larger than 2 microns present and some YSZ surfaces nearly devoid of nickel catalyst. The ALT doped specimen retained a uniform nickel network with nickel cluster sizes consistently less than 0.5 microns, qualitatively indicating the effectiveness of the chemical anchors in binding the nickel to the scaffold and thus retaining interconnection of the nickel clusters.

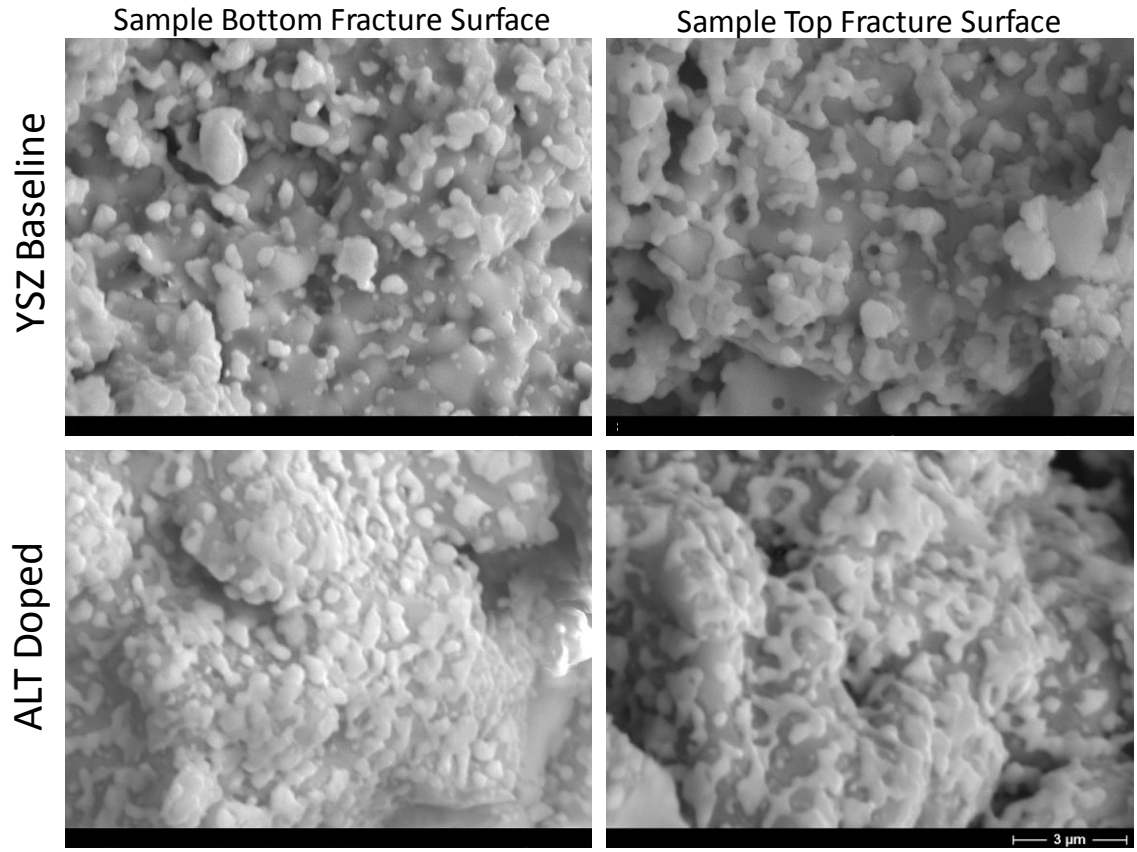

Figure 2.5: Micrographs of YSZ substrate with infiltrated nickel after 72 hours at 800^{o}C in a reducing atmosphere.

Cell Tests

The fuel cell anodes were infiltrated with low quantities of nickel, which while anticipated to yield low expected performance, provided an accelerated time table for which coarsening and nickel migration yielded observable degradation. The first (single anode nickel infiltration step) and second (dual anode nickel infiltration step) set of samples were identically prepared and experienced identical operating conditions in the test fixture to eliminate variations from processing such that performance degradation can be traced back to the anode function. The current density of infiltrated fuel cells, with

and without the ALT dopant, as a function of time was shown in Figure 2.6. An interesting outcome not directly related to degradation was that the doped cells yielded high power output for both sets of fuel cells. Based on the method by which the anchors form, one was able to deduce, that these boundaries were no longer capable of electrochemical conversion indicating the potential methodology for a decrease in initial performance. The electrolyte supported SOFC test results indicated, however, that the ALT doped cells produced better performance regardless of operational duration. This indicated that the anchors facilitated increased nickel/YSZ interface length. The doped specimen in the first sample set showed significantly lower degradation rates, based on the slope of the steady state portion of the curve. This supported the microstructural observations seen in Figure 5 such that the nickel network is locked in placed. The second set of cells generated more current as was expected due to the higher nickel loading. However, the degradation rates of the undoped and doped specimen were nearly identical. This indicated that the current method of scaffold processing by the introduction of the ALT into the scaffold powder may be insufficient to create enough anchors for the higher nickel loadings.

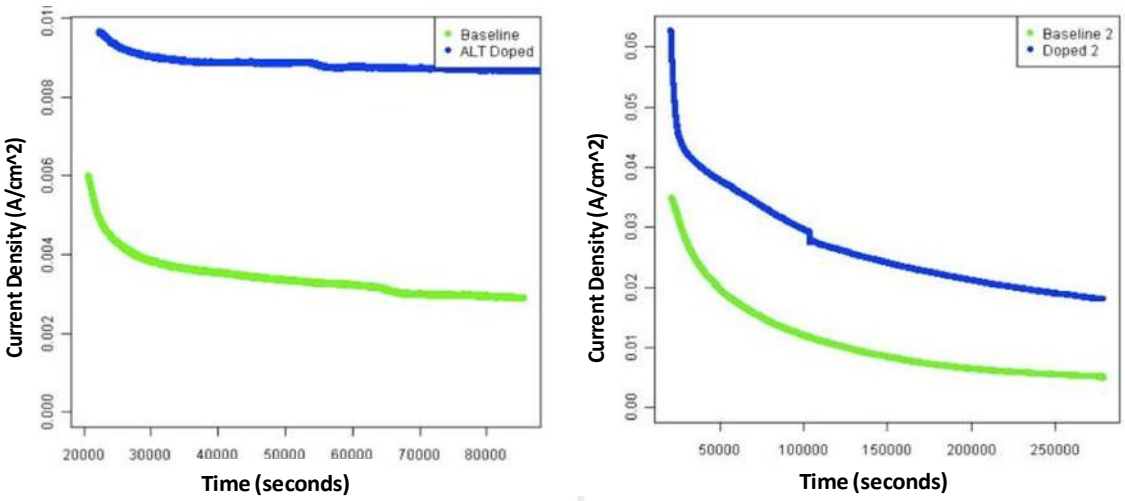

Figure 2.6: Electrolyte supported SOFC tests at 800°C with single infiltration test (left) and dual infiltration test (right) comparing baseline and ALT doped scaffolds infiltrated with saturated nickel nitrate.

The use of electrolyte supported cells in this initial study was beneficial to eliminate the effects of bulk anode conductivity degradation for an anode supported cell. While minor coarsening would not be as deleterious to net conductivity as much as triple phase boundary length in the in the electrochemically active portion of the cell, the study was designed to mitigate secondary effects associated with the thicker anodes. However, the benefits of infiltration are perhaps more relevant to anode supported cells in which better anchoring coverage may be necessary to support sufficient nickel loading for bulk anode electrical conduction. Additionally, the presence of hydrogen sulfide in fuel streams was shown to deteriorate nickel catalysts due to accelerated coarsening in electrolyte supported fuel cells [20], for which this anchoring system may also be effective at inhibiting chemically induced nickel migration due to fuel contaminants.

Conclusions

The addition of aluminum titanate (Al_2TiO_5) was shown to form a beneficial secondary phase in the interaction with YSZ and infiltrated nickel metal in the anode of a solid oxide fuel cell. The formation of the chemical anchors was found to be stepwise in which the decomposition of aluminum titanate yielded an initial chemical interaction with nickel oxide after 1100°C, followed chemical interaction with YSZ after 1300°C. In this manner, nickel aluminate and zirconium titanate were key anchor forming phases in the NiO/YSZ cermet system. The formation of chemical anchors was shown to inhibit fine (<0.5 microns) nickel catalyst migration under SOFC relevant temperatures. Furthermore, the use of ALT as a YSZ dopant showed not only increased initial performance of fuel cell anodes infiltrated with nickel nitrate solution, but also decreased the rate of degradation due to coarsening and separation of the nickel catalyst network. Future efforts are focused on developing improved methods of treating the surface of YSZ with aluminum titanate as opposed to introducing the dopant into bulk powder, to decrease the size and thus improve the number of anchoring sites available to interact with the nickel metal electro-catalyst. Additionally, applying this anchoring concept to systems other than Ni/YSZ is also being investigated.

Acknowledgments

This work was supported by the Department of Defense under Award No. FA8650-08-D-2806-0002. Any opinions, findings, conclusions, or recommendations

expressed herein are those of the author(s) and do not necessarily reflect the views of the DOD.

References

1. M. Xigeng, D. Sun, P. W. Hoo, J. Liu, Y. Hu, and Yanming Chen, *Ceramics International*, 30 (2004)

2. B. Hua, F. Lu, J. Zhang, Y. Kong, J. Pu, B. Chi, and L. Jian, *J. Electrochem. Soc.*, 156, 10 (2009)

3. M. Pihlatie, T. Ramos, A. Kaiser, *J. Power Sources*, 193 (2009)

4. A. McEvoy, S.C. Singhal, and K. Kendall, High Temperature Solid Oxide Fuel Cells: Fundamentals, Design and Applications, Elsevier, 2003 (Chapter 6)

5. A. Atkinson, S. Barnett, R.J. Gorte, J.T.S. Irvine, A.J. McEvoy, M. Mogensen, S.C.Singhal, and J. Vohs, *Nat. Mater.*, 3 (2004)

6. W.Z. Zhu, and S.C. Deevi, *Mater. Sci. Eng.*, A362 (2003)

7. D. Sarantaridis, and A. Atkinson, *Fuel Cells*, 7 (2007)

8. D. Sarantaridis, and A. Atkinson, Proceedings of the 7th European SOFC Forum, Lucerne, Switzerland 2006, paper P0728.

9. K. Kendall, C.M. Dikwal, and W. Bujalski, *ECS Trans*., 7, 1 (2007)

10. C.M. Dikwal, W. Bujalski, and and K. Kendall, *J. Power Sources*, 181 (2008)

11. A.N. Busawon, D. Sarantaridis, and A. Atkinson, *Electrochem. Solid-State Lett.*, 11, 10 (2008)

12. P.H. Grahl-Madsen, N. Larsen, J. Bonanos, J. Engell, and S. Linderoth, *J. Mater. Sci.*, 41 (2006).

13. L. Young, V. Vedahara, and S. Kung, S. Xia, V.I. Birss, *ECS Trans*., 7, 1 (2007)

14. James R. Wilson and Scott A. Barnett, *Electrochem. Solid-State Lett*, 11, 10 (2008) \

15. S.W. Sofie and D.R. Taylor, *Ceramic Engineering and Science Proceedings*, 28, 4 (2008)

16. D. Lawrence, and R.I. Smith, *J. Am. Ceram. Soc*., 88, 10 (2005)

17. G. Tilloca, *J. Mater. Sci*., 26 (1991)

18. M. Nagano, S. Nagashima, H. Maeda, and A. Kato, *Ceramics International*, 25 (1999)

19. B. Freudenberg and A. Mocellin, *J. Am. Ceram. Soc*., 70, 1 (1987)

20. A. Lussier, S. Sofie, J. Dvorak, and Y.U. Idzerda, Int. J. of Hydrogen Energy 33, 3945 (2008)

CHAPTER THREE

CHEMICAL ANCHORING OF INFILTRATED NICKEL METAL CATALYSTS FOR IMPROVED STABILITY AT HIGH TEMPERATURE

Contribution of Authors and Co-Authors

Chapter 3:

Author: Cameron H. Law

Contributions: Processed samples and performed the experiments, collected and analyzed output data, and primarily wrote the manuscript.

Co-Author: Dr. Stephen W. Sofie

Contributions: Discussed the results and implications of data and commented on the manuscript at all stages.

Manuscript Information Page

Cameron H. Law and Stephen W. Sofie
Journal Name: Journal of the Electrochemical Society
Status of Manuscript:
_____Prepared for submission to a peer-reviewed journal
_____Officially submitted to a peer-reviewed journal
__X__Accepted by a peer-reviewed journal
_____Published in a peer-reviewed journal

Published by The American Institute of Physics

Abstract

Solid oxide fuel cell electrodes based on catalyst coatings offer substantial potential for creating improved anode and cathode structures. Infiltrated anodes based on nickel metal can yield finer catalyst phase distribution at volumetric concentrations well below percolation for traditional cermets. The coarsening of nickel after high temperature thermal treatment poses substantial degradation to the deposited structure, therefore, methods of anchoring the nickel metal to the yttria-stabilized zirconia (YSZ) scaffold have been evaluated to stabilize fine scale electro-catalyst particles. Metastable aluminum titanate was introduced into the porous YSZ anode scaffold to facilitate a step-wise chemical reaction in the formation of nickel aluminate followed by zirconium titanate to anchor the nickel metal catalyst. SEM observation of thermally treated nickel infiltrated scaffolds indicates excellent preservation of the nickel network at 800°C for 72 hrs. Electrochemical tests show not only decreased degradation rates, but also increased initial performance levels due to the additive.

1.0 Introduction

Anode supported solid oxide fuel cells (SOFCs) have shown the best potential for high power densities due largely to the thin electrolytes, but also due to the catalytic characteristics of nickel as well as the excellent conductivity [2-4,7,12]. The implementation of traditional nickel oxide processed anodes, however, requires in excess of 35 vol% reduced nickel metal to satisfy full percolation of the catalyst network and hence current collection conduits [4-6,12-14]. Infiltration of electro-catalysts offers substantial potential in creating finer metal networks to enhance triple phase boundary length, while requiring substantially less metal content. In addition to finer catalytic structures, benefits in weight and cost can be attained through infiltration in which more exotic catalysts can become viable given the substantially decreased loading. This methodology has several advantages, the first in that the coefficient of thermal expansion (CTE) of an infiltrated anode is dictated by the support scaffold, most notably yittria stabilized zirconia (YSZ), and the fabrication of tailored pore structures in the single phase scaffold can reduce diffusion limitations which has been shown to yield lag in redox cycling and concentration polarization [7-14]. In this manner, a porous substrate can be infiltrated with a metal salt or other solution precursor to coat the walls of the pores thus creating a 3-D catalyst network and allowing an electron path to the interconnect [5,6,11]. Infiltration can also yield better mechanical performance by allowing more YSZ to remain in the anode [12,14]. However, the nickel metal coarsens rapidly at operational temperatures causing a discontinuous path and decreased triple

phase boundary length [13]. For this reason, most metal catalysts, in addition to nickel, are currently poor choices for infiltrated anode catalysts.

The objective of this study was to evaluate the use of aluminum titanate to chemically anchor the nickel catalyst on the porous YSZ scaffold. Aluminum titanate anchoring additives were introduced to the anode substrate and thermally treated to facilitate chemical interactions with both the substrate and the infiltrated nickel to reduce the effects of thermally-induced nickel coarsening thus mitigating rapid degradation of fine infiltrated metal catalysts. The chemical interactions between the metastable aluminum titanate additives and both the nickel and YSZ were evaluated by x-ray diffraction (XRD) as a function of temperature. In addition, microscopy and electrochemical testing were performed to characterize the effects of the chemical anchors.

2.0 Experimental Procedure

2.1 Chemical Reactivity

To evaluate the feasibility of anchors, the chemical interactions of the possible anchors with regard to the YSZ scaffold and infiltrated catalyst were analyzed by XRD as a function of thermal treatment. The chemical reactivity of aluminum titanate powder (ALT) (Al_2TiO_5, AlfaAesar #14484) as well as ALT decomposition products including Al_2O_3 (Inframat 26R-0801) and TiO_2 (Inframat 22N-0801A) were investigated by mixing with traditional anode cermet precursors including NiO (AlfaAesar #12359) and YSZ (Tosoh TZ-8YS) powers. Additionally, reactions with Al_2O_3 were investigated

independently with NiO and reactions of TiO_2 independently with YSZ. All pellets had equal weights of all the constituent materials. Each combination of powders was homogenized in ethanol with an ultrasonic mixer. The solution was then set in a drying oven to allow the ethanol to evaporate. Several pellets from each batch were pressed in a 2.5 cm diameter stainless steel die at 138 MPa weighing 2 grams each. These pellets were then sintered to temperatures up to 1400°C at 10°C per minute, held for one hour, and returned to room temperature at 15°C per minute. After sintering, the dense pellets were ground in an aluminum oxide mortar and pestle and analyzed via XRD (Scintag Inc XGEN-4000). XRD scans were performed from 15 – 70° 2-theta at room temperature. After the initial runs were completed to evaluate the chemical interaction, NiO/ALT/YSZ pellets were sintered at 1400°C and thermally treated at 800°C for 150 hours under 250 ml/min of 5% H_2/N_2 gas (forming gas).

2.2 Infiltration

To analyze the effectiveness of anchoring systems, porous YSZ powders were prepared with the addition of thermal fugitives. YSZ powder, used as received, was mixed with 45 wt% cornstarch. Ammonium polymethacrylate (Darvan C-N, RT Vanderbilt) was added as a dispersant at 1 wt% to ensure proper homogenization of the powder mixture. An identical powder mixture also contained 5 wt% ALT so that both the baseline and doped mixture were prepared in the same manner. Both slurries were placed in a centrifugal mixing device (ARE-250, Thinky Corporation) for 5 minutes at 1500 revolutions per minute for homogenization. The powders were prepared by freeze-drying to eliminate settling, and hence segregation, of the minor dopant phase in addition

to the thermal fugitive. The slurries were poured directly into liquid nitrogen and flash frozen. The frozen slurry was then placed in a freeze-dryer and the solvent sublimed under a 50 mb vacuum. Pellets approximately 2 grams in mass were uni-axially pressed in a 1.9 cm die lubricated with pressing lubricant at 195 MPa. These pellets were then sintered in a furnace up to 1450°C, held at temperature for 2 hours, and allowed to cool to room temperature.

The pellets then underwent a two-step infiltration process involving an intermediate low temperature heat treatment. After weighing the porous specimens, fully saturated nickel nitrate solution was dripped onto the surface of the porous pellets and allowed to infiltrate until it pooled on the sample's surface. The pellet was then placed in a vacuum chamber for 5 minutes to assist nickel nitrate penetration into the substrate pores. The pellet was then placed in a furnace at 500°C for 15 minutes to decompose the nickel nitrate into nickel oxide prior to additional infiltration steps [21]. After the pellets were infiltrated they were heated in a furnace up to 1400°C to activate the chemical anchors. The furnace ramped up to 1400°C at 10°C per minute, held at 1400°C for 1 hour, and then returned to room temperature at a rate of 15°C per minute. The infiltrated pellets, with and without the ALT dopant, were then subjected to thermal treatment to mimic fuel cell and reformation processes. The specimens were thermally treated at 800°C for 72 hours to mimic SOFC operation under 250 ml/min of forming gas flow. Finally, the thermally treated pellets were examined using a Field Emission Scanning Electron Microscope (FE-SEM, Zeiss Supra 55VP) to examine any changes in microstructure of the nickel network.

2.3 Electrochemical Testing

In addition to the fundamental studies of anchoring dopants, electrochemical tests were performed to show the anchoring effects in operation. An electrolyte supported SOFC was fabricated with a 125 μm thick 8YSZ electrolyte (ESL Electro-Science, Tape 42401). The YSZ anode scaffold was applied by aerosol spraying of the slurry with and without dopant onto the anode side and the electrolyte and electrode substrate were co-sintered to 1450°C. The nickel nitrate solution from the prior infiltrations was added uniformly to the anode substrates. Nickel nitrate infiltration was performed as before with only 1 or 2 infiltration steps in order to limit nickel content, thus accelerating the coarsening effect on performance. The cells were placed in a furnace and re-heated to 1400°C for one hour to activate the chemical anchors. A standard lanthanum strontium manganate (LSM) cathode was then aerosol sprayed onto the cathode side and the entire cell was sintered to 1150°C. These cells were then tested in a solid oxide fuel cell testing apparatus at 800°C under 250 ml/min air on the cathode, and 125 ml/min H_2 and 125 ml/min N_2 on the anode side as described in detail elsewhere [20]. The cells were left running under a 0.7 volt constant voltage condition for 72 hours. After testing, the cells current outputs were compared against time to show the degradation.

3.0 Results and Discussion

3.1 Chemical Reactivity

Initial literature studies using ALT as an anode dopant were evaluated in traditional Ni/YSZ cermets with the intention of reducing the coefficient of thermal expansion of the anode given the low CTE, approx. 0.5 ppm/°C, for the ALT [15]. While this previous study indicated the formation of major secondary phases including $ZrTiO_4$ and $NiAl_2O_4$, the temperature effects and order of formation of these phases was unknown. Utilizing a catalyst infiltration route, the mechanisms by which chemical interactions proceed is critical to anchoring nickel among other metal catalysts to ceramic substrates. All the powder diffraction cards used for identification of the peaks are listed in Table I for reference of relevant detected phases. In addition to the readily identifiable primary and secondary phases, many smaller unidentified peaks in the XRD scans were most closely associated with $Al_2Ti_7O_{15}$, $AlZr_9O_{1.9,}$ and TiO trace phases.

From the XRD analysis in Figure 3.1, the NiO/YSZ/ALT powder mixture sintered at 1400°C showed retention of YSZ and NiO compounds as expected given the excess stoichiometric content of YSZ and NiO with regard to the ALT decomposition content. Further, Figure 3.1 indicated that the ALT dopant reacted almost completely with the YSZ and NiO yielding several additional new phases including: $NiAl_2O_4$ and $ZrTiO_4$ as major secondary phases with $Al_2Ti_7O_{15}$, and TiO as trace secondary phases. The $ZrTiO_4$ has the highest intensity peak at 30.4 degrees, which made it difficult to identify due to overlap with a YSZ peak, however additional $ZrTiO_4$ peaks indicate that this is a major secondary phase. The presence of $ZrTiO_4$ and $NiAl_2O_4$ indicated the breakdown of ALT

into its constituents of Al_2O_3 and TiO_2 followed by subsequent reaction with NiO and YSZ. The trace phase $Al_2Ti_7O_{15}$ was also indicated in Figure 3.1 primarily as a shoulder on the most intense YSZ/$ZrTiO_4$ peak, beyond which peak overlap with the primary and secondary phases occurred.

XRD scans of the NiO/ALT pellets in Figure 2 indicated peaks of retained NiO and secondary $NiAl_2O_4$. Further, the NiO/Al_2O_3 pellet sintered to 1400°C, also shown in Figure 3.2, indicated peaks of $NiAl_2O_4$ and NiO. By isolating the nickel and the aluminum constituent of the anchoring dopant, the half reaction of the anchoring process was tested. The multiple temperature XRD scans of the NiO and ALT pellets in Figure 2.2 showed that the ALT readily decomposed to facilitate chemical reaction with NiO in the formation of $NiAl_2O_4$ at less than 1200°C, mimicking the reaction products of the pure NiO and Al_2O_3 powder mixture. No apparent reaction between NiO and the complimentary decomposition product of TiO_2 was indicated. The ALT peaks, with no peak overlap at 47.8° and 50.8°, show a clear decrease in phase content as temperature is increased from 1100 to 1300°C indicating the progressive decomposition of ALT. Furthermore, the unheated ALT indicates significant Al_2O_3 and TiO_2 in the unheated specimen indicating that the ALT powder is not fully phase pure. The trace phase $Al_2Ti_7O_{15}$ is also noted in Figure 3.2, which is longer present in the XRD scans at 1200°C.

The XRD scan of the YSZ/ALT powder mixture sintered at several temperatures, shown in Figure 2.3, yielded primary phases of YSZ, Al_2O_3 and $ZrTiO_4$ with additional trace phase content of $Al_2Ti_7O_{15}$ and $AlZr_9O_{1.95}$. The YSZ/TiO_2 pellet, which was also

sintered at 1400°C, indicated the presence of YSZ, TiO_2, and $ZrTiO_4$ phases to isolate the reaction between zirconia and titania for comparison. The 1200°C XRD scan of the YSZ/ALT mixture showed a prominent shift towards the phase content of $Al_2Ti_7O_{15}$ and $AlZr_9O_{1.95}$ prior to the formation of $ZrTiO_4$ at 1300°C which is indicated as the onset for the formation of the final half anchor. The half reaction involving the YSZ and titanium component of the anchor indicated a higher activation energy for chemical interaction such that $ZrTiO_4$ was not formed in appreciable quantity until 1300°C in addition to other trace compounds.

From the XRD study, it was apparent that the reaction occurred sequentially to form all anchoring phases given that ALT is well understood to spontaneously decompose to its constituents in the 850 – 1200°C temperature range [16-19]. Al_2O_3 as decomposed from ALT initially reacts with NiO after temperatures of 1100°C are achieved in the formation of the half-anchor $NiAl_2O_4$. Upon exposure to reducing gases, the remaining NiO will decompose to nickel metal, while the $NiAl_2O_4$ anchor will be unaffected. Further, the TiO_2 as decomposed from the ALT reacts with YSZ, or more specifically ZrO_2, at temperatures above 1300°C to form the other half-anchor $ZrTiO_4$. The use of ALT as opposed to simply adding discrete alumina and titania is of key importance with regard to the concept of anchoring. To successfully bond the YSZ with the NiO phase, the TiO_2 and Al_2O_3 must be sufficiently close in proximity to facilitate mutual chemical interactions that are bound in between by trace host phase, thus yielding the chemical anchoring concept as depicted in Figure 3.4. The use of discrete particles will add kinetic diffusional limitations that may retard the formation of the desired full

anchors. While $NiAl_2O_4$ and $ZrTiO_4$ compounds have negligible electronic and ionic conductivity, it is indicated that the majority of nickel will remain in metallic form and in contact with pure YSZ, thus preserving the triple phase boundary length required for electrochemical operation. If excessive quantities of $NiAl_2O_4$ or $ZrTiO_4$ compounds were used, the entire nickel/YSZ interface could become compromised given the excessive formation of secondary anchoring phase.

3.2 Infiltration

The infiltrated samples' fractured surfaces were examined under the SEM to determine the microstructural evolution of the nickel catalyst after exposure to elevated temperatures in a reducing atmosphere. Electron micrographs of the reduced nickel catalyst network on a doped and baseline sample are shown in Figure 3.5 to indicate the morphology of nickel within the bulk cross-section of the infiltrated anode. To point out both the uniformity of nickel infiltration and provide multiple micrographs from different areas of the anode a bulk region nearer to both the upper and lower surface, each individual sample was examined to determine potential variations in the effectiveness of the anchoring process. The vacuum assisted infiltration appears to yield very uniform nickel nitrate coverage through the pellet and no appreciable variation is noted indicating that the capillarity of the interconnected porosity was effective in homogenously distributing the precursor solution. Based on electron microscopy, the continuity and size scale of the nickel network was directly compared between undoped and ALT doped YSZ to evaluate the effectiveness of the anchors to inhibit nickel migration and coarsening. The effects of coarsening are exaggerated in the baseline sample for which

the nickel network is deteriorated on a 2-D surface with discrete nickel clusters larger than 2 microns present and some YSZ surfaces nearly devoid of nickel catalyst. The ALT doped specimen retained a uniform nickel network with nickel cluster sizes consistently less than 0.5 microns, qualitatively indicating the effectiveness of the chemical anchors in binding the nickel to the scaffold. The doped samples also seemed to have significantly better wetting characteristics than the undoped sample.

3.3 Electrochemical Testing

The fuel cell anodes were infiltrated with low quantities of nickel, which while yielding low expected performance, provided an accelerated time table for which coarsening and nickel migration yielded observable degradation. The first (single anode nickel infiltration step) and second (dual anode nickel infiltration step) set of samples were identically prepared and experienced identical operating conditions in the test fixture to eliminate variations from processing such that performance degradation can be traced back to the anode function. The current density of infiltrated fuel cells, with and without the ALT dopant, as a function of time was shown in Figure 3.6. An interesting outcome not directly related to degradation was that the doped cells yielded high power output for both sets of fuel cells. Based on the method by which the anchors form, one was able to deduce, that these boundaries are no longer capable of electrochemical conversion indicating a likely decrease in initial performance. The electrolyte supported SOFC test results indicated, however, that the ALT doped cells produced better performance regardless of operational duration. This indicated that the anchors facilitated increased nickel/YSZ interface length. The doped specimen in the first sample

set showed significantly lower degradation rates, based on the slope of the steady state portion of the curve. This supported the microstructural observations seen in Figure 3.5. The second set of cells generated more current as was expected due to the higher nickel loading. The step change observed in the ALT doped specimen at 30 hours (Figure 6 – right) was due to a momentary power disruption of the LabVIEW interface software controlling the mass flow controllers and electronic load. The degradation rates of the dual infiltration runs for both the undoped and doped specimens were however nearly identical. This indicated that the current method of scaffold processing by the introduction of 5 wt% ALT (-325 mesh) into the scaffold powder by mechanical mixing may be insufficient to create enough anchors for the higher nickel loadings in which higher ALT loading or finer particulate would be more effective.

The use of electrolyte-supported cells in this initial study was beneficial to eliminate the effects of bulk anode conductivity degradation for an anode-supported cell. While minor coarsening would not be as deleterious to net conductivity as much as triple phase boundary length in the in the electrochemically active portion of the cell, the study was designed to mitigate secondary effects associated with the thicker anodes. However, the benefits of infiltration are perhaps more relevant to anode supported cells in which better anchoring coverage may be necessary to support sufficient nickel loading for bulk anode electrical conduction. Additionally, the presence of hydrogen sulfide in fuel streams was shown to deteriorate nickel catalysts due to accelerated coarsening in electrolyte supported fuel cells [20], for which this anchoring system may also be effective at inhibiting chemically induced nickel migration due to fuel contaminants.

4.0 Conclusions

The addition of aluminum titanate (Al_2TiO_5) was shown to form beneficial secondary phases in the interaction with YSZ and infiltrated nickel metal within the anode of a solid oxide fuel cell. The formation of the chemical anchors was found to be stepwise in which the decomposition of aluminum titanate yielded an initial chemical interaction with nickel oxide after 1100°C, followed chemical interaction with YSZ after 1300°C. In this manner, nickel aluminate and zirconium titanate were key anchor forming phases in the NiO/YSZ cermet system. The formation of chemical anchors was shown to inhibit fine (<0.5 microns) nickel catalyst migration under SOFC relevant temperatures. Furthermore, the use of ALT as a YSZ dopant showed not only increased initial performance of fuel cell anodes infiltrated with nickel nitrate solution, but also decreased the rate of degradation due to coarsening and separation of the nickel catalyst network. Future efforts are focused on high resolution TEM studies to directly observe the morphology of anchoring phases in addition to developing improved methods of treating the surface of YSZ with aluminum titanate as opposed to introducing the dopant into bulk powder, thus decreasing the size for improving the number of anchoring sites available to interact with the nickel metal electro-catalyst. Additionally, applying this anchoring concept to systems other than Ni/YSZ is also being investigated.

Acknowledgments

This work was supported by the Department of Defense under Award No. FA8650-08-D-2806-0002. Any opinions, findings, conclusions, or recommendations

expressed herein are those of the author(s) and do not necessarily reflect the views of the DOD.

Table 3.1: Compounds identified by XRD and their respective JCPDS card numbers.

Compound	JCPDS Card Number
Al_2O_3	88-0826
• - $(Al_2Ti_7O_{15})^*$	39-0052
♦ - $(AlZr_9O_{1.95})^*$	53-0559
NiO	89-7131
$NiAl_2O_4$	71-0965
TiO	89-3076
TiO_2	89-6975
YSZ - $(Zr_{0.92}Y_{0.08}O_{1.96})$	48-0224
$ZrTiO_4$	34-0415

*** indicated as trace phases**

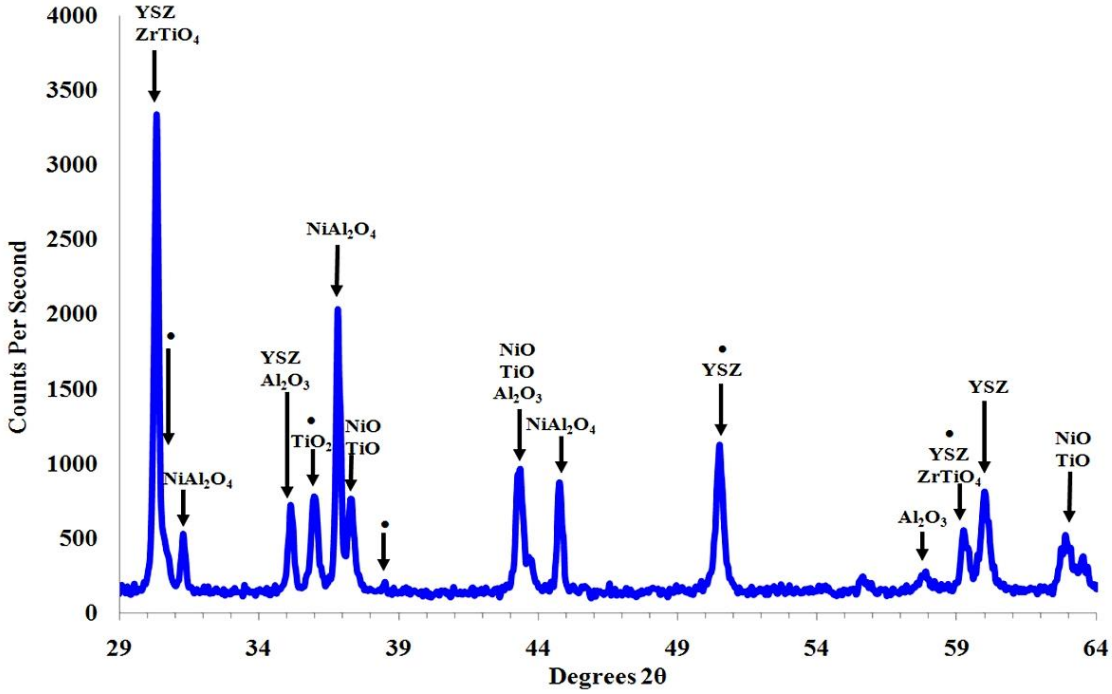

Figure 3.1: XRD pattern for NiO/YSZ/ALT powder blend sintered at 1400°C, indicating the complete chemical interaction of ALT with NiO/YSZ in the formation of Al_2NiO_4 and $ZrTiO_4$ secondary phases.

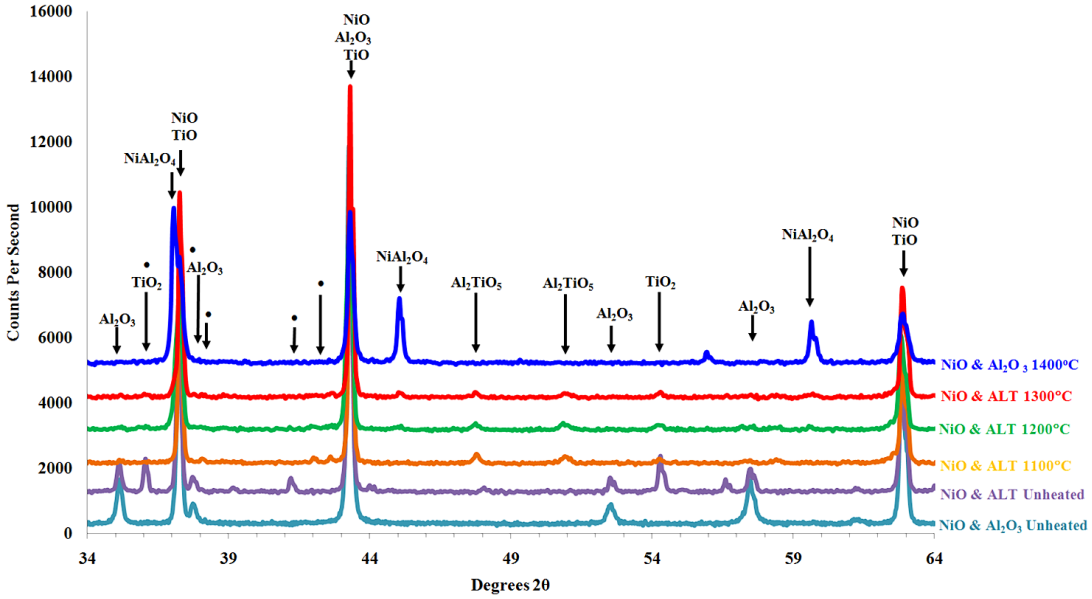

Figure 3.2: XRD patterns of NiO/ALT powders for unheated, 1100°C, 1200°C, and 1300°C sintering temperatures compared to reference NiO/Al_2O_3 powder unheated and sintered at 1400°C.

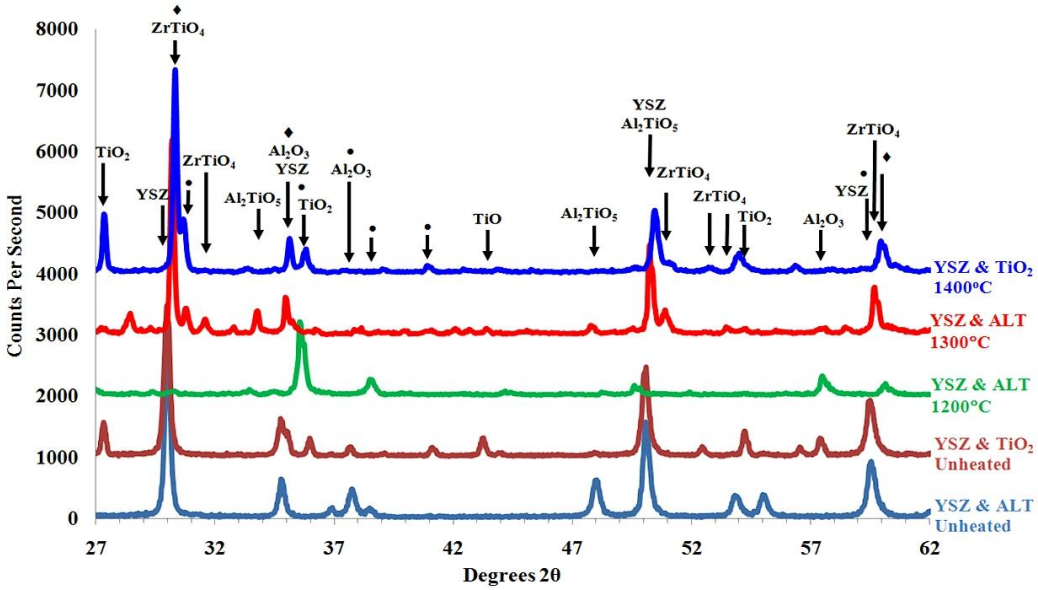

Figure 3.3: XRD patterns of YSZ/ALT powders for unheated, 1200°C, and 1300°C compared to reference YSZ/TiO_2 powder unheated and sintered at 1400°C.

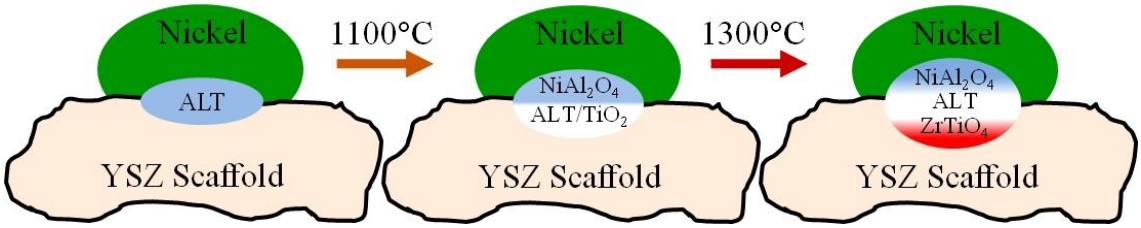

Figure 3.4: Illustration of infiltrated nickel on a YSZ substrate with ALT anchoring mechanism.

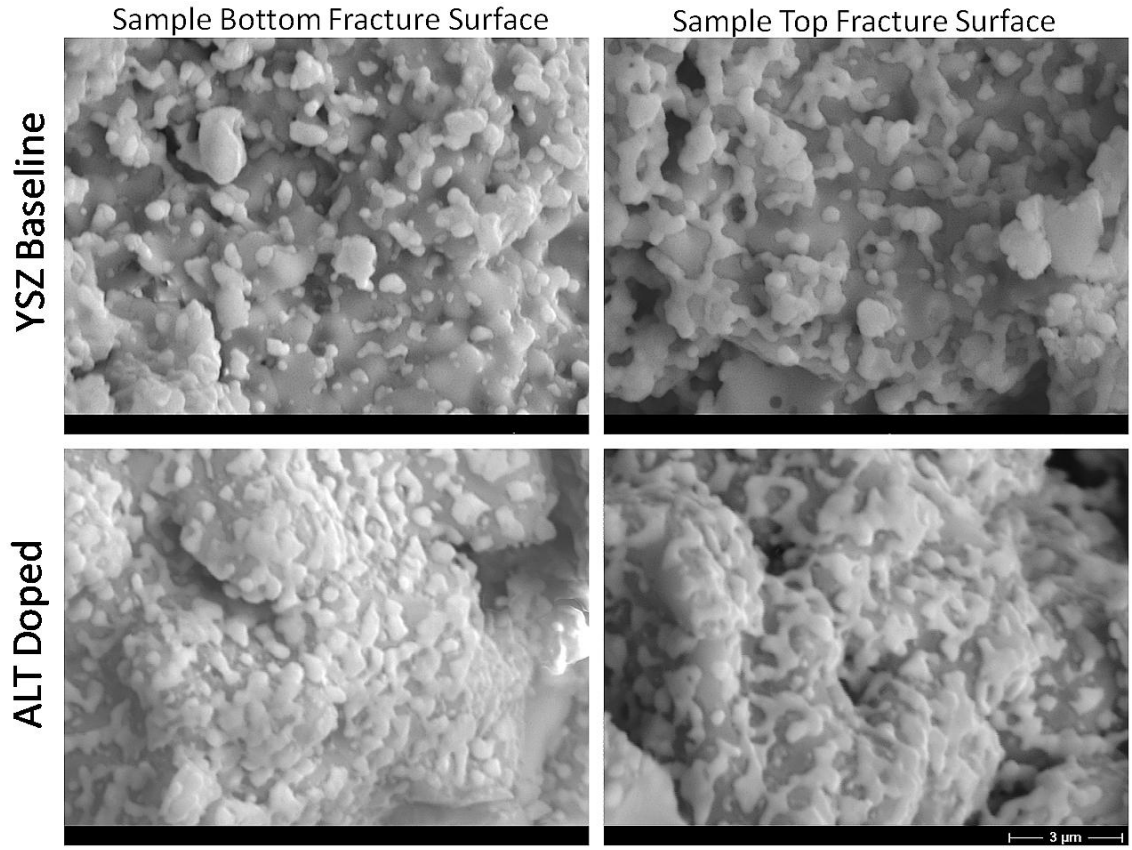

Figure 3.5: Micrographs of interior YSZ scaffold cross-sections (left nearer to the upper surface of the pellet and right nearer to the bottom surface) with infiltrated nickel after 72 hours at 800^{o}C in a reducing atmosphere.

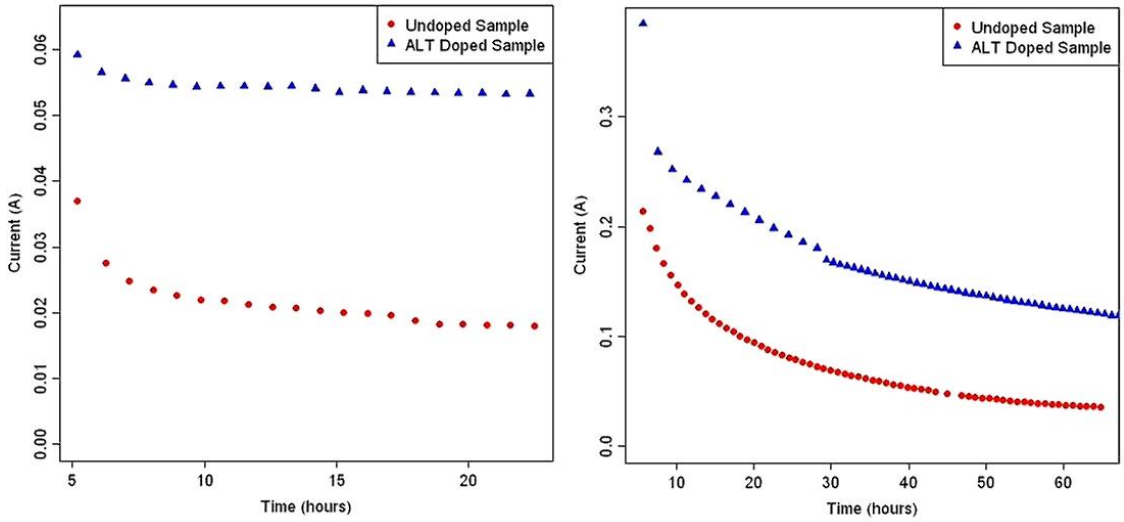

Figure 3.6: Electrolyte supported SOFC tests at 800°C with single infiltration test (left) and dual infiltration test (right) comparing baseline and ALT doped scaffolds infiltrated with saturated nickel nitrate.

References

1. M. Xigeng, D. Sun, P. W. Hoo, J. Liu, Y. Hu, and Yanming Chen, Ceramics International, 30 (2004).

2. B. Hua, F. Lu, J. Zhang, Y. Kong, J. Pu, B. Chi, and L. Jian, J. Electrochem. Soc., 156, 10 (2009).

3. M. Pihlatie, T. Ramos, A. Kaiser, J. Power Sources, 193 (2009).

4. A. McEvoy, S.C. Singhal, and K. Kendall, High Temperature Solid Oxide Fuel Cells: Fundamentals, Design and Applications, Elsevier, 2003 (Chapter 6).

5. A. Atkinson, S. Barnett, R.J. Gorte, J.T.S. Irvine, A.J. McEvoy, M. Mogensen, S.C.Singhal, and J. Vohs, Nat. Mater., 3 (2004).

6. W.Z. Zhu, and S.C. Deevi, Mater. Sci. Eng., A362 (2003).

7. D. Sarantaridis, and A. Atkinson, Fuel Cells, 7 (2007).

8. D. Sarantaridis, and A. Atkinson, Proceedings of the 7th European SOFC Forum, Lucerne, Switzerland 2006, paper P0728.

9. K. Kendall, C.M. Dikwal, and W. Bujalski, ECS Trans., 7, 1 (2007).

10. C.M. Dikwal, W. Bujalski, and and K. Kendall, J. Power Sources, 181 (2008).

11. A.N. Busawon, D. Sarantaridis, and A. Atkinson, Electrochem. Solid-State Lett., 11, 10 (2008).

12. P.H. Grahl-Madsen, N. Larsen, J. Bonanos, J. Engell, and S. Linderoth, J. Mater. Sci., 41 (2006).

13. L. Young, V. Vedahara, and S. Kung, S. Xia, V.I. Birss, ECS Trans., 7, 1 (2007).

14. James R. Wilson and Scott A. Barnett, Electrochem. Solid-State Lett, 11, 10 (2008).

15. S.W. Sofie and D.R. Taylor, Ceramic Engineering and Science Proceedings, 28, 4 (2008).

16. D. Lawrence, and R.I. Smith, J. Am. Ceram. Soc., 88, 10 (2005)

17. G. Tilloca, J. Mater. Sci., 26 (1991)

18. M. Nagano, S. Nagashima, H. Maeda, and A. Kato, Ceramics International, 25 (1999)

19. B. Freudenberg and A. Mocellin, J. Am. Ceram. Soc., 70, 1 (1987)

20. A. Lussier, S. Sofie, J. Dvorak, and Y.U. Idzerda, Int. J. of Hydrogen Energy 33, 3945 (2008)

21. M. A. A. Elmasry, A. Gaber, and E. M. H. Khater, Journal of Thermal Analysis and Calorimetry, 47, 3 (1996)

CHAPTER FOUR

INVESTIGATION OF ALUMINUM TITANATE FOR CHEMICAL ANCHORING OF INFILTRATED NICKEL CATALYST IN SOLID OXIDE FUEL CELL ANODE SYSTEMS

Contribution of Authors and Co-Authors

Author: Cameron H. Law

Contributions: Processed samples and performed experiments, collected and analyzed output data, and primarily wrote the manuscript.

Co-Author: Dr. Stephen W. Sofie

Contributions: Discussed the results and implications of data and commented on the manuscript at all stages.

Manuscript Information Page

Cameron H. Law and Stephen W. Sofie
Journal Name: Journal of Power Sources
Status of Manuscript:
X Prepared for submission to a peer-reviewed journal
_____ Officially submitted to a peer-reviewed journal
_____ Accepted by a peer-reviewed journal
_____ Published in a peer-reviewed journal

Publisher: Elsevier

Abstract

Development of Solid Oxide Fuel Cells (SOFCs) has been largely leveraged on nickel/YSZ cermets. However, more recent efforts have been involved in examining all-ceramic systems and infiltrated catalyst approaches. While enhanced mechanical strengths and decreased weight can be achieved by infiltrating nickel into a porous yttria-stabilized zirconia (YSZ) electrode when compared to traditional nickel/YSZ cermets, the electrochemical performance readily degrades due to coarsening of the initial nickel network. The stabilization of metallic electro-catalysts for use at high temperatures provides an opportunity to extend the potential of nickel based anodes. While this methodology has application potential in a variety of industries where micro or even nano-sized clusters of metal catalyst are desired, this study focused much more on the application to SOFCs and further characterization of the chemical additive aluminum titanate (ALT). The decomposition behavior of ALT and formation of chemical reactions with Ni/YSZ cermets was evaluated with a detailed XRD diffraction study from 1000 – 1400°C. XRD also indicated that the $NiAl_2O_4$ half anchor formed at temperatures as low as 1100°C and the $ZrTiO_4$ half anchor formed around 1205°C, depending on the precursor used. Transmission electron microscopy was employed to investigate the proposed mechanism by which chemical anchors restrain nickel metal migration, in which it has been established that two discrete configurations of chemical anchors were formed. Further, testing of SOFCs with optimized ALT addition utilizing infiltrated anodes from metal salt solution was used to compare the effectiveness of the anchors in regard to electrochemical performance.

1.0 Introduction

Solid Oxide Fuel Cells (SOFCs) are a continually developing technology which integrates aspects of electrochemistry, materials, and structures for fabricating effective and robust devices. From a materials aspect, SOFCs have several challenges to overcome to be implemented as an effective and viable power source for both terrestrial and space applications. The several layers of an SOFC include the anode, electrolyte, and cathode; often with interlayers between the electrodes and electrolytes to improve electrochemical performance and to decrease chemical reactivity [1-3]. Traditionally, anodes are made of a ceramic/metal (cermet) material consisting of nickel metal catalyst and yttria-stabilized zirconia (YSZ). Nickel provides an inexpensive catalyst when compared to more exotic materials in the platinum metals group, but still has a high catalytic activity at the elevated operating temperatures of SOFCs.

It has been common practice to mix nickel oxide, YSZ, and a pyrolizable thermal fugitive together to achieve an equal volume mixture [4]. This satisfies the percolation limit of all the materials (3-D connectivity) and allows simultaneous gas flow and electron flow through the anode, with ion transport extended farther into the anode than the planar anode-electrolyte interface. While this method is convenient for commercial production and has been extensively studied to manipulate particle size and pore size [1, 5-7], it does have several shortcomings. The high nickel concentration of over 33 vol% limits the mechanical strength of the YSZ and shifts the coefficient of thermal expansion for the anode to approximately 13.4 ppm/^{o}C, much higher than that of the YSZ electrolyte at approximately 10.8 ppm/^{o}C. The stresses induced by thermal cycling can

be detrimental to a cell/stack and cause catastrophic failures [4]. From a weight perspective, the density of nickel, 8.9 g/cc, is substantially higher than that of YSZ at 5.9 g/cc. The high solids loading of nickel therefore results in increased system mass which can be critically important in aero applications.

A different approach to anode fabrication is to introduce the nickel anode catalyst by infiltration. Instead of a bulk mixture of nickel oxide, YSZ, and a thermal fugitive, a YSZ scaffold is fabricated with porosity by one of several available methods. These methods can include pyrolyzable thermal fugitives, freeze tape casting which leaves porosity in a green state, or a chemical leaching method [8-10]. The sintered, porous YSZ is then infiltrated with a solution-based nickel precursor. The first benefit of this method is that only 10 - 15wt% nickel metal is needed instead of the higher quantities necessary for bulk mixtures to satisfy percolation [4,8]. This not only reduces cell weight, but in cases where a more specialized anode catalyst is needed, such as the use of hydrocarbon fuels or combined electrolysis operation, this method promises reduced costs. The second benefit is that the majority of the anode is comprised of the YSZ scaffold, improving overall strength and providing a better matched coefficient of thermal expansion to the electrolyte [9]. This method has not been fully taken advantage of because the nickel metal migrates and coarsens substantially, degrading cell performance at rates much greater than traditional anodes [11]. At SOFC operational temperatures (700^{o}C to 1000^{o}C) the nickel has been shown to coarsen and agglomerate into larger particles that break up the original nickel network [11]. This causes two key problems; first, the larger particles are less catalytically active than the smaller, original network of

particles due to the substantial decrease in surface area. Second, the coarsening of nickel causes voids and separation in the nickel network, breaking down the electron path for current collection and hindering overall performance of the anode [8,12-13].

Previous work has introduced a novel concept of chemical anchoring which mitigates the nickel coarsening. By introducing a minor amount of anchoring additive that forms a bond between the catalyst and substrate, portions of the nickel network that previously necked down to a discontinuous path were stabilized at 800°C [11]. This chemical anchoring concept can be applied to several industries where migration of a catalyst on a surface has been shown to lead to failures such as automotive catalytic converters[14-15], methane reforming systems [16-17], and multilayer capacitors [18], in addition to SOFCs . While the results are promising in the previous study, the mechanism by which the anchors formed and direct observation of the anchors by electron microscopy has yet to be ascertained. Studying the qualitative effects of thermal coarsening, X-ray Diffraction (XRD) spectra, Scanning Electron Microscopy (SEM)/Transmission Electron Microscopy (TEM)/Focused Ion Beam (FIB) tools, and infiltrated electrode conductivity testing yielded a more defined system that can be carried on for future work across a multitude of platforms including new material systems such as gadolinium doped ceria and barium cerate based fuel cell ceramics.

2.0 Experimental Procedure

2.1 Thermal Coarsening

To fully understand the relevance of chemical anchoring nickel metal catalysts, determining the effect of temperature on coarsening was paramount. Experiments were setup to determine temperatures that have the most substantial coarsening effects on infiltrated nickel and compare these with the mitigation of the coarsening by chemical anchors to establish the effectiveness of the anchors at temperatures that reach 900°C. While this temperature was higher than normal for terrestrial use, it may be required in aero applications to improve the specific power density (kW/kg). Dense pellets of only yttria-stabilized zirconia (YSZ, Tosoh TZ-8Y) or YSZ with 10 wt% aluminum titanate (ALT - Al_2TiO_5, AlfaAesar #14484) were mechanically mixed and pressed in a 1.27 cm diameter die to 231 MPa then sintered at 5°C/min up to 1400^{o}C for 1 hour with 10^{o}C/min ramp rate down. Pellets of pure YSZ were similarly sintered but then coated via the aerosol spray method with dilute ALT that was ground in an automated mortar and pestle for 2 hours. Once dry, all pellets were coated with a thin layer of fully saturated nickel nitrate solution (Nickel Nitrate Hexahydrate, AlfaAesar A15540) via the aerosol spray method. Pellets dried almost instantly and were heat treated to 1400^{o}C again for 1 hour to activate the anchors as determined in a previous study [11]. To maintain continuity between all the samples, the pellets without anchoring additives were also heat treated.

All samples were then simultaneously reduced at 600^{o}C for 1 hour in a 5% H_2/95%N_2 atmosphere. This temperature was selected because it provided a sufficient reducing atmosphere to reduce the NiO to nickel metal but limited the effects of

thermally induced coarsening. Once reduced, one pellet of each type (baseline, 10wt%ALT, and aerosol sprayed ALT) were placed in the tube furnace again for 100 hours at temperatures between 650^{o}C and 900^{o}C ramping to temperature over the course of 30 minutes and cooling as quick as possible at approximately 10^{o}C/min. Once the run was completed, samples were mounted for observation under a Field Emission Scanning Electron Microscope (FE-SEM, Zeiss Supra 55VP) to examine and qualitatively compare the reference coarsening and the two methods of anchoring.

2.2 X-ray Diffraction

Previous studies had performed very coarse XRD scans to find evidence of anchor formation [11]. In this study, a detailed scan of various temperatures between 1100^{o}C and 1400°C was completed to identify specific formations and possible temperatures of interest. Powders of NiO (AlfaAesar #12359), YSZ, and ground ALT were pressed in a 1.9 cm diameter die to 172 MPa and sintered to temperatures between 1100 and 1400°C at 5°C/min up and 10°C/min down with a 1 hour dwell. Equal volumes of the three constituents were used and initial powders were prepared by ultrasonic mixer in ethanol and dried at 70^{o}C. Pellets were ground back to a powder in an aluminum oxide mortar and pestle and scans were taken from 15^{o} to 75° 2θ with an XRD (Scintag Inc. XGEN-4000). Powder spectra were then compared to relevant powder diffraction files and compared to other temperatures. The same process was performed with Al_2O_3 (Inframat 26R-0801) and TiO_2 (Inframat 22N-0801A) since these two compounds are formed when ALT decomposes in the metastable region. Instead of 33 vol% ALT, a 50% molar ratio

of each Al_2O_3 and TiO_2 were used to have the same ratio of aluminum to titanium as the ALT powder.

2.3 Microscopy and Elemental Analysis

Use of several microscopes at the Environmental Molecular Science Laboratory (EMSL) at the Pacific Northwest National Laboratory (PNNL) was awarded through a rapid access proposal prepared at Montana State University. Samples were prepared specifically for examination at EMSL and contained significantly higher ALT percentages. Three FE-SEMs with Focused Ion Beam Milling attachments were used at EMSL (FEI Helios, and two FEI Quanta) for detailed elemental mapping and to prepare samples for HR-TEM (Titan 80-300). Samples of YSZ were freeze tape cast in aqueous solution as described elsewhere [19] [10]. Freeze tape casting was chosen because of the graded pores available by the nature of ice crystal formation. This produced an easily identifiable pore surface for infiltration and location under the microscopes. The frozen tapes were then set in a freeze dryer (Virtis AdVantage) to sublime the ice crystals yielding porous green tapes. Using a 2.5cm diameter punch, disks were cut from the tape and sintered up to 1400°C with 1 hour dwell, and a rate of 5°C/min up and 10°C/min back down to room temperature. A tape was also made with 50wt% ALT and 50wt% YSZ in place of the YSZ in the previous tape. This slurry was cast and processed the same as the YSZ only tape. Disks from both tapes were infiltrated with nickel nitrate to a calculated nickel solids loading in the range of 18-30 wt% as listed in Table 1. Nickel nitrate would be applied to the surface of the disks until saturated, then placed under a vacuum for 60 seconds. The samples were placed in a 500°C furnace to decompose the

nickel nitrate into nickel oxide. Infiltration was then repeated until loading reached the desired threshold. The sample with ALT in the bulk was placed in the furnace and heated to 1400°C to activate the anchors with a 1 hour dwell and the standard heating and cooling rate of 5°C/min and 10°C/min, respectively. Samples were finally placed in a reducing atmosphere of 5%H_2/95%N_2 at 800°C for 48 hours. This allowed the nickel oxide to reduce and mild thermal coarsening to occur with the intention of easing the location of anchor points for the microscope studies such that areas of higher nickel concentration should correspond to sites of anchor formation. Disks were placed in the SEM with FIB and, through the focused ion beam attachment, samples of approximately 10μm in width were removed.

2.4 Infiltrated Electrode Conductivity

As a final method to test the effectiveness of anchoring additives in a nickel catalyst-based electrode, porous electrode scaffolds were fabricated, infiltrated, and tested to provide an opportunity to evaluate the anchoring process and effects on overall conductivity. Electrodes were tape cast as a mixture of YSZ, a thermal fugitive, binders, and plasticizers . The ALT doped sample used the same total weight as the YSZ only tape, but instead was composed of 90wt% YSZ and 10 wt% ALT.

Disks 2.5cm in diameter were punched from the anode tapes and were sintered up to 1400°C at 5°C/min up and 10°C/min down with a 1 hour dwell, combusting the thermal fugitive and sintering the oxide support. Nickel nitrate described previously in the thermal coarsening section was then introduced to the surface of the anode until saturated, placed under a low vacuum to maximize penetration of the nitrate, and heat

treated at 500°C for 15 minutes to decompose the nitrate. This process was repeated until the calculated nickel loading met a threshold of approximately 20 wt%. The loaded anode was then heated to 1400°C at 5°C/min up and 10°C/min down with a 1 hour dwell to either activate the chemical anchors, or maintain continuity in the case of the baseline.

The disks were then coated with silver slurry (SPI High Purity Silver Paint) and had two leads of silver wire attached on each side. The disk was then clamped between two alumina blocks to minimize stress on the leads and placed inside a tube furnace (MTI GSL1500X). The leads were connected to a micro ohm meter such that a 4 point resistance measurement was made (Agilent 34420A Nano Volt / Micro Ohm Meter) and a 5%H_2/95%N_2 forming gas atmosphere was introduced. After approximately 15 minutes, the furnace heated to 800°C at 10°C/min and dwelled for 50 hours. During the ramp up, the resistance of the cell would be measured approximately every 200^{o}C. Once 800^{o}C was reached, the resistance was recorded every 10 minutes.

3.0 Results and Discussion

3.1 Thermal Coarsening

Surface images of nickel coarsening obtained by FE-SEM are shown in Figure 4.1. These images of samples heat treated at 700°C and 800°C were arranged such that the far left was the baseline sample, the middle was the sample with 10 wt% ALT in the bulk, and the far right was the sample with a dilute ALT solution applied to the surface via aerosol method. While the images of thermal coarsening were acquired from different specimens where variances in ALT and nickel nitrate coverage were expected, the images

provide a qualitative analysis of the effects of thermal coarsening based on a planar YSZ/Ni interface. To verify initial application of the nickel, an aliquot of the pellets were sampled after the 600°C reduction run and indicated that the nickel network was consistent across all the samples. This was sufficient evidence that the coatings of nickel nitrate were similar in nature and quantity. While the images were collected from separate samples, the goal of qualitatively comparing the coarsening of nickel and the effects of anchors provides an important visual basis for the merits of this study.

At the 700°C temperature, the baseline sample was a well dispersed network with coarsening of the nickel just beginning to occur. However, compare the baseline to the anchored samples and it was obvious that the 10 wt% ALT sample had larger nickel clusters but better connectivity while the aerosol applied ALT maintained a higher quantity of nickel at a finer scale. The aerosol applied ALT was introduced as a possible method of infiltration. This solution of finely ground ALT in ethanol appeared to wet well and anchored the nickel as effectively as the mechanically mixed ALT in the bulk. Use of this solution for infiltration in porous electrodes may be possible due to this success. Figure 5.1 also indicated that the baseline sample underwent moderate to severe coarsening since the finer network of the 700°C specimen was no longer apparent, but instead larger clusters of nickel at least doubled in size remained. The change in the baseline sample from 700°C to 800°C indicated that the nickel network was indeed coarsening and should have been apparent in the nickel network of other samples as well. The 10 wt% ALT at 800°C did indeed show some coarsening but maintained good connectivity throughout the network and maintained a distribution of nano-size

particulates of nickel. ALT applied via the aerosol method showed an incredible network remained with both connectivity and smaller particles of nickel. It was noted that at 900^{o}C all samples appeared to have similarly coarsened networks, with the samples with aerosol method ALT being slightly more connected. While ALT anchor sites help mitigate coarsening, there clearly was a limit to the anchoring additives capability and the higher temperatures may have imposed a force greater than the anchors could overcome. Remarkably, the chemical anchors did maintain networks significantly better than the baseline samples at the desired operating temperatures of SOFCs. The ALT applied via aerosol method was so dilute in concentration (less than 1 wt%) that any issue of saturation or reacting with all the nickel catalyst was dismissed. Further optimization of ALT characteristics may extend the effective temperature range well beyond the 900^{o}C mark, although that was beyond the scope of this work. Figure 5.1 clearly displayed the change in nickel networks between the temperatures and between the samples.

A high magnification image of the baseline sample and the 10 wt% ALT sample after being held at 900°C has been displayed in Figure 4.2. Several pits were apparent in the images with nickel clusters still centered in some of the depressions and others completely empty. This was indicative of nickel previously being held in the areas of the depressions but coarsened to the surrounding clusters. At 900^{o}C the 10 wt% ALT sample had coarsened, but still has superior connectivity over the baseline sample. These pockets were exceptional evidence of the previous nickel network and the drastic effects coarsening can have on an anode. While several authors discuss coarsening, high magnification images such as this are not common [4, 8-9, 11-12].

This study provided a very unique insight to the coarsening and microstructure of nickel metal catalyst on a YSZ substrate as used with many SOFC anodes. While the results were qualitative, they were fully supported by the remaining studies and thus contributed to the objectives of this report.

3.2 X-ray Diffraction

Earlier studies had focused on ALT as a sintering or strengthening dopant but it was quickly realized that other reactions were occurring based on the metastability of ALT that form the basis of the anode anchoring process [11,20]. It has been reported that ALT begins to decompose between 600^{o}C [21] and 1400^{o}C [22], with several formation temperatures reported in between[23-26]. Previous identification of the decomposition and chemical interaction of ALT with the two anode constituents was reported elsewhere, however, studiers were only completed on a rough temperature scale [11]. The expected reactions were listed in Equations 4.1-3 where it was known that the nickel aluminate formed prior to the zirconia titanate. The propensity to form nickel aluminate may assist with the decomposition and allow the remaining titante to react with the zirconia.

$$Al_2TiO_5 \leftrightarrow Al_2O_3 + TiO_2 \qquad \text{Equation 4.1}$$

$$Al_2O_3 + NiO \rightarrow NiAl_2O_4 \qquad \text{Equation 4.2}$$

$$TiO_2 + ZrO_2 \rightarrow ZrTiO_4 \qquad \text{Equation 4.3}$$

These reactions would allow the anchoring additive, ALT, to be introduced to the sample. When thermally activated, ALT decomposed into its constituents at the same local area. These constituents would react with either the catalyst or the substrate and ease the varying materials. Physically, the nickel aluminate should form a bond with the nickel metal catalyst, but also interact better with the zirconia titanate due to being an oxide. The zirconia titanate would then interface with the YSZ and the catalyst at that area would be considered anchored.

XRD spectra for different powder compositions thermally treated at progressively increased temperature were shown in Figures 4.3 and 4.4. The peaks for the XRD spectra were indexed to indentify primary phases, secondary phases, and trace phases. Peak overlap occurred substantially with many of the primary and secondary phases in this system including $NiAl_2O_4$ and TiO_2 at 35.95^o, NiO, Al_2O_3, and TiO_2 at 43.35^o, and NiO and TiO at 37.25^o and 62.9^o. The formation and decomposition of key anchoring phases was, however, identified with less prominent peaks to isolate the temperature steps associated with the formation of chemical bonds.

When comparing the two spectra, a very interesting change was noted regarding TiO_2. First, looking at the Al_2O_3 and TiO_2 sample in Figure 3, the TiO_2 peaks at 27.3^o and 54.02^o diminish to the level of noise at 1190^{o}C and 1265^{o}C, respectively. Since several other peaks overlap, this peak can be productive to give some indication of when the YSZ reacts with TiO_2. Previous studies indicated that the Ni and Al_2O_3 reacted much more readily with YSZ and TiO_2 requiring a higher thermal energy before reactions would occur. Thus, using the TiO_2 peak should be indicative of complete reaction

between all the compounds. Based on this assumption, the final reaction occurs around 1265^{o}C. Comparing this to the ALT composition in Figure 4.4, the TiO_2 peaks now appear to decrease to negligible heights almost exclusively at 1205^{o}C. As discussed as an option later, the use of separate Al_2O_3 and TiO_2 seems to require a higher processing temperature than simply using ALT. It is very counterintuitive that a reaction which first requires decomposition of a compound, ALT, required less thermal energy than that of a reaction of the constitutive compounds alone. However, the model in the top of Figure 5, would indicate that the Al_2O_3 and TiO_2 benefit from a physical closeness to each other such that the nickel forms the nickel aluminate and the titanium reacts with the zirconium. The nickel aluminate appeared in both cases as low as 1100^{o}C. Also, by assessing the TiO_2 peaks and the lack thereof, it was safely assumed that the peaks with overlapping NiO and TiO_2 are actually only NiO.

There were a few peaks in both spectra which were not accounted for, such as at 39.85^{o} and 59.13^{o}. These trace phases were identified to possibly be $Al_2Ti_7O_{15}$ or $Al_{0.1}Zr_{0.9}O_{1.95}$. A scan of the ALT as received indicated that these peaks specifically were not present, although the powder was not pure ALT. The absence of trace phase peaks in the XRD scan performed at traditional YSZ sintering temperatures indicated that once the 1350^{o}C temperature mark was reached, many of the secondary and undesirable phases no longer appeared in either scan. This could indicate that the $Al_2Ti_7O_{15}$ or $Al_{0.1}Zr_{0.9}O_{1.95}$ phases were additional metastable phases that eventually decomposed and contributed to the formation of the primary anchoring phases, $ZrTiO_4$ and $NiAl_2O_4$. The results of this new XRD study show clearly that the full anchoring process was complete

just above 1200°C. However to ensure phase purity for the microscopy and conductivity study, along with continuity of the previous study, 1400^{o}C was used for thermal treatment to activate the chemical anchors.

Most relevant from the XRD spectra were the similarities of using ALT compared to the decomposed aluminum oxide and titanium oxide. The detailed spectra showed nearly identical peaks between the two compositions. This justified previous works which examined the half reactions (nickel/aluminum oxide and YSZ/titainium oxide [11]) and will simplify future analysis. If these spectra were significantly differing, the compositions could only be analyzed as a whole system and the assumption of decomposition of ALT would be incorrect. Equations 4.1-3 agree with the XRD results such that the ALT is present at lower temperatures, with nickel aluminate forming at lower temperatures, and finally the titanium reacted with the zirconia.

3.3 Microscopy and Elemental Analysis

One of the most critical elements to this study was microscopic evidence of the anchors to validate the modeled behavior as depicted in Figure 4.5 along with XRD spectra discussed above. Figure 6 shows an SEM micrograph of a region from an ALT doped sample in which elemental mapping was overlaid on the SEM image to extrapolate spatial distribution of the key elements. The elemental mapping acquired from a ground particle of a doped sample infiltrated with nickel. The green coloring in the top left image of Figure 4.6 represented a strong aluminum phase while the yellow represented a strong nickel phase. The brightest yellow (lower right corner of lower left image) was indicative of a pure nickel metal cluster. All other overlapping areas of green and yellow

indicated a nickel/aluminum composition. While elemental mapping could not identify the specific composition, this does support the conclusion that nickel and aluminum form a chemical bond identified in the previous XRD.

In the lower right corner of Figure 4.6, the elemental mapping was focused on the zirconia (pink) and titanium (blue) elements. When this image was compared with the nickel/aluminum map, the dark areas of one map correlate to the bright areas of the other. That fact indicated that very little reaction occurred between the two proposed phase combinations. For instance, an aluminum zirconia oxide was not forming since the aluminum and zirconia maps were completely isolated from one another. When referencing the titanium and zirconia overlap, again it was evident that they were forming a composition that included both of the constituents as identified in the XRD spectra to most likely be $ZrTiO_4$.

The top right image in Figure 4.6 was of aluminum and titanium. This image had some points where the green and blue colors mixed mildly. Those locations were indicative of remaining ALT. Noting the correlation of these ALT phases to the nickel/aluminum and zirconium/titanium overlapping phases, it appeared that the ALT was remaining in between these other phases and would indicate an incomplete reaction. This remaining ALT may benefit the anchoring process by further reducing the change in composition between the nickel catalyst and the zirconia substrate.

SEM-FIB systems were used to prepare the samples to a standard set of dimensions and mount the sample to a TEM grid. Several areas in Figure 4.7 were selected for elemental analysis with the goal of observing the anchoring phases and their

respective size to validate the concepts in Figure 4.5. Since the electrons are being transmitted through the sample in TEM, varying shades are indicative of different materials. The area imaged in Figure 4.7 was specifically selected because of these varying shades and the expectation that they would indicate predicted anchoring phases. The granular nature of Figure 7 was unexpected since, previously, the predicted model was a homogeneous or very gradual change in anchoring compounds. TEM systems allow much more reliable EDX spectra to be collected since the collection of elemental data was not clouded by the compounds beneath the surface. The EDX analysis indicated that several phases strongly correlated to an aluminum/nickel composition, as in area 1 of Figure 4.7. This followed the elemental mapping and XRD in being an indicator that the predicted phases were indeed occurring. Similarly, areas 2 and 3 displayed very dominant yttria, zirconia, and titanium peaks. Between these two areas, as expected from the change in coloring, were differences in the intensity of the peaks. The minor differences shown in the spectra in Figure 4.8 could be indicative of varying compounds. Differences in color can also be caused by shifts in the lattice, and may only be indicating that one area was aligned significantly different than the other. Copper peaks were detected and ignored for the purpose of analysis since they were known artifacts from the TEM grid and no known sources of copper contamination were available.

The sample examined in Figure 4.7 was intentionally prepared with significantly more ALT than previous samples with the purpose of increasing the likelihood of finding an anchoring point. This act may have serendipitously led to the realization of a saturation limit and the resulting change in a predicted model. Defining a new model

based on the results of this TEM image required the nickel to be anchored on the edges instead of directly in the center of a particle. Several problems arise with an oversaturated sample model. First, ALT and its decomposed entities are known to yield less catalytic activity than nickel. By introducing more ALT than necessary, vital nickel catalyst is displaced and the activity of the region is decreased. Also, the true triple phase boundary of a particle of nickel on a YSZ substrate is at the edge where the catalyst and ion conductor meet together with a pore. This allows the fuel to be delivered to the point where an oxygen ion can reach and the nickel network can carry electrons away. By causing anchor sites to be formed at the edge, this could limit the overall triple phase boundary and decrease activity. However, if sufficient gain occurred, there are also benefits to this new model with anchor points at the edge. The diffusion of titanium and aluminum to the edges may allow separate infiltration of anchor constituents and avoid the infiltration of ALT as a solid suspended in solution. Hydrated aluminum nitrate and titanium isopropoxide could be infiltrated simultaneously or sequentially and would diffuse to anchor locations and self-assemble the necessary bonds. The lower top image in Figure 4.5 displays how this method contrasts to the originally proposed anchor model. Initially, the ALT would separate and form an anchor in the middle of the nickel particle. This would allow the entire circumference of the particle to be open and act as a triple phase boundary. However, it also only anchors the center of the particle. The model developed by oversaturation of the ALT appears to anchor the nickel around the edges of the particle. This limits the triple phase boundary by taking up valuable area with the anchor. Surrounding areas are still available for the electrochemical activity necessary

for the operation fuel cell and may be sufficient. This model may better anchor the particle by bonding it at the edges. Future investigation should be made into the effectiveness of each model.

A TEM image of the boundary between nickel and YSZ was displayed as Figure 4.9 where a small discreet area appears labeled “Nickel Compound”. The elemental analysis detected that the area was nickel with no other peaks, but for some reason the appearance had changed for this one section as with area 3 in Figure 4.7. This could be indicative of a nano-sized anchor but could not be confirmed. The interaction between the nickel and YSZ as described earlier was also evident in Figure 4.9 as the interface between nickel metal and the YSZ was very definite. The interface of nickel metal to the nickel compound was less distinct, as was the interface with the nickel compound and the YSZ. Thus, the nickel compound may indeed be such an anchor with a gradual progression of nickel metal catalyst to the YSZ substrate.

These maps were immensely helpful in providing local support of a nickel aluminate and zirconium titanate forming. When coupled with the previous XRD data, the story clarifies to show the reactions indicated in XRD were most likely occurring in the sample at the locations identified by mapping.

3.4 Infiltrated Electrode Resistance

Measured resistance can be used with geometry to determine the resistivity or its inverse, the conductivity, of a material. Unfortunately, the geometry used of cross sectional area and length are more convoluted with a porous, infiltrated substrate than with a dense pellet. The measurable dimensions of area and length relate to the overall

macroscopic porous substrate which is electronically non-conducting. Infiltrated nickel networks allow electron conduction throughout the sample, but are essentially miniscule filaments of nickel that form an intricate network throughout the pores. As particles of nickel neck down due to the coarsening, the cross sectional area in that location changes. Similarly, as paths coarsen and disconnect, the electron flow must use an alternate route to traverse the substrate, effectively increasing the length. One particle coarsening and disconnecting could disconnect a very large portion of the nickel network and show a significant change in resistance. These complications from material properties directed the study to use a common measurement, the area specific resistance (ASR). Determining the ASR of each disk allowed the measured resistance and the overall area to be incorporated and the data was plotted. ASR is commonly used as a method to determine the in situ change in coatings [27] and SOFC electrodes [28-30]. By incorporating the cross sectional area into the value, variability in the pellets was normalized out of the results. Thus ASR was used as a common value with a decent physical understanding.

The ASR measurements were plotted and displayed in Figure 4.10 with redundant samples in Figure 4.11. As the nickel paths coarsen in the baseline samples, the networks become more and more discontinuous. This discontinuity in turn increases the path length for electrons from one side to the other and increased the measured resistance. Anchored samples retard this coarsening and allow the electron paths to maintain in the originally, or similar, infiltrated state. The sample anchored with 10 wt% ALT in the bulk shown in Figure 4.10 underwent 36.5%/1000 hr degradation. The baseline sample 1

underwent a degradation of 6419%/1000 hr. The 10 wt% ALT sample in Figure 4.11 degraded more than the previously doped sample at 104%/1000 hr while baseline sample was calculated at a 625%/1000 hr degradation rate. The degradation was calculated by a linear fit over the last 20 hours of the run, with percentages based of the ASR at the beginning of the linear fit. Even with the very low increase in the second baseline sample, it was clear that the anchored sample did reduce the overall increase in ASR.

It was clear from Figure 4.10 and 4.11 that a spread between ASRs occurred for samples very close in physical characteristics. All baseline samples were from the same tape cast slurry, sintered, and infiltrated simultaneously. ALT doped samples were prepared in identical fashion. As displayed in Figure 4.12, the weight percent of nickel in each sample was very similar. This variance in ASR was attributed to the chaotic nature of tape cast porous structures and infiltration. While the samples all had approximately equal porosity, the pore tortuosity could be very different. When the infiltration is then varied within 1 wt%, the nickel network could be very complex and unique sample to sample. In all samples, the trend was quite obvious between baseline samples and ALT doped samples.

Previous studies using SOFC systems as a catalytic activity metric always displayed increased performance initially as well as a decreased degradation rate [11]. The obvious difference between these results and those results was the catalytic activity. Catalysis and electrical conduction were occurring in full cell tests while these tests were purely of conductivity. The catalytic activity must also be affected by the anchors and in

such a way to offset for the loss in conductivity from the nonconductive oxide anchor compounds.

Conclusions

Work on anchoring fine nickel particulate networks has sparked interest in several institutions and for good reason. The results clearly display the formation of phases involving the catalyst and substrate and the decomposed portions of the anchoring additive, ALT. Migration was shown to indeed be a problem as evidenced in the FEM images. As particles coarsen, pockets are visible where the nickel particulate was but no longer occupied. The ALT deposited via aerosol and the bulk ALT had minor differences; both exhibited superiority over the baseline sample. This will allow future works to investigate infiltration of the anchor after a simple particle size reduction and suspension in ethanol. The detailed XRD plots demonstrated that the ALT was indeed breaking down and forming similar reactions as aluminum oxide and titanium oxide combined. The use of Al_2O_3 and TiO_2 separately required temperatures between 1190^{o}C and 1265^{o}C while ALT provided a tighter range centered at 1205^{o}C. After higher temperatures, the ALT compared well to the sample with the decomposed constituents simplifying future analysis, and justified previous studies where the half reactions were analyzed. Grant approval from EMSL can lead to future collaborations and show the formation of anchors on atomic scales. The TEM work previously done brings up the interesting possibility of selection of anchor model depending on the saturation level. Finally, infiltrated electrode ASR tests conclusively displayed the reduced degradation as

a result of ALT anchoring with improvements of 6 times less degradation from the best baseline sample to the worst ALT sample. The knowledge gained in this study provides the framework for which this methodology can be applied to other systems where mutually interacting phase formation can be predicted with thermodynamic modeling and validated with high temperature XRD studies.

Acknowledgments

A portion of the research was performed using EMSL, a national scientific user facility sponsored by the Department of Energy's Office of Biological and Environmental Research and located at Pacific Northwest National Laboratory.

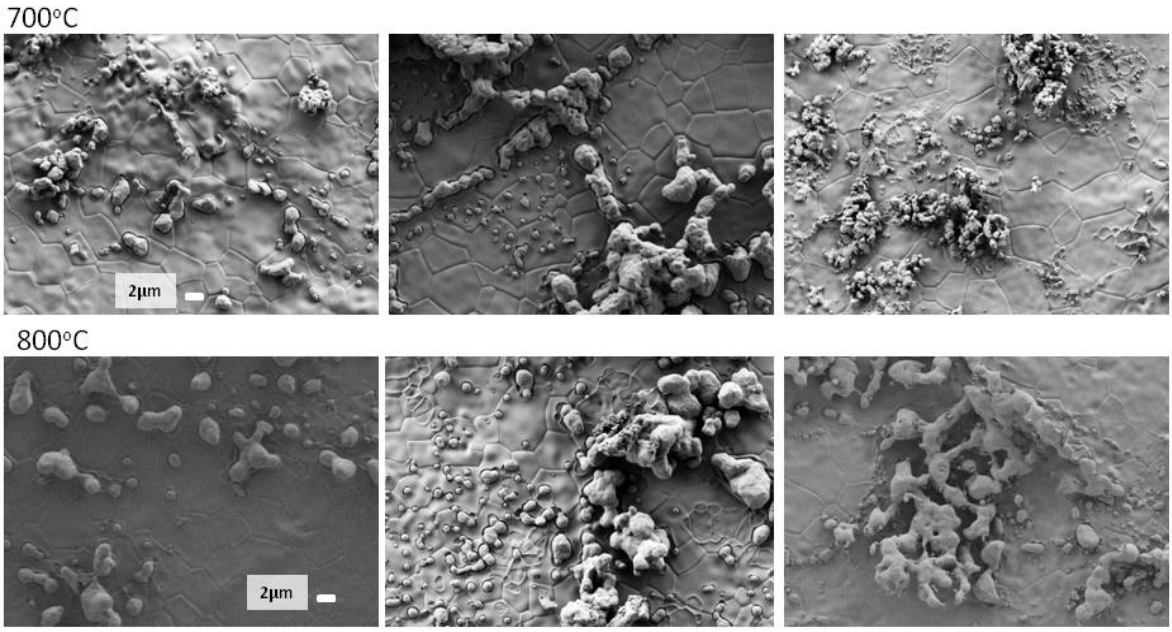

Figure 4.1: FE-SEM images of the nickel network after 100 hours at 700°C (top) and 800°C (bottom). The baseline (left), 10 wt% ALT mechanically mixed (center), and ALT applied via aerosol method (right) displaying a variety of anchoring effectiveness.

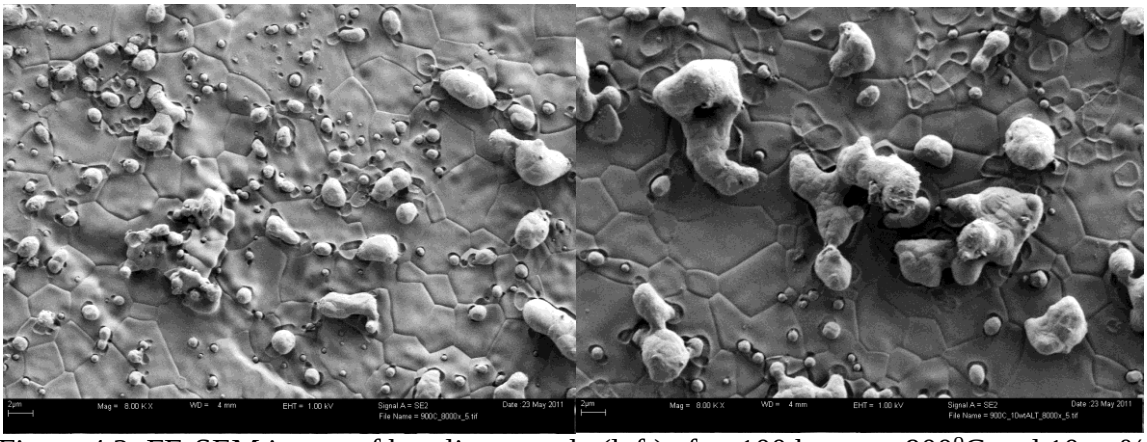

Figure 4.2: FE-SEM image of baseline sample (left) after 100 hours at 900°C and 10 wt% ALT (right). Pits in surface are indicative of nickel present earlier but have coarsened.

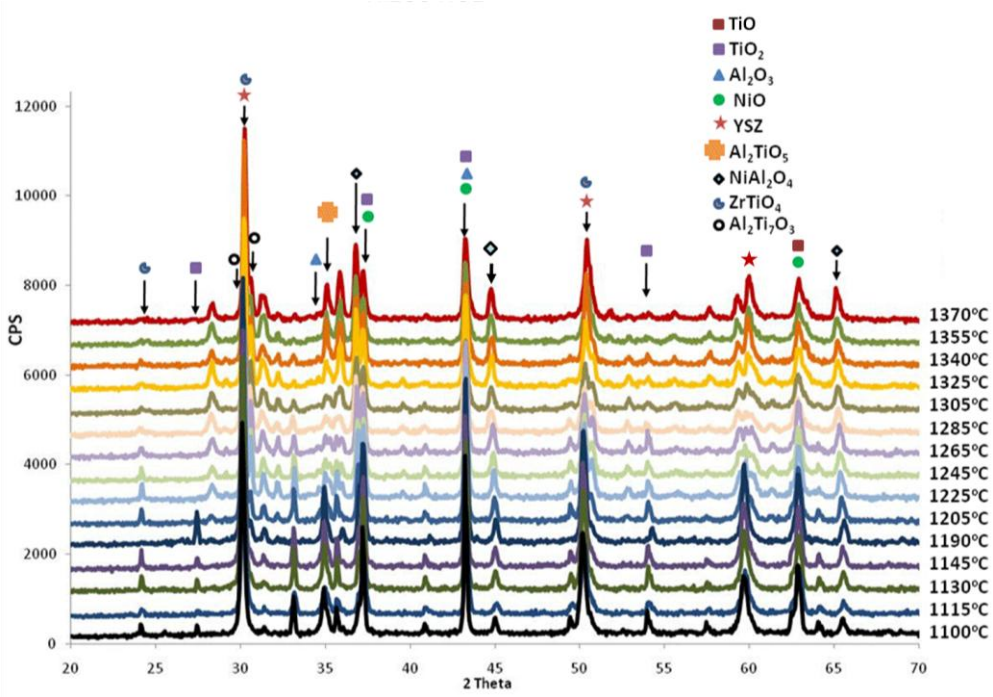

Figure 4.3: XRD Plot of NiO, YSZ, Al_2O_3, and TiO_2 at various temperatures with prominent peaks indexed.

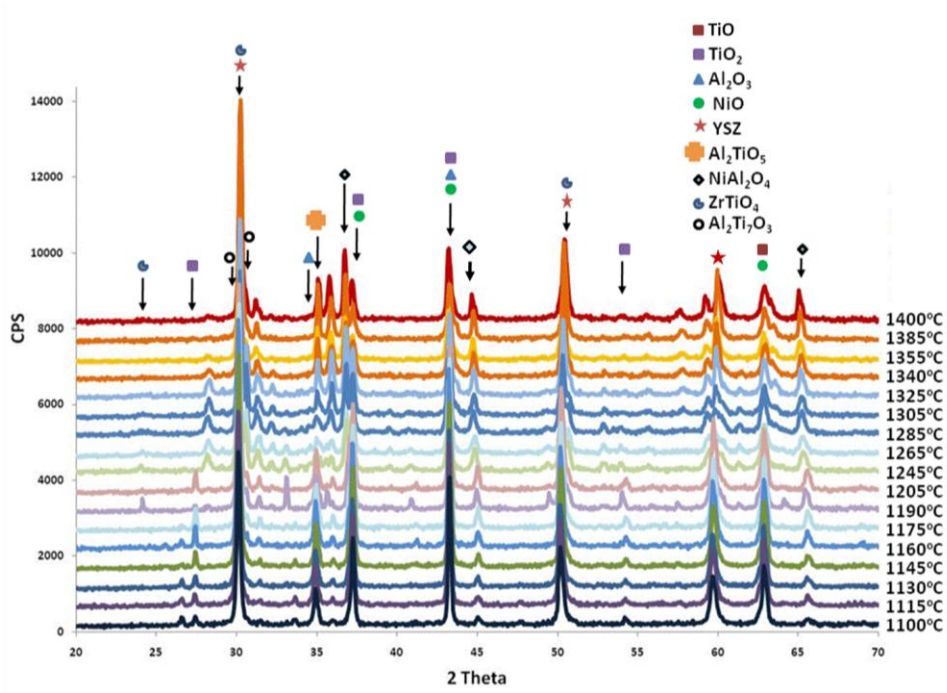

Figure 4.4: XRD Plot of NiO, YSZ, and ALT at various temperatures with prominent peaks labeled.

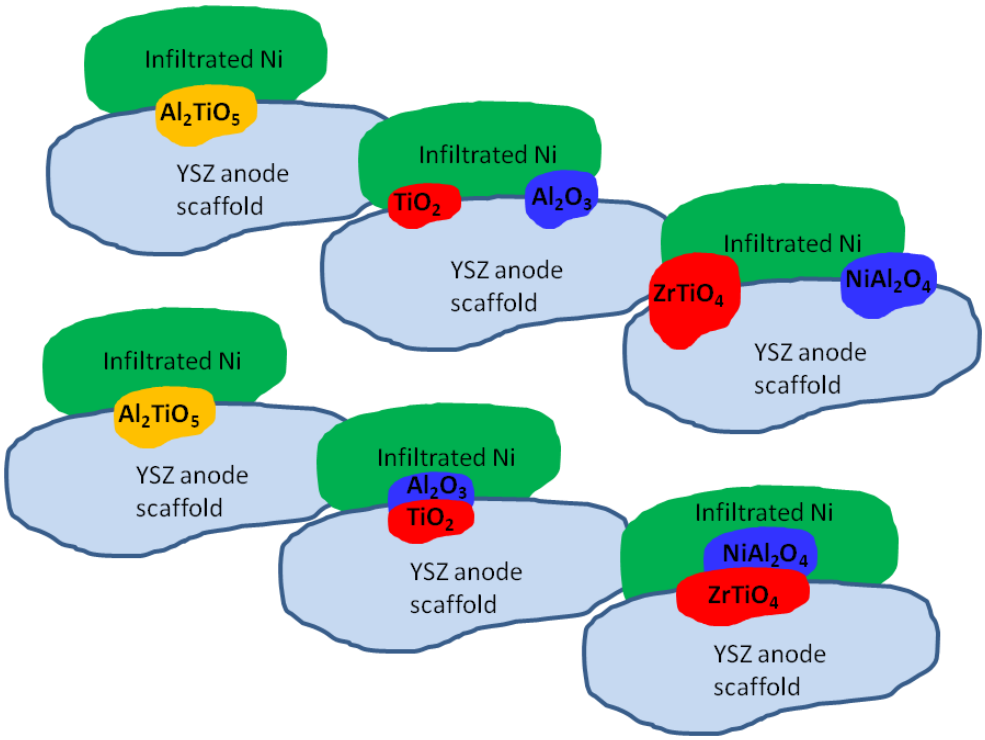

Figure 4.5: Possible methods of anchor formation

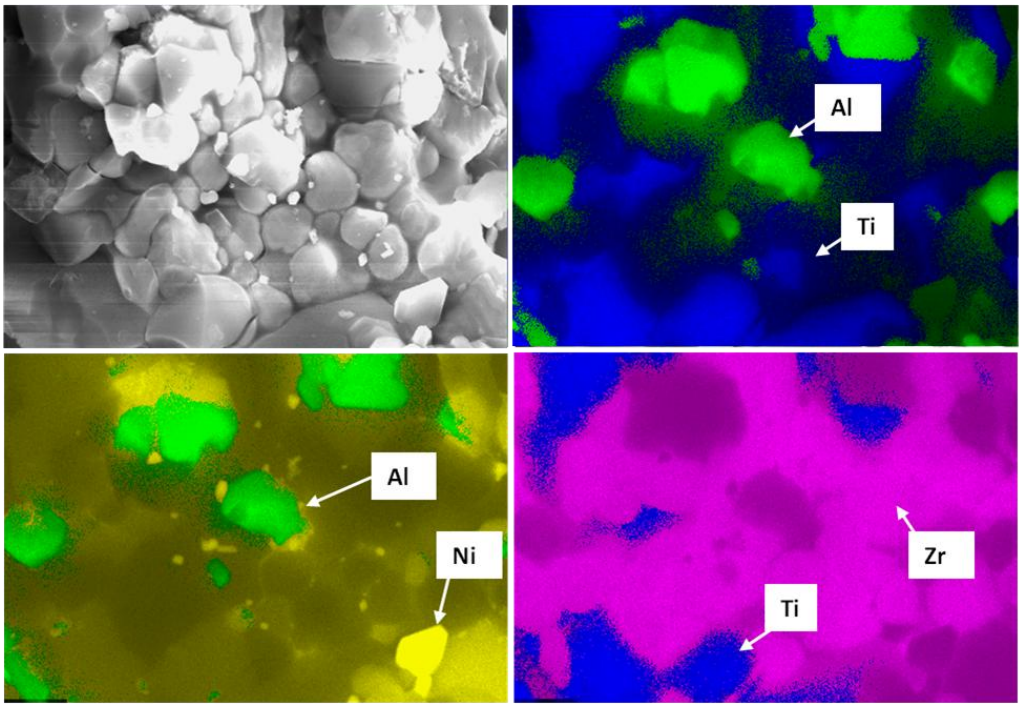

Figure 4.6: Energy Dispersive X-ray Spectroscopy of an infiltrated nickel anode on an ALT anchored YSZ scaffold with elemental mapping overlaid on an SEM micrograph.

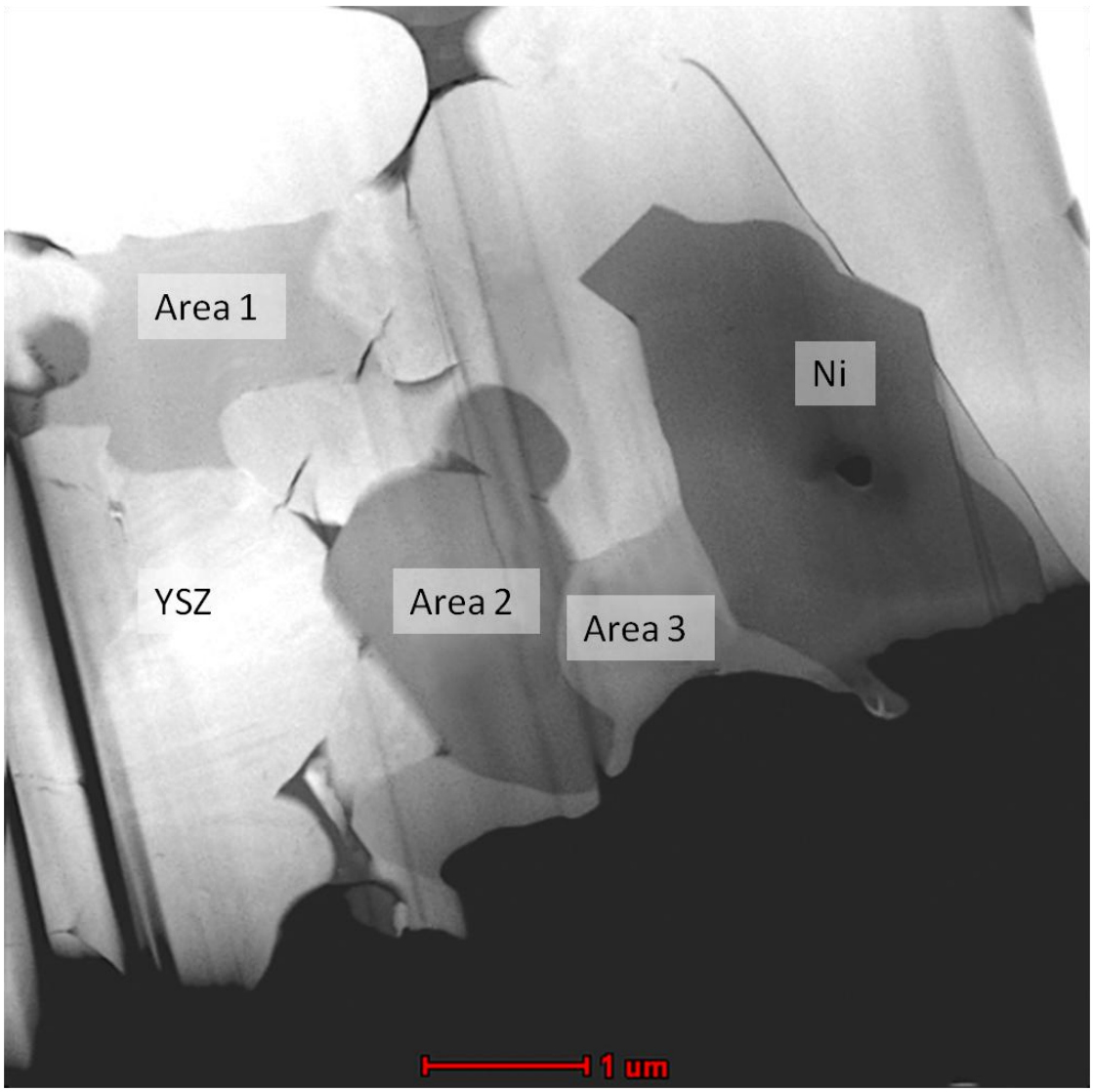

Figure 4.7: TEM image of prepared sample with anchors and several different phases between areas 1, 2, and 3.

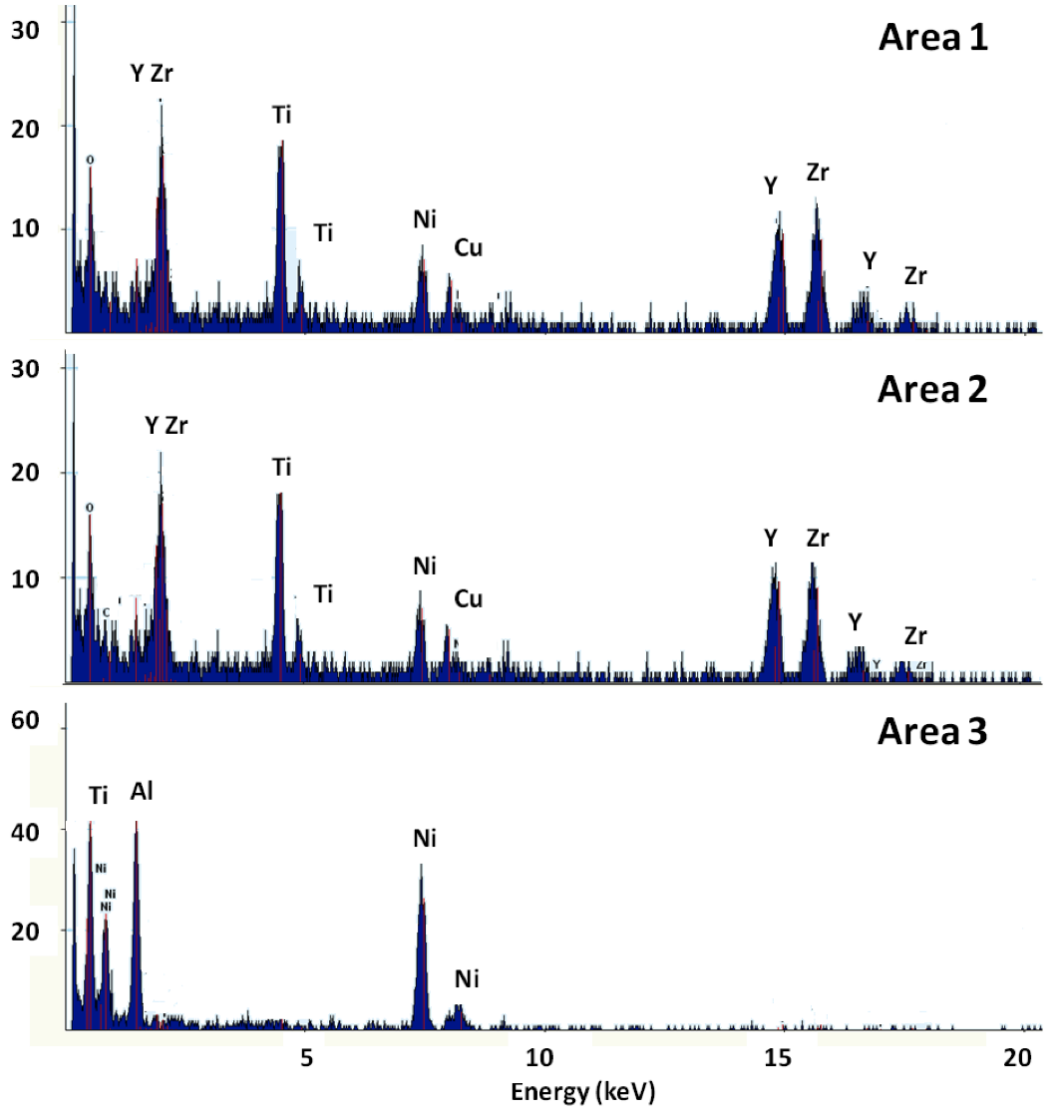

Figure 4.8: EDX spectra of areas depicted in Figure 4.8

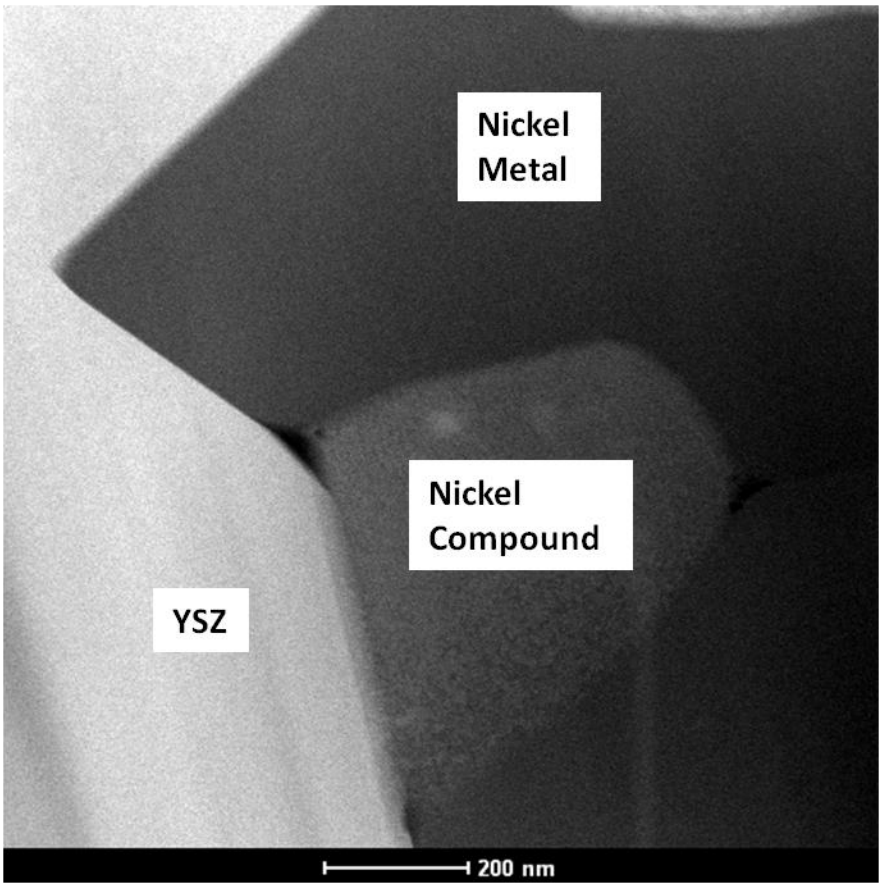

Figure 4.9: Boundary between nickel and YSZ

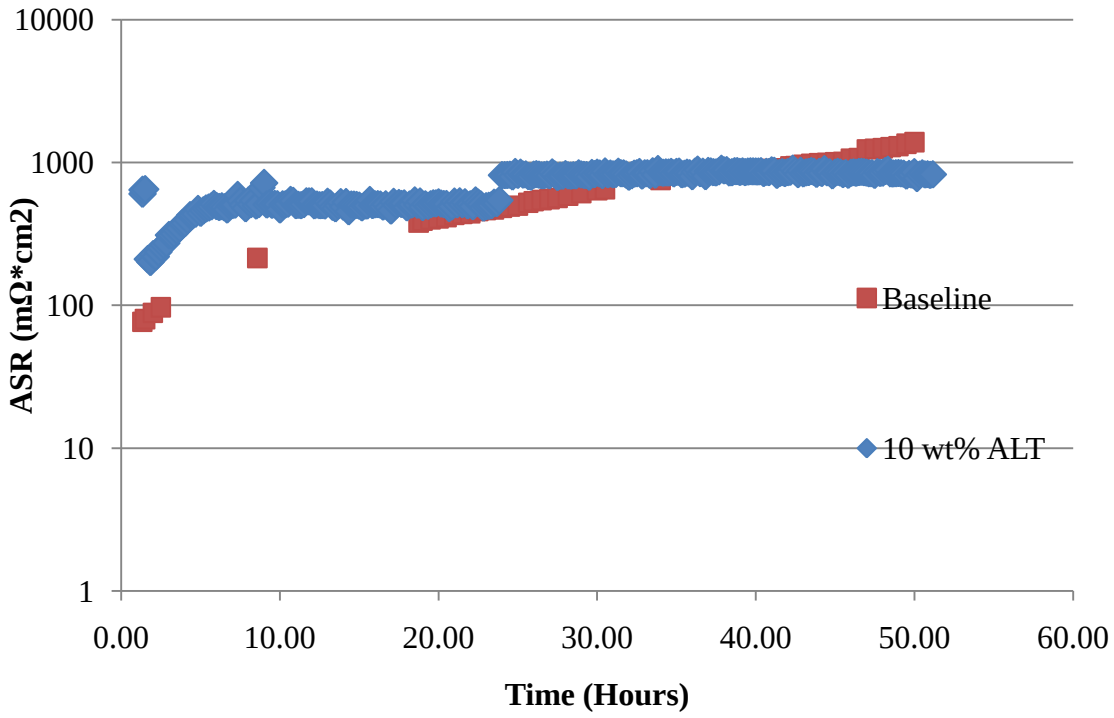

Figure 4.10: Plot of ASR (mΩ cm^2) as a function of time for baseline sample (red) and 10 wt% ALT doped sample (blue) at 800°C.

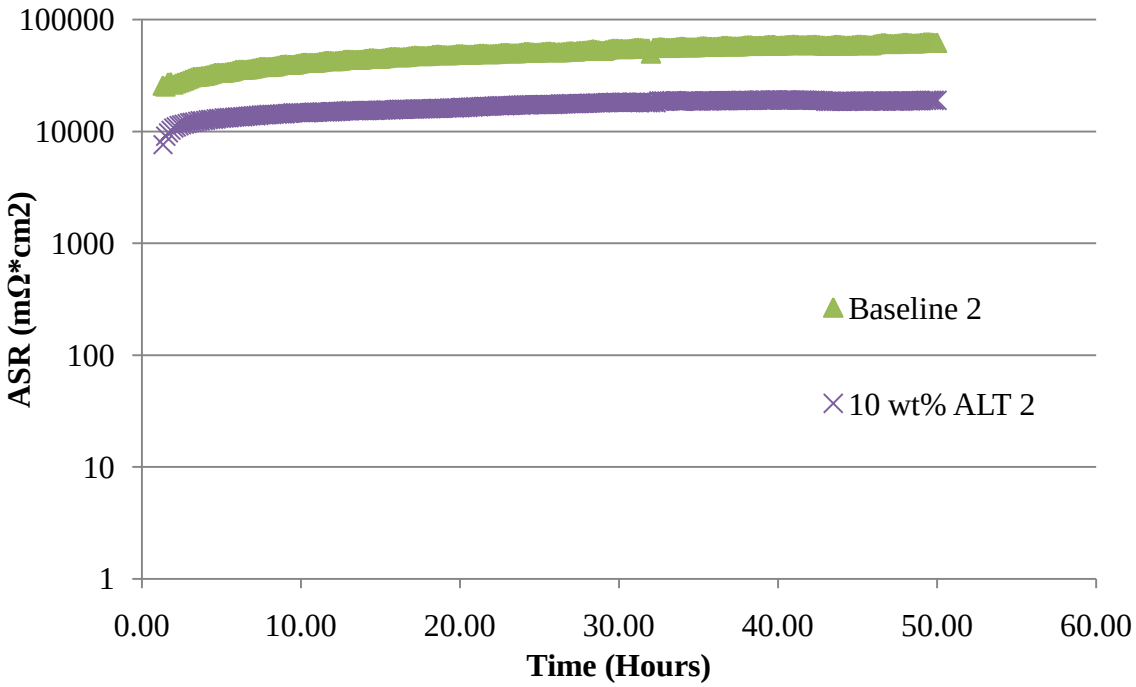

Figure 4.11: Redundant plot of ASR (mΩ cm^2) as a function of time for baseline sample (green) and 10 wt% ALT doped sample (purple) at 800°C.

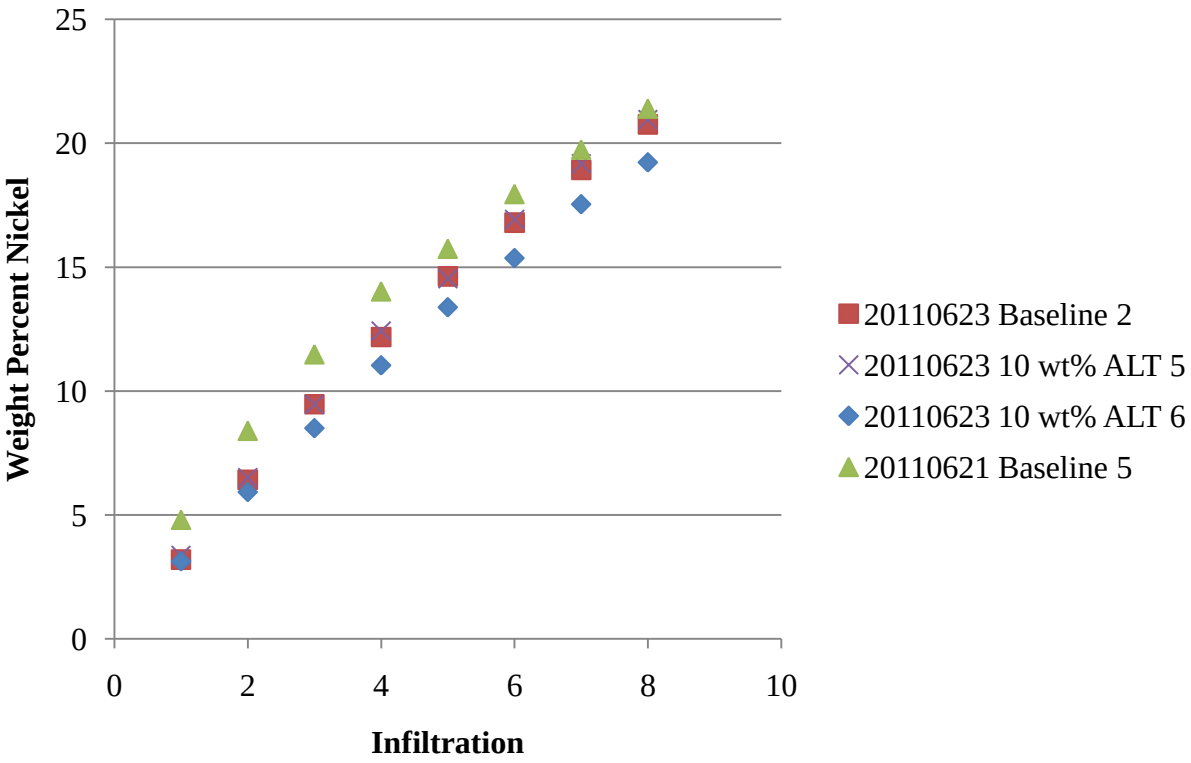

Figure 4.12: Weight percent of nickel as a function of infiltration iterations in baseline and doped samples.

References

1. *Processing and properties of the ceramic conductive multilayer device solid oxide fuel cell (SOFC).* Stover, D., Buchkremer, H.P. and Uhlenbruck, S. 2004, Ceramics International , Vol. 30, pp. 1107-1113.

2. *Fabrication and Electrochemical Performance of ANode-Supported Solid Oxide Fuel Cells by a Single-Step Cosintering Process.* Ding, J. and Liu, J. 10, 2008, J. Am. Ceram. Soc., Vol. 91, pp. 3303-3307.

3. *Development of yttria-stabilized zirconia thin films via slurry spin coating for intermediate-to-low temperature solid oxide fuel cells.* Chen, K., et al. 2006, Journal of Power Sources, Vol. 160, pp. 436-438.

4. *Nanostructured anodes for solid oxide fuel cells.* Gorte, R.J. and Vohs, J.M. 2009, Current Opinion in Colloid & Interface Science, Vol. 14, pp. 236-244.

5. *Influence of porous composite microsctructure on the processing and properties of solid oxide fuel cell anodes.* Clemmer, R.M.C. and Corbin, S.F. 2004, Solid State Ionics, Vol. 166, pp. 251-259.

6. *Mechanical properties of tape cast nickel-based anode materials for solid oxide fuel cells before and after reduction in hydrogen.* Radovic, M. and Lara-Curzio, E. 2004, Acta Materialia, Vol. 52, pp. 5747-5756.

7. *Processing Microstructure Property Correlation of Porous Ni-YSZ Cermets Anode for SOFC Application.* Pratihar, S.K., Dassharma, A. and Maiti, H.S. 2005, Materials Research Bulletin.

8. *Quantitative analysis of microstructure and its related electrical property of SOFC anode, Ni-YSZ cermet.* Lee, J.-H., et al. 2002, Solid State Ionics, Vol. 148, pp. 15-26.

9. *Ni Infiltration as a Possible Solution to the Redox Problem of SOFC Anodes.* Busawon, A.N., Sarantaridis, D. and Atkinson, A. 10, 2008, Electrochem. And Solid-State Lett., Vol. 11.

10. *A symmetrical, planar SOFC design for NASA's high specific power density requirements.* Cable, T.L. and Sofie, S.W. 2007, Journal of Power Sources, Vol. 174, pp. 221-227.

11. *Anchoring of Infiltratred Nickel Electro-Catalyst by Addition of Aluminum Titanate.* Law, C. H. and Sofie, S. W. 11, 2010, ECS Transactions, Vol. 28, pp. 217-226.

12. *Nickel coarsening in annealed Ni/8YSZ anode substrates for solid oxide fuel cells.* Simwonis, D, Tietz, F and Stover, D. 2000, Solid State Ionics, Vol. 132, pp. 241 -251.

13. *Performance and durability of Ni-coated YSZ anodes for intermediate temperature solid oxide fuel cells.* Kim, Sun-Dong, et al. 2006, Solid State Ionics, Vol. 177, pp. 931-938.

14. *Environmental risk of particulate and soluble platinum group elements released from gasoline and diesel engine catalytic converters.* Moldovan, M., et al. 2002, The Science of the Total Environment, Vol. 296, pp. 199-208.

15. *Coarsening Kinetics of Alloy Platinum-Palladium Particles on Oxide Substrates.* Clark, R.W., Wynblatt, P. and Tien, J.K. 1982, Acta Metallurgica, Vol. 30, pp. 139-146.

16. *Comparison of iron-, nickel-, copper- and manganese-based oxygen carriers for chemical-looping combustion.* Cho, P., Mattisson, T. and Lyngfelt, A. 2004, Fuel, Vol. 83, pp. 1215-1225.

17. *Hydrogen From Steam Reforming of Ethanol. Characterization and Performance of Copper-Nickel Supported Catalysts.* Marino, F.J., et al. 12, 1998, Int. J. Hydrogen Energy, Vol. 23, pp. 1095-1101.

18. *Correlation of Silver Migration with Temperature-Humidity-Bias (THB) Failures in Multilayer Ceramic Capacitors.* Ling, H.C. and Jackson, A.M. 1, 1989, IEEE Transactions on Components, Hybrids, and Manufacturing Technology, Vol. 12.

19. *Fabrication of Functionally Graded and Aligned Porosity in Thin Ceramic Substrates With the Novel Freeze-Tape-Casting Process.* Sofie, S. 7, 2007, J. Am. Ceram. Soc, Vol. 90, pp. 2024-2031.

21. *Controlled Thermal Expansion Anode Compositions with Improved Strength for Use in Anode Supported SOFCs.* Stephen W. Sofie, Davis R. Taylor. 4, 2009, Advances in Solid Oxide Fuel Cells III: Ceramic and Engineering Science Proceeding, Vol. 28.

22. *Low Temperature Sol-Gel Preparation of the B-Al2TiO5 Thin Films: Spectroscopic Analysis of the Precursors.* Licoccia, S., Di Vona, M.L. and Martucci, A. 2000, Journal of Sol-Gel Science and Technology, Vol. 19, pp. 577-580.

23. *Thermal Anisotropy of Tialite (Al2TiO5) By Powder XRD.* Zabicky, J., et al. 1995, NanoStructured Materials, Vol. 6, pp. 675-678.

23. *Phase Transformations in the Al2O3/TiO2 System and Metastable Phase Formation at Low Temperatures.* Camaratta, R., Acchar, W. and Bergmann, C.P. 2011, Rev. Adv. Mater. Sci, Vol. 27, pp. 64-68.

24. *Formation of Composite Structure in Alumosilicate Systems with the Introduction of Potassium Titanates.* Sanchez-Valdes, E., et al. 2010, Glass and Ceramics, Vol. 67, pp. 5-6.

25. *Al2TiO5 - New Contributions to its Preparation Via the Sol-Gel Technique.* Tudyka, S., et al. 4, 2010, 22nd Annual Conference on Composites, Advanced Ceramics, Materials, and Structures: B: Ceramic Engineering and Science Proceedings, Vol. 19.

26. *Synthesis, Densification, and Phase Evolution Studies of Al2O3-Al2TiO5-TiO2 Nanocomposites and Measurement of Their Electrical Properties.* Somani, V. and Kalita, S.J. 8, 2007, J. Am. Ceram. Soc., Vol. 90, pp. 2372-2378.

27. *Deposition and Evaluation of Protective PVD Coatings on Ferritic Stainless Steel SOFC Interconnects.* Gorokhovsky, V.I., et al. 10, 2006, Journal of The Electrochemical Society, Vol. 153, pp. A1886-A1893.

28. *Effect of Precious-Metal Dopants on SOFC Anodes for Direct Utilization of Hydrocarbons.* McIntosh, S and Vohs, J.M., Gorte, R.J. 11, 2003, Electrochemical and Solid State Letters, Vol. 6, pp. A240-A243.

29. *Kinetic parameters influencing the performance of IT-SOFC composite electrodes.* Steele, B.C.H., Hori, K.M. and Uchino, S. 1-4, 2000, Solid State Ionics, Vol. 135, pp. 445-450.

30. *Influence of composition and Cu impregnation method on the performance of Cu/CeO2/YSZ SOFC anodes.* Jung, Sukwon, et al. 1, 2006, Journal of Power Sources, Vol. 154, pp. 42-50.

CHAPTER FIVE

SUPPLEMENTAL DATA

ALT Grinding Effects on XRD Spectra

ALT was the prime chemical anchoring candidate for all of the previous studies. Through the use of XRD, several scans at different temperatures and various combinations of constituent powders illustrated an interesting story of sequential compound formations. One issue appeared from the stressful grinding to reduce particle size. ALT as received was too large to remain in suspension in ethanol or water. To avoid the addition of chelating agents or attempting to form the anchors in situ, the ALT was placed in an automated mortar and pestle for two hours to reduce the particle size. This process was successful in reducing the particle size to less than one sixth of the initial size as shown in Figure 5.1

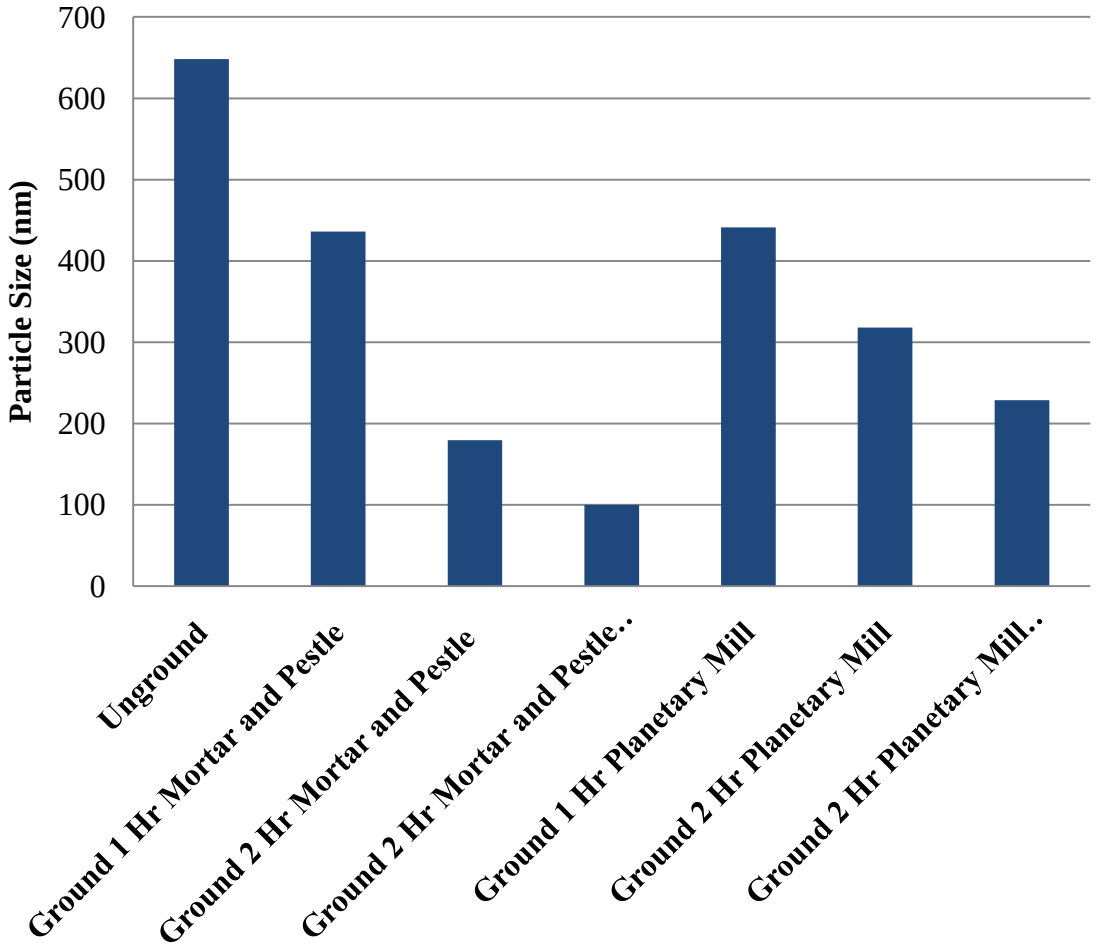

Figure 5.1: Plot of particle size for each method of processing. Ultrasonic indicates that powders were ultrasonically mixed prior to testing, which gives the most accurate results.

Figure 5.1 clearly indicated that grinding for 2 hours in the mortar and pestle gives the smallest particle size of approximately 100nm. It was qualitatively observed that the 100nm ALT stayed in suspension much better than the unground ALT or any other particle size reduction method. However, an interesting change in XRD data was found when the ground powder was compared to the as received powder. The spectra, Figure 5.2, illustrated several peaks which changed in relative intensity or in their

entirety. Some examples were the peaks at 18 and 25 which appeared or disappeared, respectively. The peak at 35 had a drastic change in relative intensity. While the majority of these peaks were defined as ALT, Al_2O_3, or TiO_2 in the previous XRD studies, several peaks remained unidentified. The mortar and pestle used was an agate (SiO_2) system, but no SiO_2 peaks were found, and the new peaks match no other expected compounds.

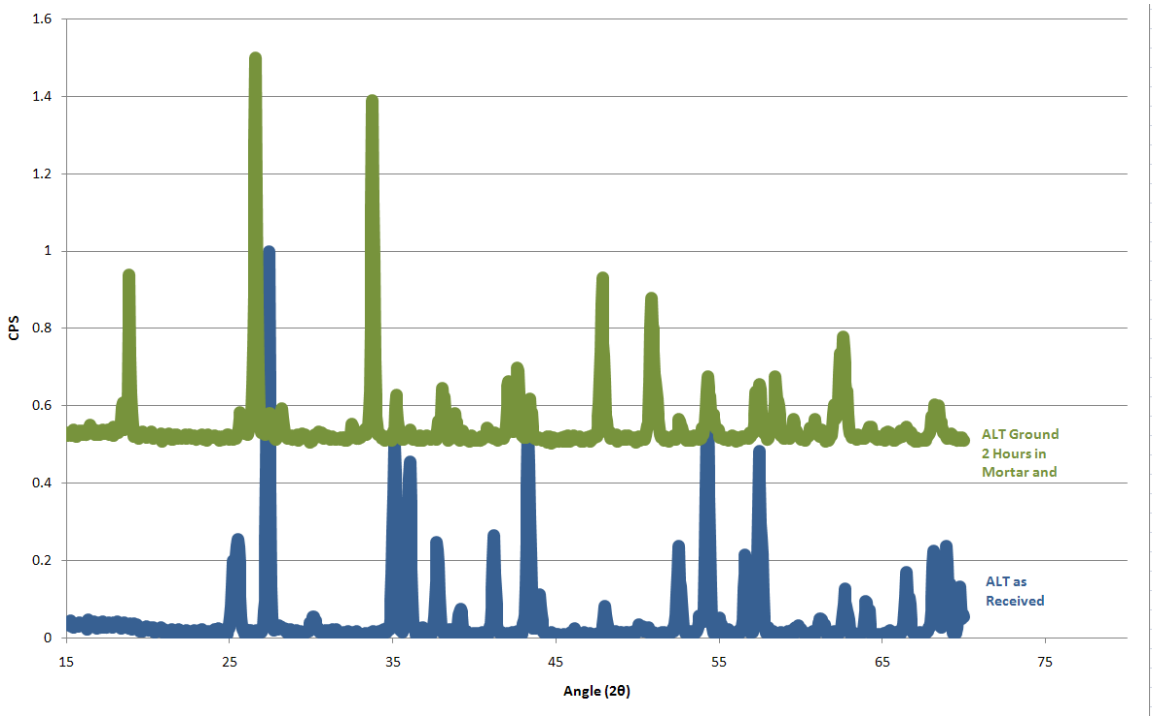

Figure 5.2: XRD scans of ALT as received (bottom) compared to ALT ground for 2 hours in a mortar and pestle (top).

This shift in XRD spectra attributed to milling has been reported elsewhere [42-43] and has been investigated in other material systems [44-45]. One publication implied mechanically induced self-propagating reactions can occur where constituents react to form compounds at much lower temperatures than are normally required [46]. The

possibility of other Al/Ti phases forming would open a plethora of XRD cards to investigate and is only offered as a possible explanation.

CHAPTER SIX

CONCLUSIONS

The chemical anchoring of nickel in regards specifically to SOFC anodes has been shown to occur and characterized by several means. The publication in Appendix A related sintering and general ceramic processing techniques to several dopants. The work in Appendix B displayed the incredible conducting capabilities of small nickel paths. This coupled with the introduction to nickel as a catalyst indicated that nickel was an ideal phase for SOFCs due to the catalytic activity and electron conduction. Nickel wire filaments can conduct incredibly high currents, relative to common cell performance, at SOFC operating temperatures. This current capacity increases as the filament diameter decreases possibly due to the increase in surface area to volume ratio. The filaments can then radiate the thermal energy away from the bulk and minimize the detrimental effects of joule heating. Clearly this mode of failure is not the primary cause of SOFC degradation, possibly indicating that coarsening plays a very significant role. Thus the motivation for the first three publications was justified.

Images in the first three manuscripts provided several FE-SEM micrographs that also indicated severe coarsening. These images ranged from lower magnification and indicating the overall segregation of the nickel network to higher magnification where the "footprint" of the initial nickel particle is clearly imaged with the coarsened particle imaged as well. The images were very interesting and useful to the SOFC community in communicating the effect coarsening has on nickel networks and anodes as a whole.

XRD data clearly identified that ALT can and will decompose into Al_2O_3 and TiO_2, which will then readily react with the nickel catalyst precursor and the YSZ substrate. These reactions occurred in a sequential order. The data also suggests that the reactions can occur at temperatures already relevant to SOFC anode processing techniques. While ALT was determined to work as an anchor with nickel and YSZ, modeling based on thermodynamic reaction calculations could be used to determine new possible anchors for other material systems with confirmation by thorough XRD studies.

HRTEM and elemental mapping provided incredible data which indicated that the initial predicted model could be correct, but also that over saturation of the ALT in the sample may lead to a different model that could be beneficial to other systems. EDX at the HRTEM nano-scale clearly indicated grains of nickel, YSZ, a YSZ and titanium rich area, and a nickel and aluminum rich area. This data in conjunction with the XRD data persuasively indicates that the ALT does decompose and form the expected compounds.

Conductivity tests with infiltrated electrode materials gave a clear definition to the positive effects of chemical anchoring. While all systems did show some overall degradation, the doped systems retained a lower rate of degradation throughout the last 10 hours. Baseline samples produced an overall increase in ASR of 625 to 6419%/1000 hr over the last 20 hours, while ALT samples exhibited 35 to 103.8%/1000 hr degradation in ASR over the last 20 hours.

Full cell testing also indicated several times that minor quantities of ALT dopant in the anode correlated to an initially higher performance and a reduced degradation. As with the conductivity tests, optimized systems could be fabricated and compared but

sufficient data was collected to show without a doubt that the chemical anchoring increased performance. Baseline samples produced a rate of degradation of 1621 to 19411%/1000 hr at the end of the testing, while ALT doped samples degraded no more than 835%/1000 hr at the end of testing.

The concept of chemical anchoring can be applied to many other systems. As another SOFC example, gadolinium doped ceria (GDC) may even be able to ALT again as a chemical anchor since nickel is a common catalyst and both gadolinium and ceria have been known to form various compounds with aluminum and/or titanium. Copper on YSZ is a system of interest because copper resists coking, but has shown serious coarsening issues. Recalling other systems from Chapter 1, platinum and silver anchoring could both be investigated due to the several systems which incorporate these metals. While these are only a few of the common catalysts in use today, all have shown coarsening to some extent and could be improved upon via chemical anchoring.

References

1. *Processing and properties of the ceramic conductive multilayer device solid oxide fuel cell (SOFC).* Stover, D., Buchkremer, H.P. and Uhlenbruck, S. 2004, Ceramics International , Vol. 30, pp. 1107-1113.

2. *Fabrication and Electrochemical Performance of ANode-Supported Solid Oxide Fuel Cells by a Single-Step Cosintering Process.* Ding, J. and Liu, J. 10, 2008, J. Am. Ceram. Soc., Vol. 91, pp. 3303-3307.

3. *Development of yttria-stabilized zirconia thin films via slurry spin coating for intermediate-to-low temperature solid oxide fuel cells.* Chen, K., et al. 2006, Journal of Power Sources, Vol. 160, pp.436-438.

4. *Nanostructured anodes for solid oxide fuel cells.* Gorte, R.J. and Vohs, J.M. 2009, Current Opinion in Colloid & Interface Science, Vol. 14, pp. 236-244.

5. *Influence of porous composite microsctructure on the processing and properties of solid oxide fuel cell anodes.* Clemmer, R.M.C. and Corbin, S.F. 2004, Solid State Ionics, Vol. 166, pp. 251-259.

6. *Mechanical properties of tape cast nickel-based anode materials for solid oxide fuel cells before and after reduction in hydrogen.* Radovic, M. and Lara-Curzio, E. 2004, Acta Materialia, Vol. 52, pp.5747-5756.

7. *Processing Microstructure Property Correlation of Porous Ni-YSZ Cermets Anode for SOFC Application.* Pratihar, S.K., Dassharma, A. and Maiti, H.S. 2005, Materials Research Bulletin.

8. *Quantitative analysis of microstructure and its related electrical property of SOFC anode, Ni-YSZ cermet.* Lee, J.-H., et al. 2002, Solid State Ionics, Vol. 148, pp. 15-26.

9. *Ni Infiltration as a Possible Solution to the Redox Problem of SOFC Anodes.* Busawon, A.N., Sarantaridis, D. and Atkinson, A. 10, 2008, Electrochem. and Solid-State Lett., Vol. 11.

10. *A symmetrical, planar SOFC design for NASA's high specific power density requirements.* Cable, T.L. and Sofie, S.W. 2007, Journal of Power Sources, Vol. 174, pp. 221-227.

11. *Anchoring of Infiltratred Nickel Electro-Catalyst by Addition of Aluminum Titanate.* Law, C. H. and Sofie, S. W. 11, 2010, ECS Transactions, Vol. 28, pp. 217-226.

12. *Nickel coarsening in annealed Ni/8YSZ anode substrates for solid oxide fuel cells.* Simwonis, D, Tietz, F and Stover, D. 2000, Solid State Ionics, Vol. 132, pp. 241-251.

13. *Performance and durability of Ni-coated YSZ anodes for intermediate temperature solid oxide fuel cells.* Kim, Sun-Dong, et al. 2006, Solid State Ionics, Vol. 177, pp. 931-938.

14. *Environmental risk of particulate and soluble platinum group elements released from gasoline and diesel engine catalytic converters.* Moldovan, M., et al. 2002, The Science of the Total Environment, Vol. 296, pp. 199-208.

15. *Coarsening Kinetics of Alloy Platinum-Palladium Particles on Oxide Substrates.* Clark, R.W., Wynblatt, P. and Tien, J.K. 1982, Acta Metallurgica, Vol. 30, pp. 139-146.

16. *Comparison of iron-, nickel-, copper- and manganese-based oxygen carriers for chemical-looping combustion.* Cho, P., Mattisson, T. and Lyngfelt, A. 2004, Fuel, Vol. 83, pp. 1215-1225.

17. *Hydrogen From Steam Reforming of Ethanol. Characterization and Performance of Copper-Nickel Supported Catalysts.* Marino, F.J., et al. 12, 1998, Int. J. Hydrogen Energy, Vol. 23, pp. 1095-1101.

18. *Correlation of Silver Migration with Temperature-Humidity-Bias (THB) Failures in Multilayer Ceramic Capacitors.* Ling, H.C. and Jackson, A.M. 1, 1989, IEEE Transactions on Components, Hybrids, and Manufacturing Technology, Vol. 12.

19. *Fabrication of Functionally Graded and Aligned Porosity in Thin Ceramic Substrates With the Novel Freeze-Tape-Casting Process.* Sofie, S. 7, 2007, J. Am. Ceram. Soc, Vol. 90, pp. 2024-2031.

20. *Controlled Thermal Expansion Anode Compositions with Improved Strength fo Use in Anode Supported SOFCs.* Stephen W. Sofie, Davis R. Taylor. 4, 2009, Advances in Solid Oxide Fuel Cells III: Ceramic and Engineering Science Proceeding, Vol. 28.

21. *Low Temperature Sol-Gel Preparation of the B-Al2TiO5 Thin Films: Spectroscopic Analysis of the Precursors.* Licoccia, S., Di Vona, M.L. and Martucci, A. 2000, Journal of Sol-Gel Science and Technology, Vol. 19, pp. 577-580.

22. *Thermal Anisotropy of Tialite (Al2TiO5) By Powder XRD.* Zabicky, J., et al. 1995, NanoStructured Materials, Vol. 6, pp. 675-678.

23. *Phase Transformations in the Al2O3/TiO2 System and Metastable Phase Formation at Low Temperatures.* Camaratta, R., Acchar, W. and Bergmann, C.P. 2011, Rev. Adv. Mater. Sci, Vol. 27, pp. 64-68.

24. *Formation of Composite Structure in Alumosilicate Systems with the Introduction of Potassium Titanates.* Sanchez-Valdes, E., et al. 2010, Glass and Ceramics, Vol. 67, pp. 5-6.

25. *Al2TiO5 - New Contributions to its Preparation Via the Sol-Gel Technique.* Tudyka, S., et al. 4, 2010, 22nd Annual Conference on Composites, Advanced Ceramics, Materials, and Structures: B: Ceramic Engineering and Science Proceedings, Vol. 19.

26. *Synthesis, Densification, and Phase Evolution Studies of Al2O3-Al2TiO5-TiO2 Nanocomposites and Measurement of Their Electrical Properties.* Somani, V. and Kalita, S.J. 8, 2007, J. Am. Ceram. Soc., Vol. 90, pp. 2372-2378.

27. *Deposition and Evaluation of Protective PVD Coatings on Ferritic Stainless Steel SOFC Interconnects.* Gorokhovsky, V.I., et al. 10, 2006, Journal of The Electrochemical Society, Vol. 153, pp. A1886-A1893.

28. *Effect of Precious-Metal Dopants on SOFC Anodes for Direct Utilization of Hydrocarbons.* McIntosh, S and Vohs, J.M., Gorte, R.J. 11, 2003, Electrochemical and Solid State Letters, Vol. 6, pp. A240- A243.

29. *Kinetic parameters influencing the performance of IT-SOFC composite electrodes.* Steele, B.C.H., Hori, K.M. and Uchino, S. 1-4, 2000, Solid State Ionics, Vol. 135, pp. 445-450.

30. *Influence of composition and Cu impregnation method on the performance of Cu/CeO2/YSZ SOFC anodes.* Jung, Sukwon, et al. 1, 2006, Journal of Power Sources, Vol. 154, pp. 42-50.

31. *Sub-micron sized Al2TiO5 powders prepared by high-energy ball milling.* Uribe, R., et al. 2001, Journal of Materials Science, Vol. 36, pp. 5105-5113.

32. *In Situ Synthesis of Rod-like Tielite/Alumina Ceramic Composites via Mechanical Activation.* Chen, Xiaohu, et al. 2007, Key Engineering Materials, Vol. 352, pp. 111-114.

33. *Change in the Structure of Niobium Pentoxide Due to Mechanical and Thermal Treatments.* Ikeya, T. and Senna, M. 1988, Journal of Non-Crystalline Solids, Vol. 105, pp. 243-250.

34. *Phase transformation of cobalt induced by ball milling.* Huang, J.Y., Wu, Y.K. and Ye, H.Q. 3, 1995, Applied Physics Letters, Vol. 66, pp. 308-310.

35. *Self-sustaining reactions induced by ball milling.* Takacs, L. 2002, Progress in Materials Science , Vol. 47, pp. 355-414.

APPENDICES

APPENDIX A

SINTERING PERFORMANCE OF YSZ CERAMICS WITH TRANSITIONMETAL OXIDE SINTERING AID

Contribution of Authors and Co-Authors

Manuscript in Appendix A

Author: Stephen Sofie

Contributions: Developed the concept and primarily wrote the manuscript.

Co-Author: Zane Townsend

Contributions:

Co-Author: Max Lifson

Contributions:

Co-Author: Cameron Law

Contributions: Assisted with the sample preparation, testing, and analysis.

Manuscript Information Page

S. Sofie, Z. Townsend, M. Lifson, C. Law
Journal Name: TMS Supplemental Proceedings
Status of Manuscript:
_____Prepared for submission to a peer-reviewed journal
_____Officially submitted to a peer-reviewed journal
_____Accepted by a peer-reviewed journal
_____Published in a peer-reviewed journal
X_____Published in a conference proceedings

Publisher:
Issue in which manuscript appears: Supplemental Proceedings: Volume 2: Materials Characterization, Computation, Modeling, and Energy (2010)

Abstract

Transition metal oxides were found to dramatically alter the sintering behavior of micron sized yttria stabilized zirconia at concentrations of 1 mol%. Cobalt, nickel, and chromium oxide yielded enhancement in sintering performance, while copper oxide yielded a detriment to the sintering process. The effects of nickel oxide were examined with the primary goal to reduce the sintering temperature of solid oxide fuel cell electrolyte fabrication. The effects of nickel oxide were evaluated in both partially (3Y) and fully (8Y) stabilized zirconia with 0 to 1 mol% nickel addition, as NiO, and characterized from 1300°C to 1400°C with a 1 hr dwell. Utilizing low temperature 1300°C sintering, 8YSZ powder doped with nickel oxide yielded a density of 95% theoretical, whereas the 3YSZ was more sensitive to the dopant yielding 97% density with the nickel oxide additions. Grain growth for the doped specimens is increased and an early transition to transgranular fracture is noted for the doped specimens. The total ionic conductivity of the doped specimens remained constant, however, the grain boundary contribution showed an improvement from the dopant. Further, ring on ring flexural testing of tape cast electrolytes indicates up to 46% increase in flexural strength from the dopant addition.

Introduction

Oxygen ion conducting yttria stabilized zirconia remains heavily studied in solid oxide fuel cell (SOFC) development given the stable ionic conduction and thermal stability in dual atmospheres. A key detriment to the development of better catalytic and conductive electrodes hinges on the chemical reactivity of materials with YSZ at elevated sintering temperatures which typically requires in excess of 1400°C for several hours to close off open porosity. This also limits the implementation of co-sintering processes in which chemical interaction with lanthanum based cathode materials form insulating pyrochlore phases at the interface above 1300°C [1-3]. Traditional YSZ powders employed in electrolyte fabrication are sub-micron sized with particle sizes ranging from 0.3 to 0.6 microns to achieve good dispersion and suspension characteristics. While nano-particulate can reduce sintering temperatures, the ability to use nano-particles in traditional slurry fabrication processes is difficult and often inconsistent. Lower sintering temperature also has the benefit of generating finer grain structures that can yield improved strength and toughness with negligible change in ionic conduction.

Several approaches have been employed in the past to improve the sintering behavior of YSZ materials. Aluminum oxide (Al_2O_3) powder is commonly added to YSZ to improve the sintering behavior as well as the grain boundary ionic conduction [4-5]. The addition of aluminum oxide as a secondary phase yields chemical reactivity with lanthanum manganate (LSM) cathodes and Ni/YSZ anodes in form of insulating $(Mn,Al)_3O_4$ spinel and nickel aluminate ($NiAl_2O_4$) yielding substantial performance degradation [5-6]. Bismuth oxide has a clear benefit as a sintering aid due to the formation of a liquid phase

at the grain boundaries. It was observed that less than 3 mol% Bi_2O_3 yielded densification of YSZ below 1100°C, however, the reactivity of bismuth phases presents a substantial detriment to fuel cell stability [7-8]. Copper oxide (CuO) has also been studied as a dopant for lowering the sintering temperature of YSZ again through the formation of liquid phases [9]. The accumulation of copper; hence secondary phases at the grain boundary does however degrade the ionic conductivity and even small quantities of CuO greater than 1 mol% are shown to inhibit the densification process [10]. More recently several studies have shown that cobalt has benefits over aluminum oxide, bismuth oxide, and copper oxide in that it has been successfully utilized in anodes as cobalt metal catalysts, in addition to improving cathode performance as cobalt oxides. Cobalt oxide (Co_3O_4) has shown excellent performance as a sintering aid at approx. 1-3mol% [11], and further the ionic conductivity of cobalt doped YSZ has been shown to improve from the dopant addition, particularly the grain boundary contribution [12]. Nickel oxide has not been studied as an intentional dopant for lowering the sintering temperature of YSZ, however, given the extensive use of Ni/YSZ anode materials the effects of nickel as a diffusional impurity into the electrolyte has been evaluated. Nickel oxide (NiO) has an approximate 1-2mol% solubility in YSZ, which presents itself as an ideal dopant in that low quantity dopants have the potential to yield uniform distributions of nickel through the electrolyte without excessive accumulation at the grain boundary [13-14]. The effects of dissolved NiO in YSZ have been analyzed to show that the ionic conductivity of nickel-containing YSZ can degrade rapidly when dissolved nickel oxide can precipitate as metallic nickel in the grain boundaries [13]. However, the extent at

which this precipitation process can occur in a fuel cell with an active oxygen flux through the electrolyte has not been ascertained.

The purpose of this study is to identify the extent of sintering enhancement achieved with low levels of nickel oxide dopant in contrast to other transition metal oxides. This study focuses on densification behavior of nickel oxide doped partially and fully stabilized zirconium oxide micron sized powder compacts based on the broad availability of nickel oxide to the SOFC manufacturer as well as the proven compatibility and stability of NiO/YSZ during high temperature sintering processes. The densification, grain growth characteristics, microstructure, ionic conductivity, and mechanical properties of nickel oxide doped YSZ will be explored.

Procedure

Preliminary sintering studies were performed with 8 mol% YSZ (Tosoh TZ-8YS) utilizing nickel oxide (NiO - Alfa Aesar), chromium oxide (Cr_2O_3 - Alfa Aesar), cobalt oxide (Co_3O_4 - Alfa Aesar), and copper oxide (CuO - Alfa Aesar). The effects of nickel oxide on sintering were further evaluated at 0.1, 0.5, and 1mol% nickel oxide (NiO - Alfa Aesar), utilizing both 8 mol% and 3 mol% YSZ (Tosoh TZ-8YS and TZ-3YS). The oxide dopants were mechanically homogenized in water with the addition of ammonium polymethacylate dispersant (Darvan C-N, R.T. Vanderbilt) by centrifugal mixing (ARE-250, Thinky Corporation) for 5 minutes at 1000 rpm. To preserve the slurry homogeneity during the drying process the powders were flash frozen utilizing liquid nitrogen. The frozen mixture was then placed into a countertop freeze dryer (Advantage EL, Virtis Co.)

and water was sublimed under a 10mbar vacuum at 40°C, leaving a free flowing fine powder. The powders were then pressed uni-axially into a 1.27 cm stainless steel cylindrical die at a pressure of 27.5MPa. Pellets were sintered at 1300°C and 1400°C with a 1 hour dwell at a 5°C/min ramp rate up and 10°C/min ramp rate down. The density of the pellets were measured geometrically based on a density of 5.9 g/cc for 8YSZ and 6.05 g/cc for 3YSZ.

Scanning electron microscopy (Jeol 8500) was utilized on fracture surfaces of sintered pellets to determine grain size and fracture mode. Average grain size was calculated using the linear intercept method.

Impedance spectroscopy (5897 Impedance Analyzer, Solartron Analytical) was utilized to determine the ionic conductivity of the doped specimens. Samples utilized for the density study, ~1cm after sintering, were prepared with silver leads and silver contact paste and run under ambient atmosphere. The samples were heated to 850°C and cooled in steps of 50°C for frequency sweeps from 1 Hz to 10 MHz.

To characterize the mechanical performance of nickel doped YSZ electrolyte substrates, tape casting was utilized with an ethanol/xylene solvent, menhaden fish oil dispersant, polyvinyl butyral binder, and poly alkylene glycol plasticizer. The tape casting process yielded sintered substrates approximately 120 microns in thickness. Identical 3YSZ and 8YSZ (Tosoh TZ-3YS and TZ-8YS) tapes were prepared with and without dopant for ring on ring flexural testing and cut into 5.5cm circular specimens and sintered at respective temperatures on alumina setter plates. An aluminum concentric ring-on-ring test fixture was fabricated in compliance with ASTM standard C 1499-05 to apply a

distributed monotonic uni-axial load on ceramic membranes at ambient temperature. Ring-on-ring testing was employed to limit the edge effects of the samples where the stress is the weakest. Tape cast specimens were sintered for 2 hours to mimic fuel cell fabrication processes with slurry cast electrolytes.

Results & Discussion

Comparison of Transition Metal Oxides

Based on the literature findings several transition metal oxides appear to have some benefit towards the enhanced sintering of YSZ at reduced temperature. However, there has been no direct comparison between the effectiveness of these additives using a common precursor, host YSZ powder lot, and mixing procedure.

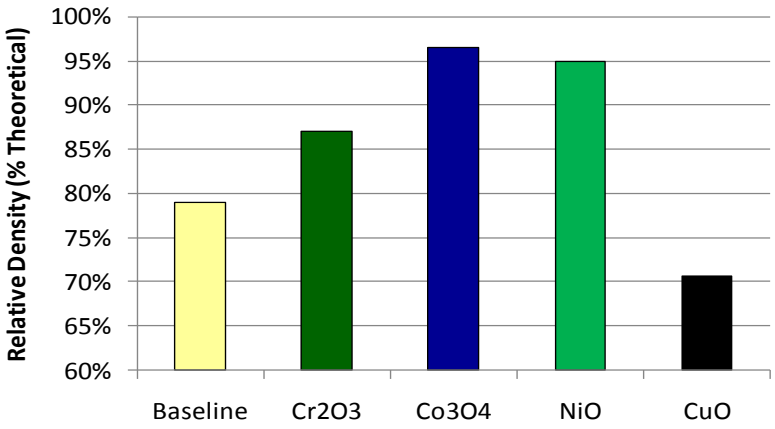

Figure A.1: Relative density of uni-axially pressed 8YSZ specimens doped with 1 mol% transition metal sintered at 1300°C for 1 hr (based on a density of 5.9 g/cc for 8YSZ).

The sintering behavior of 8YSZ powder with 1mol% TM (TM – 1mol% Cr, 1mol% Co, 1 mol% Ni, 1 mol% Cu) based on metal content to ensure an accurate

comparison with nickel is shown in Figure A.1. It is clear that both nickel and cobalt oxides yield the best sintering enhancement, however, the trend (transition metal oxides in Figure A.1 are arranged such that the metals are in order from left to right on the periodic table) shows a dramatic decrease in performance around Ni and Co. The nature of this trend is not trivial such as decreasing atomic radii, given that not all the dopants represent a solid solution and therefore secondary phase formation also plays a role in the densification process. The liquid secondary phase formation in the CuO-YSZ system at 1 mol% inhibited densification even though liquid phases at the grain boundaries typically improve densification [10]. While cobalt yields slightly better densification, it was noted that the use of cobalt results in extensive staining and contamination of the both the setter plate and furnace walls yielding an electrolyte with a strong blue color. Chromium also yielded substantial contamination of the setter plates. On the other hand, the nickel dopant yielded no color change of the YSZ as well as no visible contamination of the alumina setter plate, which was expected given the favorable formation of $NiAl_2O_4$. The NiO appears to be well locked up in solid solution, which is consistent with the reported 1-2 mol% NiO solubility in YSZ [14]. XRD analysis showed no evidence of secondary phase presence and SEM/EDS mapping showed a uniform distribution of Ni throughout the YSZ with no evidence of increased concentration at the grain boundaries.

Sintering Performance & Conductivity with NiO

To further establish the effect of the nickel dopant, NiO was added to both 3YSZ and 8YSZ powders at 0.1, 0.5, and 1.0 mol% Ni to ascertain an optimum dopant quantity. The relative density of sintered pellets is shown in Table A.1.

Table A.1: Density of 3YSZ and 8YSZ uni-axially pressed pellets with nickel oxide dopant at 1300°C and 1400°C.

Relative Density - 1300°C 1 hr

Mol% Nickel	0	0.1	0.5	1
8YSZ	79%	84%	95%	95%
3YSZ	68%	81%	93%	97%

Relative Density - 1400°C 1 hr

Mol% Nickel	0	0.1	0.5	1
8YSZ	98%	98%	98%	98%
3YSZ	87%	94%	97%	97%

While 1400°C is a relatively standard sintering temperature, a key goal of this study is to develop a process for sintering YSZ at 1300°C or less to mitigate cathode interaction issues. The first clear trend that can be seen from the 1300°C data is that the density plateaus between 0.5 and 1 mol% Ni, yielding a potential optimum concentration. Furthermore, the 3YSZ is more sensitive to the nickel dopant than the 8YSZ climbing from a highly open porous structure at 68% density to a dense closed pore bulk structure at 97% density. At 1400°C the dopant is not beneficial from a sintering standpoint for

the 8YSZ specimen, yielding constant density for the range of dopant concentrations. The 3YSZ at 1400°C shows a nominal improvement in density and further indicates an optimum close to 0.5mol% Ni dopant.

To further understand how nickel oxide may be influencing the sintering process the grain sizes of the sintered specimens were determined utilizing 1 mol% Ni to maximize the sintering enhancement. The grain sizes were determined by the linear intercept method applied to SEM micrographs.

Table A.2: Average grain size calculations for YSZ uni-axially pressed pellets doped with 1 mol% Ni.

Average Grain Size - 1300°C 1 hr

Mol% Nickel	0	1
8YSZ	0.282 μm	1.040 μm
3YSZ	0.161 μm	0.249 μm

Average Grain Size - 1400°C 1 hr

Mol% Nickel	0	1
8YSZ	0.714 μm	2.477 μm
3YSZ	0.208 μm	0.289 μm

The grain sizes of uni-axially pressed specimens in Table A.2 indicate both thermal and dopant contributions to grain growth, with the dopant contribution

substantially larger than the temperature dependency. The grain growth behavior of the baseline and doped specimens is based on a starting particulate/aggregate size of ~300nm as reported from Tosoh, however, the individual crystallite size is much smaller for which grain growth is built upon. The temperature induced grain growth effect is more prevalent in 8YSZ, however based on the densification data in Table A.1, more rapid growth of 8YSZ grains is expected. The dopant effect on grain size is more remarkable for both 8YSZ and 3YSZ at 1400°C yielding excessive growth for achieving high strength fine polycrystalline YSZ. Lower temperatures, below that of 1300°C for increased time durations may provide a means of retaining smaller grains while still achieving full densification.

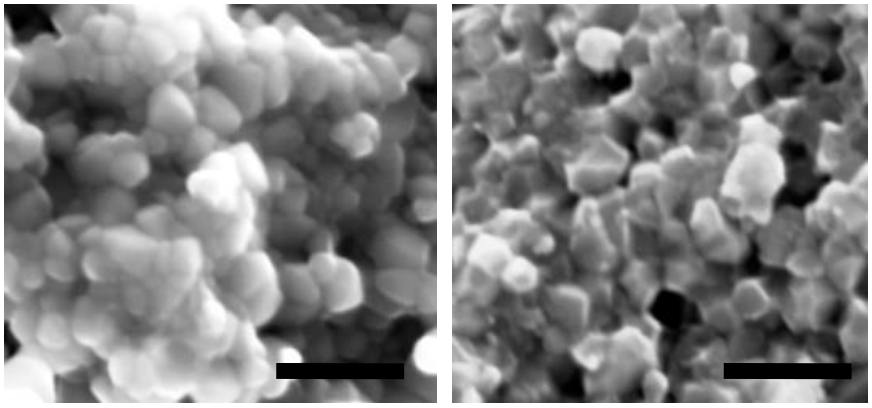

Figure A.2 SEM micrograph of fracture surfaces for uni-axially pressed 3YSZ baseline (left) and with 1mol% Ni dopant (right) specimens sintered at 1400°C for 1 hour. (bar = 1 micron)

Examination of the micrographs of the doped and undoped pellets showed some discrete differences in fracture mode. Figure A.2 shows the fracture surfaces of doped and undoped 3YSZ sintered at 1400°C, a sufficiently high temperature to promote bulk diffusion in 3YSZ. The undoped sample showed a predominantly inter-granular mode of

fracture while the nickel doped specimen showed mixed mode with more evidence of trans-granular fracture. The nickel dopant appears to improve cohesion of the grain boundary thus promoting an early transition to trans-granular fracture.

Impedance spectroscopy for 1 mol% Ni doped and undoped 8YSZ specimens sintered at 1300°C for 1 hour indicated that the grain boundary contribution of the doped specimen showed an improvement in ionic conductivity. This is also indicated in the cobalt doped system [12]. However, the total conductivity of nickel doped specimens showed a negligible change from the dopant addition. EDS mapping showed no excess nickel concentrations near the grain boundaries as initially suspected, however, nickel substitution in the zirconia lattice may promote enhanced oxygen ion conductivity given the improved cohesion, hence uniformity of the grain boundary due to the dopant. This may alter the intrinsic space charge layer behavior of the grain boundary similar to silicon impurity without the deleterious effects [15]. Additional impedance studies are needed to fully understand this phenomenon. However, the ability to enhance grain boundary conductivity with nickel oxide dopant gives rise to mechanisms of improving total conductivity by increasing the contribution of the grain boundary through very small grains.

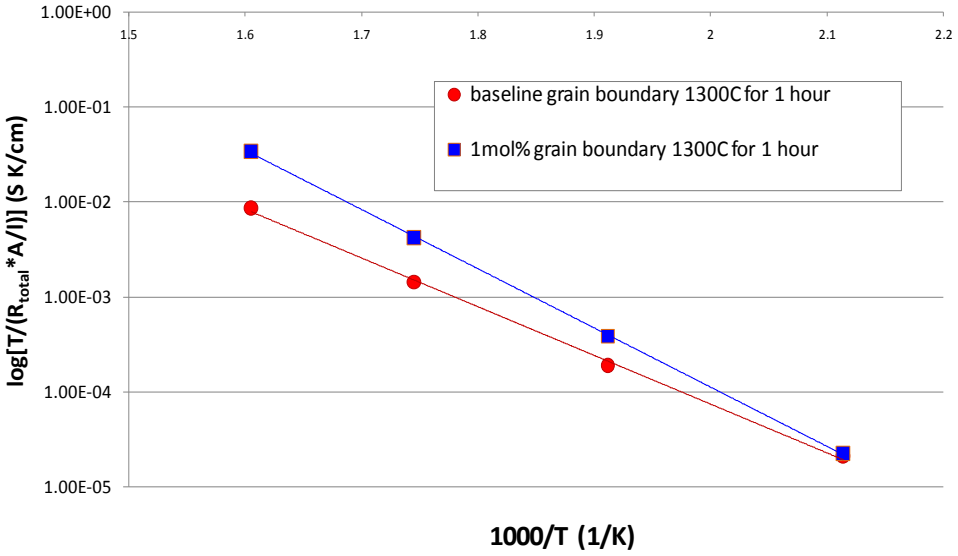

Figure A.3: Improved grain boundary conduction contribution in uni-axially pressed 1 mol% Ni doped 8YSZ at 1300°C sintering for 1 hour.

Mechanical Behavior of Tape Cast Electrolytes

Fracture behavior and grain size data suggest that improved cohesion at the grain boundary yields a mechanism to increase the strength of YSZ materials. While the nickel oxide dopant was added for the purpose of improving densification, the strength of the YSZ is also important given the multi-functionality required of YSZ in fuel cell applications. Ring on ring flexural testing was performed on tape cast YSZ electrolytes to evaluate the strength characteristics of the doped electrolyte substrates. The flexural strength data is given in Figure 4 which showed in all cases that the nickel dopant yields a significant benefit to mechanical performance with up to 46% increase. Each data point represents an average of 16 individual specimens spread over the surface of the tape to mitigate any homogeneity issues that may be present in the slurry casting and drying process. It is well understood that partially stabilized zirconia (3YSZ) is substantially stronger than 8YSZ due to the transformation toughening effect of the tetragonal to

monoclinic phase transformation. Partially stabilized zirconia is however expected to achieve nearly 1000-1200MPa when fully dense indicating small pores are still present in the tape cast specimens. Given that the tape cast specimens may not yield the same densities as the uni-axially pressed pellets, some component of the strength increase observed may be due to increased densification of the tapes with the nickel dopant. The transgranular fracture mode behavior of the nickel oxide doped specimens however supports the strengthening of the doped YSZ regardless of residual porosity, as well as the previously noted increase in fracture toughness [16]. The 1300°C results do indicate that lower temperature sintering with nickel oxide dopant can yield mechanical properties on par or better than YSZ without dopant at 1400°C. Longer dwell times at lower temperature may further improve the low temperature performance and dilatometer studies will allow for the determination of the onset of sintering to determine just how low the sintering process can be taken.

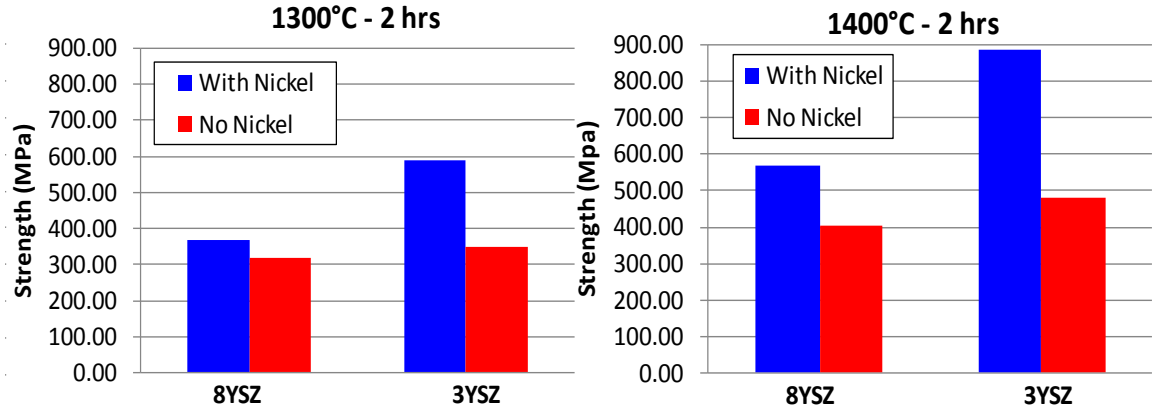

Figure A.4: Ring on Ring flexural strength data for tape cast YSZ specimens with and without 1 mol% Ni.

Conclusions

Nickel oxide has been shown to dramatically improve the densification behavior of both partially and fully stabilized YSZ electrolytes. Densities greater than 95%, representing a transition from open to closed porosity, can be achieved in standard micron sized YSZ at temperatures of 1300°C for 1 hour, which facilitates densities of only 68% (3YSZ) and 79% (8YSZ) in undoped YSZ. Nickel oxide is found to augment grain growth yielding excessively large grains at 1400°C indicating use of the dopant is more suitable for lower temperature processing to retain finer grain sizes. The grain boundary contribution for ionic conduction was improved from the nickel oxide additive at 1300°C over pure YSZ. Nickel oxide dopant promotes an early transition to transgranular fracture for YSZ providing a substantial increase in the flexural strength of the doped YSZ. Due to its prevalence in SOFC labs, small additions of nickel oxide can have significant positive impacts on YSZ ceramic processing with little additional cost.

References

1. A. Chen et al., "Characterization of lanthanum zirconate formation at the a-site -deficient strontium-doped lanthanum manganite cathode/yttrium-stabilized zirconia electrolyte interface of solid oxide fuel cells," *J. Am. Ceram. Soc., 91 (8) (2008), 2670-2675*

2. A. Grosjean et al., "Reactivity and diffusion between La0.8Sr0.2MnO3 and ZrO2 at interfaces in SOFC cores by TEM analyses on FIB samples," *Solid State Ionics, 177 (19) (2006)1977-1980*

3. C. Chervin, R. Glass, S. Kauzlarich, "Chemical degradation of La1-xSrxMnO 3/Y2O3-stabilized ZrO2 composite cathodes in the presence of current collector pastes," *Solid State Ionics, 176 (1-2) (2005) 17-23*

4. R.C. Buchanan, D.M. Wilson, "Role of Al2O3 in Sintering of Submicrometer Yttria-Stabilized ZrO2 Powders," *Advances in Ceramics, 10 (1984) 526-540*

5. R. Knibbe, J. Drennan, A. Dicks, J. Love, "Effect of alumina additions on the anode|electrolyte interface in solid oxide fuel cells," *J. Power Sources, 179 (2) (2008)511-519*

6. R. Knibbe, J. Drennan, A. Dicks, J. Love, "Effect of alumina additions in YSZ on the microstructure and degradation of the LSM-YSZ interface," *Solid State Ionics, 180 (14-16) (2009) 984-989*

7. K. Keizer, M.J. Verkerk, A.J. Burggraaf, "Preparation and Properties of New Oxygen Ion Conductors for use at Low Temperatures," *Ceramurgia International, 5 (4) (1979) 143-147*

8. Y.H. Kim, H.G. Kim, "Effect of Bi2O3 on the microstructure and electrical conductivity of ZrO2-Y2O3 ceramics," *J. Mat. Sci., 5 (5) (1994) 260-266*

9. J.L. Shi, T.S. Yen, H. Schubert, "Effect of small amounts of additives on the sintering of high-purity Y-TZP," *J. Mat. Sci., 32 (5) (1997) 1341-1346*

10. C. Bowen, S. Ramesh, C. Gill, S. Lawson, "Impedance spectroscopy of CuO-doped Y-TZP ceramics," *J. Mat. Sci., 33 (21) (1998) 5103-5110*

11. G. S. Lewis, A. Atkinson, B.C. Steele, "Cobalt additive for lowering the sintering temperature of yttria-stabilized zirconia," *J. Mat. Sci. Letters, 20 (12) (2001) 1155-1157*

12. G.C. Silva, E.N. Muccillo, "Electrical conductivity of yttria-stabilized zirconia with cobalt addition," *Solid State Ionics, 180 (11-13) (2009) 835-838*

13. W. G. Coors, J.R. O'Brien, J.T. White, "Conductivity degradation of NiO-containing 8YSZ and 10YSZ electrolyte during reduction," *Solid State Ionics, 180 (2-3) (2009) 246-251*

14. H. Hondo et al., "Phase stability and electrical property of NiO-doped yttria -stabilized zirconia," *Materials Letters 57 (2003) 1624–1628*

15. T.S. Zhanga et al., "Synergetic effect of NiO and SiO2 on the sintering and properties of 8mol% yttria-stabilized zirconia electrolytes," *Electrochimica Acta 54 (2009) 927–934*

16. H. Hondo et al., "Solid-Solution Effects of a Small Amount of Nickel Oxide Addition on Phase Stability and Mechanical Properties of Yttria-Stabilized Tetragonal Zirconia Polycrystals," *J. Am. Ceram. Soc., 86 (3) (2002) 523–25*

APPENDIX B

CRITICAL CURRENT IN NICKEL FILAMENTS ANALOGOUS TO NICKEL NETWORKS IN SOFC ANODES

A collaborative effort between the Physics department and the Mechanical Engineering Department at Montana State University was undertaken to model the degradation of the nickel network in SOFC anodes. A model of spherical nickel particles was provided by the Physics department but validation of the critical current densities (currents at which the filaments fail divided by the cross sectional area) was necessary. The Mechanical Engineering Department developed a system to consistently test nickel filaments to failure and record the maximum current.

Experimental Procedure

To determine the maximum current which the particulates of nickel in the modeled nickel network could accept prior to failure, specimens of nickel wire were tested to failure in multiple environments. Since the resistivity of a material varies with temperature, thus temperatures of 800 ^{o}C, 600 ^{o}C, 400 ^{o}C, and 20^{o}C were tested. Nickel oxide is much less electronically conductive than the nickel metal, thus testing both in air and a 5% H2/N2 reducing gas atmosphere were conducted to differentiate between the effects of an oxide scale. A DC power supply (Protek, Model 3006) was connected in series to a multimeter (HP 34401A) as shown in Figure B.1. The multimeter's min/max function was used to record the maximum current carried through the wire prior to failure. This system was determined to have insufficient power for the thicker wires. Thus, for the two larger diameter wires, a Hewlett Packard 6260B DC power supply replaced the Protek, and a Tektronix TX3 multimeter replaced the HP 34401A. All the processes for testing were identical between all the wire samples.

Five diameters of nickel wire were tested. These diameters and stock numbers are listed below in Table B.1. The thinnest wire was wrapped around 0.25mm silver wire (Alfa Aesar, Stock #12187) for a mechanical connection and coated in a high purity silver paint (SPI-Paint, CAS #: 7440-22-4) to increase the electrical connection. The silver wire was approximately 2 feet in length on each side of the sample wire. Once dried, the sample was positioned in the center of a quartz tube and placed in a tube furnace (Lindberg/Blue, Model # TF55035A-1). For the tests in a reducing atmosphere, the ends of the tube were sealed and 2 to 4 liters per hour of reducing gas were introduced to the tube for a minimum of 15 minutes prior to testing. For the samples to be tested at temperatures other than room temperature, the tube furnace was set to the temperature of interest and would achieve the set temperature in a few minutes. The silver wires were connected to the leads from the electronics by using the silver paste onto the spade connectors of the leads, and then clamped down by a thumbscrew, washers, and a wing nut. Once the sample was appropriately set up, the electronics were turned on with the min/max function of the multimeter activated and the voltage limit set to maximum on the power supply, with the current set point at zero. The current knob was increased slowly at a rate of approximately 200 mA/min. This allowed an increasing current to pass through the specimen until the voltage spiked and the current dropped to zero which indicated that the nickel wire specimen failed and the circuit was broken. This method was used by Durkan *et al* when studying electromigration in gold nanowires.

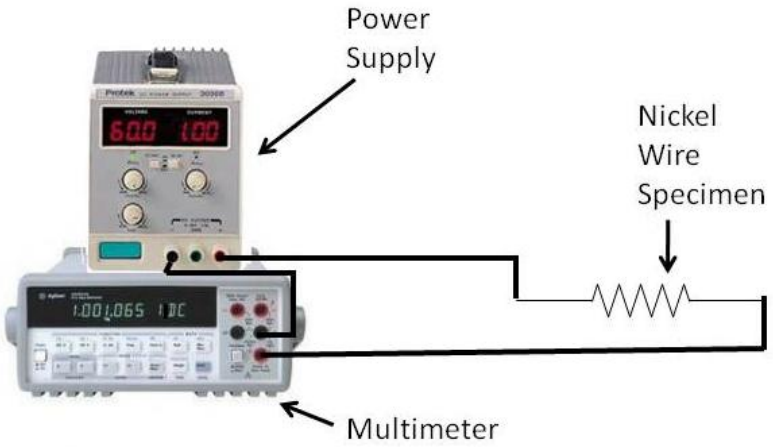

Figure B.1: Set up of nickel wire testing apparatus using the HP multimeter and Protek power supply.

Table B.1: Diameters, calculated area, and the stock number of all the wire diameters used.

Diameter (mm)	**Area (cm^2)**	**Stock Number**
0.01	0.0000007854	Alfa Aesar #40673
0.025	0.00000490874	Alfa Aesar #40672
0.05	0.000019635	Alfa Aesar #10933
0.127	0.000126677	Materials Research Corporation #117E-NI000-1046
0.25	0.000490874	Alfa Aesar #10931

Experimental Results

The resulting max current for each wire and temperature/atmosphere combination was recorded and the critical current density, $J_{critical}$, was calculated by Equation B.1 with the cross sectional area of the wire, A.

$$J_{critical} = I_{critical}/A \qquad [B.1]$$

All data from the tests was shown in Table B.2. Plots of the wires at different temperatures and in both atmospheres were also shown, as well as a plot of the room

temperature readings for all the wires in both atmospheres. The areas used in the calculations were simply the cross sectional area of the wire.

This study initially focused only on the .25 mm, .127 mm, and .025 mm nickel wires. These samples were tested once in each condition to provide an overall analysis. It was then decided to continue on with the testing and the smaller wires were tested three times for each condition. The standard deviation for most of the wires was 9% or less, indicating very good consistency over the tests. However, the .01 mm diameter wires very difficult to handle at the 800^{o}C temperatures and the data collected was much less consistent at that temperature (32% standard deviation in air) or were not able to be collected at all as with the 800^{o}C in reducing atmosphere. The .025 mm wire also gave a larger standard deviation at room temperature in a reducing atmosphere (20% standard deviation). These points could not be used for any detailed analysis but still fit the trend and thus were included. Obviously, the larger diameter wires that were run once did not yield a standard deviation but, again, the data fit the trend and was plotted to be used in a supporting role.

Experimental Discussion

Prior to full discussion of the results of the nickel wire experiments, it is most beneficial to review resistance variations with respect to temperature. Resistance for a material is known to change somewhat linearly with a temperature change. The equation for the new resistance is shown below as Equation B.2:

$$R = R_o + \alpha * \Delta T * R_o \qquad [B.2]$$

where R_o is the initial resistance, α is the temperature coefficient, and ΔT is the change in temperature. While this is commonly viewed as a change in resistance, for a sample with an unchanging geometry, this equation could also be used for the change in resistivity. For nickel, an initial resistivity of $6.99 * 10^{-8}$ Ωm and a temperature coefficient of 0.005866 $1/^oC$ were used.

As the temperature increases, the resistivity of the wire specimens increased. This would resistively heat the specimen and add to the ambient thermal energy. Also, the resistivity is a function of the resistance, area, and length of the sample. Thus, when the thicker wires were investigated, the resistances were high enough that the thermal energy from the ambient temperature plus any resistive heating would exceed the melting temperature of the wire at the higher temperatures.

Consistent for all the samples, when the data collected in air was compared to the data collected in a reducing environment the reduced sample always had the higher critical current density. This was expected when the true cross sectional area of the wire was considered. If one assumed that an oxide scale of a certain thickness formed on the exterior of the wire, the scale would essentially reduce the true nickel metal cross sectional area. When the wire was in a reducing atmosphere, the scale reduced back from a nickel oxide to pure nickel metal. Since the oxidation thickness would be consistent for all the wires, the larger diameter wires' scale was a very small percentage of the area of wire while the small diameter wires' would have a larger area of oxide and be effected much more significantly. This concurs with the data since for both the 0.127mm and the 0.25 mm wires, the reduced samples compared very close to the wire specimens in air for

critical current densities. However, the very small wire diameter meant that the scale on the exterior of the wire would make up a much higher percentage of the area than the larger wires, even though it was assumed that the scale thickness was consistent between all the samples. This also agreed with the data collected for the small wire as the critical current density for the reduced samples was significantly higher. This was readily evident in the samples tested at room temperature. The averages of these tests, displayed in Figure B.2, clearly shows that the larger diameter, 0.25 mm for example, has minimal difference between the reduced and oxidized sample.

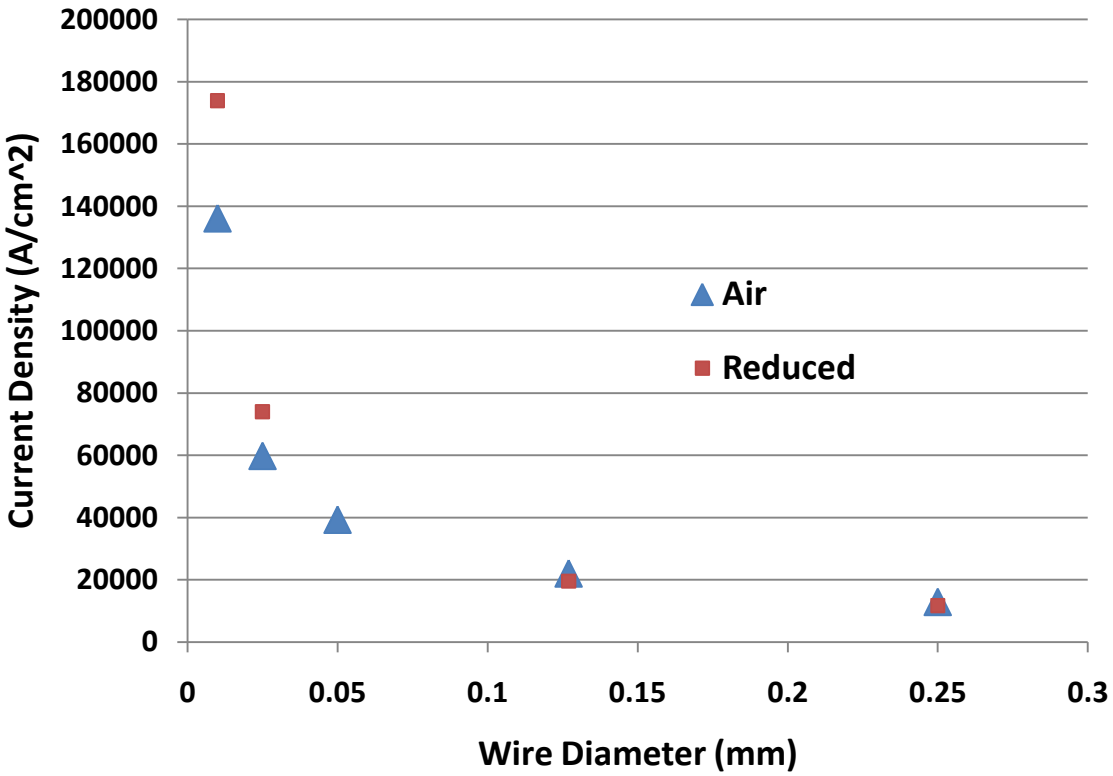

Figure B.2: Plot of current density at failure for several diameters in oxidizing and reducing atmospheres at room temperature.

The similarity between atmospheres does not continue to smaller diameter wires below the 0.127 mm samples. The 0.025 mm and 0.01 mm samples had increasing spread between the critical current densities of oxidizing and reducing atmospheres. This supported the statement that the oxide layer would affect smaller wires to a higher degree. Another possible reason that the air and reduced samples are almost identical for the larger wire is that the temperature was insufficient to reduce the nickel. This concern was dismissed when the tests at various temperatures were completed and the spread was still small for larger diameter wires as observed in Figure B.2.

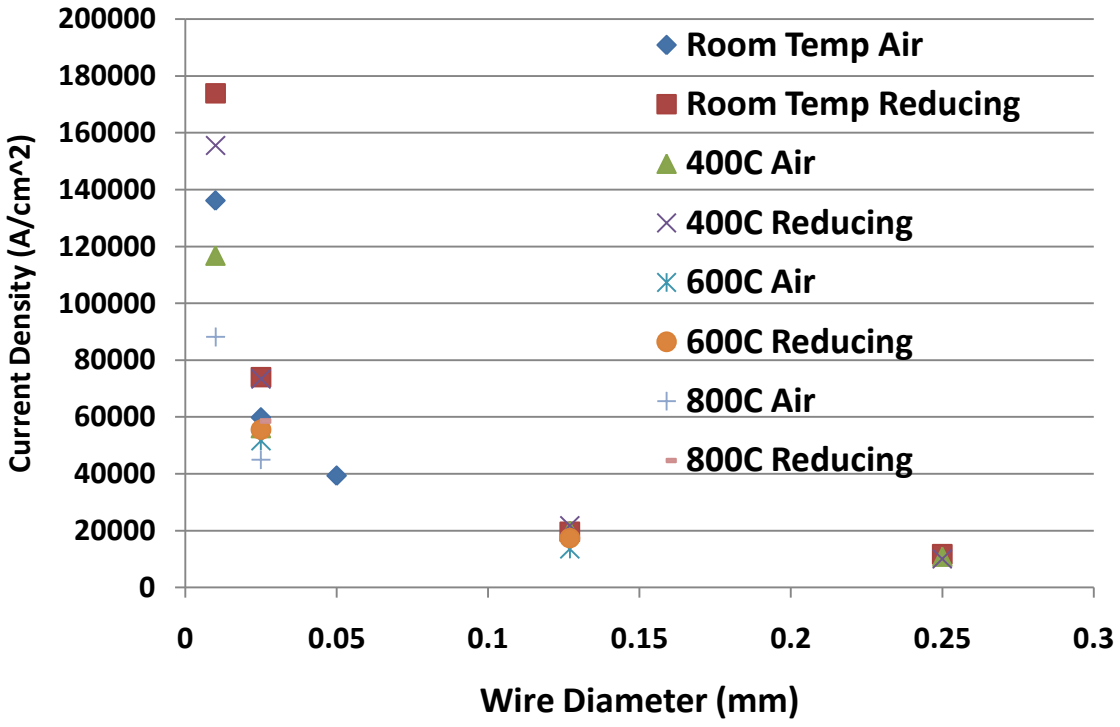

Figure B.3: Plot of current density at failure for several diameters in oxidizing and reducing atmospheres at several temperatures.

Another trend observed in Figure B.2 is that the increasing temperature decreases the overall critical current density. This is correlated back to the joule heating concept and the resistivity as a function of temperature. The temperature the tests were conducted at were all well below the melting point of nickel. However, the additional thermal energy produced by the joule heating of the filaments did provide sufficient energy to fail the wires. The resistance of the nickel wires increases as a function of temperature such that the same amount of current at different temperatures would produce a higher joule heating effect at a higher temperature.

While the variation between the atmospheres was previously explained, and the critical current for various wire diameters should change, the critical current density should be consistent for a material. This was investigated further later. However, to give an estimate of the critical current density for the nickel in a SOFC anode environment as was modeled, a simple power series regression was fitted to the data. This was used for the most basic of models where the current was related to the resistance, which is based on the resistivity and thus the geometric relationship of length over area. A good fit was achieved (R^2 >0.99) and the critical current density values for a 0.62μm wire was found to be $177.1*10^3$ Amps/cm^2 for a reducing atmosphere, as would be seen in an operating anode.

To understand why the supposedly constant critical current density was changing significantly between the larger and smaller diameter wires, two explanations were investigated concurrently. First, the surface-to-volume ratios of the wires were

investigated for possible explanations. Second, the concept of electromigration was deemed a possibility for the variations.

The surface-to-volume ratio is simply the surface area for one unit length of the sample divided by the volume of one unit length of the sample. Since the volume is calculated as a square of the radius, and the surface area is a function of the radius, the change in surface-to-volume ratio obviously follows a 1/r function. Table B.2 was the summary of these surface-to-volume ratio calculations. The surface-to-volume ratio for the 0.025 mm wire was 10 times higher than that of the 0.25 mm wire and the 0.01 mm wire had a 25 times greater surface-to-volume ratio even though the radial change. A large surface-to-volume ratio means that the surface area for a unit length can provide much better heat transfer by convection and radiation than a unit length with significantly less surface area (2,3). Since the heat was more efficiently removed from the smallest wire, it required much more joule heating to reach the melting point, and thus much more current.

Table B.2. Summary of the surface-to-volume ratios for specified wires.

Diameter of the wire (mm)	Surface-to-Volume Ratio	Radius Ratio to 0.25 mm
0.01	400	25
0.025	160	10
0.05	80	
0.127	~31.5	0.5
0.25	16	1

The second explanation commonly accepted for this increase in critical current density for smaller filaments is related to electromigration. Electromigration is the transport of material caused by the gradual movement of the ions in a conductor due to

the momentum transfer between conducting electrons and diffusing metal atoms (4). Essentially, electromigration causes material transport in the direction of the ion and electron flow by forcing atoms to separate from the grain boundaries. Thicker wire carries a higher current, but over a larger area and thus actually has a lower current density. In the case of these thick wires, the fewer electrons that were flowing through a specific grain boundary in the larger two wires were unable to effectively detach as many atoms. However, as the wire becomes smaller this current density increases and forces more electrons through fewer grain boundaries, increasing the probability that atoms would be forced to separate. If the wire becomes sufficiently small, the diameter could span only one grain which would minimize the grain boundaries where this transport could occur. Thus the electromigration is overcome by very small wires only a few grains across, and is negligible to larger wires, but in between at some range of radii it can be detrimental. The large wires used in this test may not have been so large to have resisted the electromigration, but instead fell in the middle where electromigration played a large role.

Another way that very small wires can resist electromigration is the "bamboo structure" of the grains (1,2,3,4). Instead of the traditional polygonal shapes of the grain boundaries that are often observed in larger materials, the small wires seem to have grain structures that are elongated along the length of the wire (3). This effect also minimizes the grain boundaries perpendicular to the path of the electrons and thus more effectively resists electromigration.

While both these effects were traditionally observed for nano-sized wires, it could be that the trends are noticeable over larger scales and has been confirmed by a study at sizes up to 25 microns (1). The data clearly follows the same trends, indicating that either the nickel experiences these same effects are a larger scale, or that the effects are always noticeable to some extent. The latter is the most probable since nano-sized wires would show even higher critical current densities multiple orders of magnitude larger.

Between the surface-to-volume ratios better transferring heat to the surroundings and the electromigration, a good grasp of this nonlinearity was obtained. A common third factor for nano-wire failure is an electron-phonon scattering within the incredibly small wires. Since the scale required for most of these arguments is orders of magnitude off, it was neglected as a possible solution (2,3). It also is now understood how the discrepancies in the data for the two atmospheres are obtained. By understanding all the mechanisms that can affect the nickel wire a better estimate for the critical current densities of incredibly fine nickel filaments in SOFC anodes was achieved. Since the smaller diameters of nickel particles could cause a more sever nonlinearity in the critical current densities, it is assumed that the previously calculated $177.3*10^3$ Amps/cm^2 critical current density is much lower than that truly reached. For this model though, it could be used as a very conservative estimate.

References

1. *Slit morphology of electromigration induced open circuit failures in fine liine conductors.*John E. Sanchez, Jr., L. T. McKnelly, and J. W. Morris, Jr. 7, Berkely : J. Appl. Phys., 1992, Vol. 72.

2. *Analysis of failure mechanisms in electricaly stressed Au nanowires.* C. Durkan, M. A. Schneider, and M. E. Welland. 3, Cambridge : J. Appl. Phys., 1999, Vol. 86.

3. *Diameter dependent failure current density of gold nanowires.* S Karim, K Maaz, G Ali, and W Ensinger. Islamabad : J. PHys. D: Appl. Phys., 2009, Vol. 42.

4. *Electromigration - A Brief Survey and Some Recent Results.* Black, James R. 4, s.l. : IEEE Transactions on Electron Devices, 1969, Vols. ED-16.

APPENDIX C

DESCRIPTION OF FOCUSED ION BEAM TO PREPARE TRANSMISSION ELECTRON MICROSCOPY

The use of FIB-SEM instruments provided an exceptional learning experience and HRTEM sample preparation tool. A FIB has many similarities to focused electron beam systems such as scanning electron microscopes but the main difference is ions are focused. Gallium ions (Ga^+) are most commonly used because gallium can easily be kept in liquid form due to its low melting temperature. The use of Ga^+ allows imaging resolution of approximately 5nm. Ga^+ also penetrate less into the material, resulting in a more relevant elemental mapping since material underneath the surface layer is not analyzed [1]. Obviously the greatest implementation of a FIB is the removal of material either for HRTEM sample preparation or to provide layered elemental analysis. The Ga^+ ions sputter atoms off the bulk material while incoming gas molecules adsorb to the surface. The balance between taking material off and adsorbing material onto the surface can cause an angled HRTEM sample. This can usually be offset by tilting the sample and sputtering off the added material while again competing with new material to be slowly added. Another concern which can arise from the FIB preparation techniques is the "waterfall" or "curtaining" effect in which the Ga^+ ions smear material from the upper sample edge downwards. This can cause a long, narrow artifact when imaging and occasionally cannot be avoided. However, the curtaining effect is often easy to identify and differentiate from the rest of the sample and is more of an imaging fault than an analysis problem. The other method previously mentioned and utilized at EMSL was the layered elemental analysis. FIB-SEMs can be automated such that a small layer can be cut away via the FIB attachment, the sample rotated, and elemental analysis conducted on the new face. The sample would then rotate back to the original position and repeat the

process. Since the Ga^+ ions penetrate less than the electrons, each layer can be thin and allow much higher resolution of the elemental analysis system. A possible issue with this is shadowing; where a particle is not cut and will eventually block electrons and ions from reaching the surface of interest. This issue can occur after several slices and, since this method often incorporates the machine overnight, can blemish a section of the data.

All other methods used are much more commonplace in the analysis field and have a plethora of information available. Additional and supplemental data is included after the following manuscripts which will then be followed by conclusions.

References

[1] *A review of focused ion beam milling techniques for TEM specimen preparation.* Giannuzzi, L.A. and Stevie, F.A. 1999, Micron, Vol. 30, pp. 197-204.

APPENDIX D

THERMAL COARSENING STUDY DATA

Data presented in Appendix D is an expanded collection of the data collected for the publication *Investigation of Aluminum Titanate for Chemical Anchoring of Infiltrated Nickel Catalyst in Solid Oxide Fuel Cell Anode Systems* presented in Chapter 4. These samples were pressed and sintered YSZ disks providing a dense surface to apply the catalyst. Samples listed as "YSZ and 10 wt% ALT" were pressed and sintered from a powder consisting of 90 wt% YSZ and 10 wt% ground ALT. The final samples fabricated were the dense, pure YSZ pellets and had a dilute ALT suspension applied via aerosol method. Each figure displays an arrangement of three images of 1000x (left), 4000x (center), and 8000x (right) magnification. This qualitative analysis provided an overall picture of the anchoring process and is supported by the XRD and other analysis techniques. The final figure shows a few examples of substrates where the nickel catalyst has coarsened. The impressions left in the substrate are assumed to be an area where the nickel catalyst was initially located, but the catalyst has coarsened away from the area. This also gives rise to the concern that the catalyst has coarsened such that the visible area from the top view is an exaggeration of the TPB remaining in contact with the YSZ substrate.

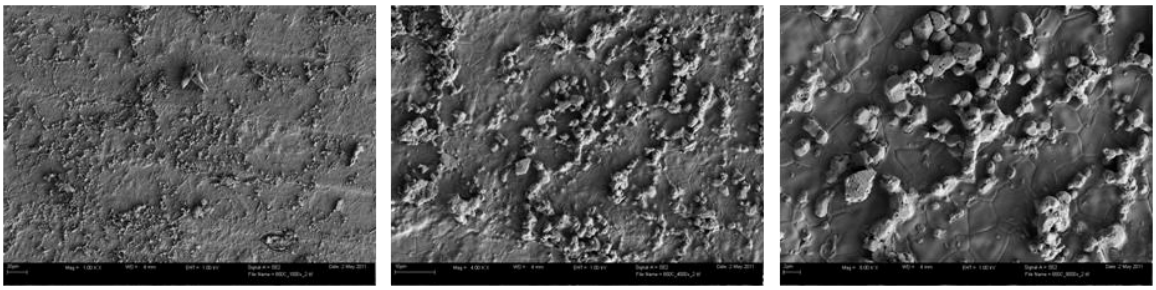

Figure D.1: YSZ baseline sample with nickel coating after being held at 650^{o}C for 100 hours in 5%H_2/95%N_2 at 1000x (left), 4000x (center), and 8000x (right) magnification.

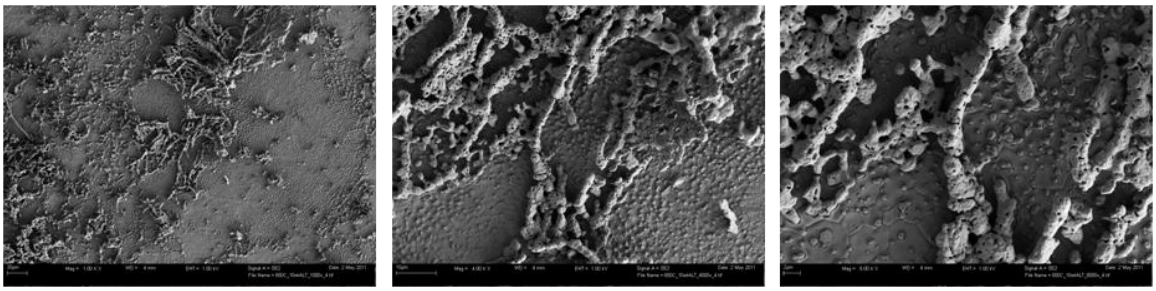

Figure D.2: YSZ and 10 wt% ALT sample with nickel coating after being held at 650^{o}C for 100 hours in 5%H_2/95%N_2 at 1000x (left), 4000x (center), and 8000x (right) magnification.

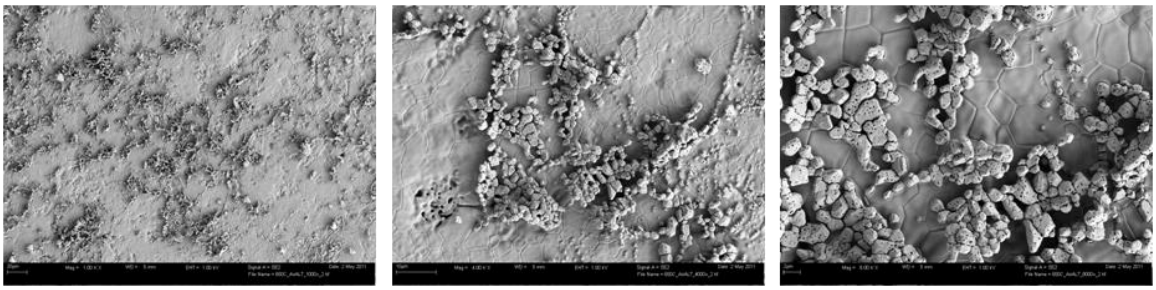

Figure D.3: YSZ and aerosol applied ALT sample with nickel coating after being held at 650^{o}C for 100 hours in 5%H_2/95%N_2 at 1000x (left), 4000x (center), and 8000x (right) magnification.

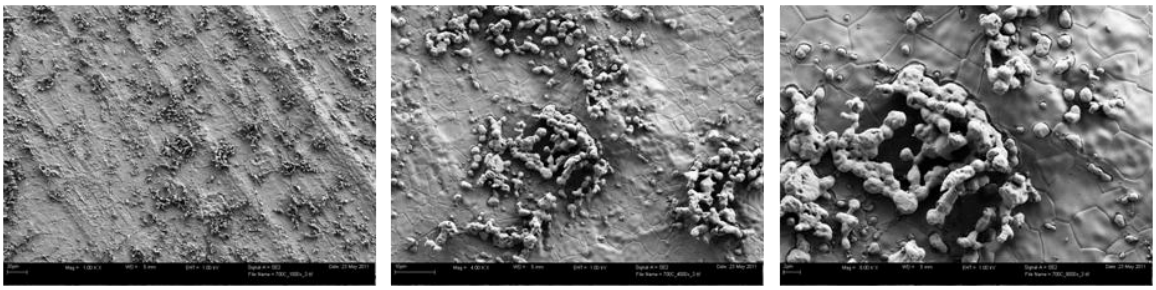

Figure D.4: YSZ baseline sample with nickel coating after being held at 700^{o}C for 100 hours in 5%H_2/95%N_2 at 1000x (left), 4000x (center), and 8000x (right) magnification.

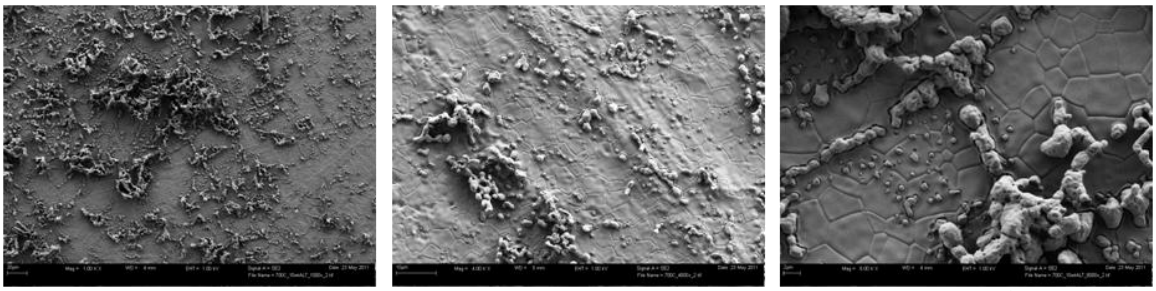

Figure D.5: YSZ and 10 wt% ALT with nickel coating after being held at 700^{o}C for 100 hours in 5%H_2/95%N_2 at 1000x (left), 4000x (center), and 8000x (right) magnification.

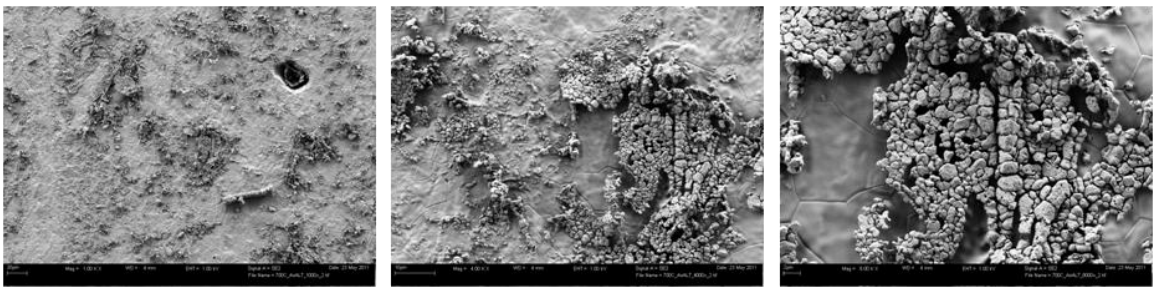

Figure D.6: YSZ and aerosol applied ALT with nickel coating after being held at 700^{o}C for 100 hours in 5%H_2/95%N_2 at 1000x (left), 4000x (center), and 8000x (right) magnification.

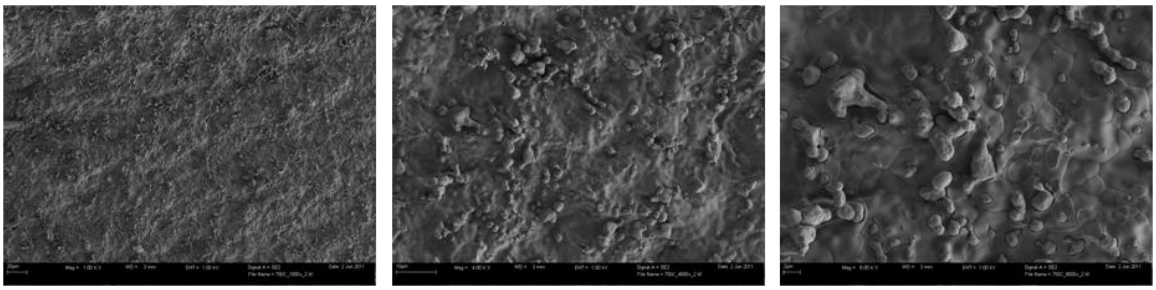

Figure D.7: YSZ baseline sample with nickel coating after being held at 750^{o}C for 100 hours in 5%H_2/95%N_2 at 1000x (left), 4000x (center), and 8000x (right) magnification.

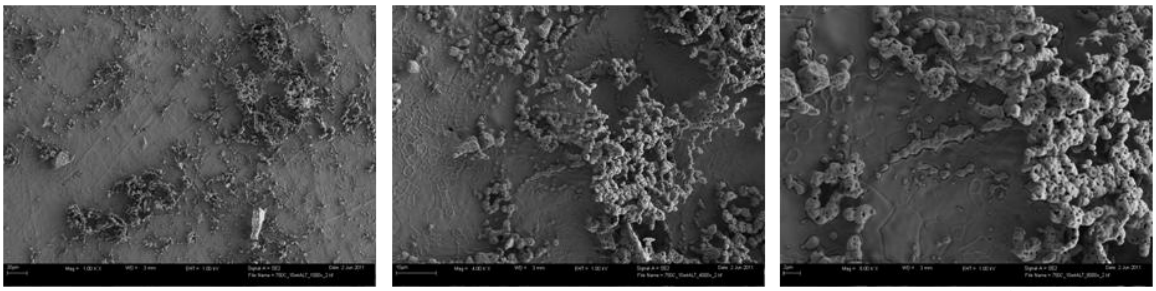

Figure D.8: YSZ and 10 wt% ALT with nickel coating after being held at 750^{o}C for 100 hours in 5%H_2/95%N_2 at 1000x (left), 4000x (center), and 8000x (right) magnification.

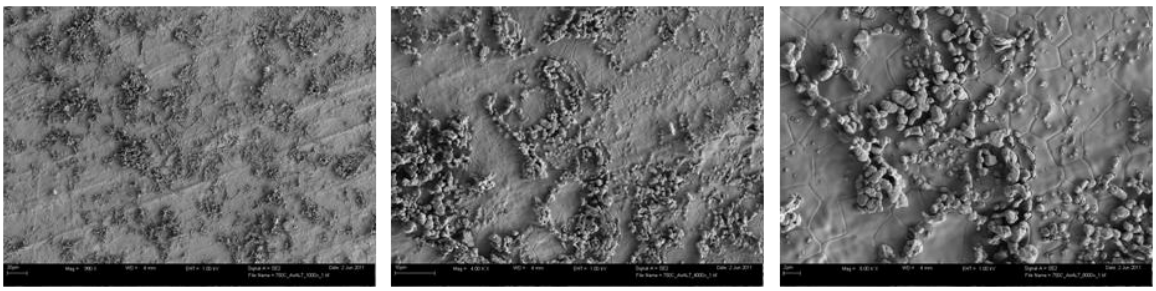

Figure D.9: YSZ and aerosol applied ALT with nickel coating after being held at 750^{o}C for 100 hours in 5%H_2/95%N_2 at 1000x (left), 4000x (center), and 8000x (right) magnification.

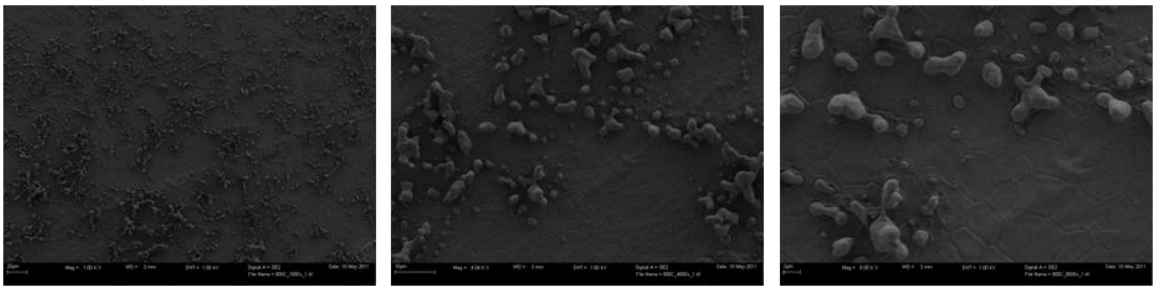

Figure D.10: YSZ baseline sample with nickel coating after being held at 800^{o}C for 100 hours in 5%H_2/95%N_2 at 1000x (left), 4000x (center), and 8000x (right) magnification.

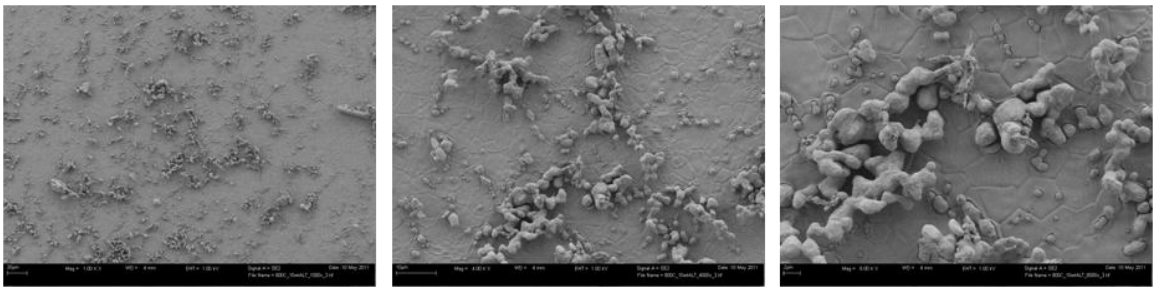

Figure D.11: YSZ and 10 wt% ALT with nickel coating after being held at 800^{o}C for 100 hours in 5%H_2/95%N_2 at 1000x (left), 4000x (center), and 8000x (right) magnification.

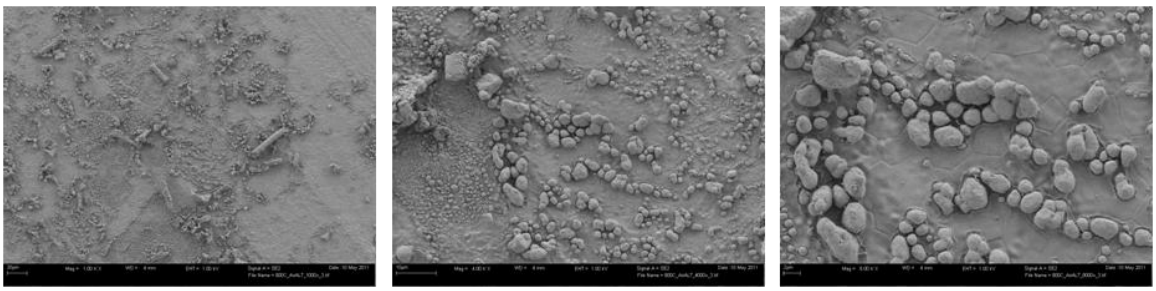

Figure D.12: YSZ and aerosol applied ALT with nickel coating after being held at 800^{o}C for 100 hours in 5%H_2/95%N_2 at 1000x (left), 4000x (center), and 8000x (right) magnification.

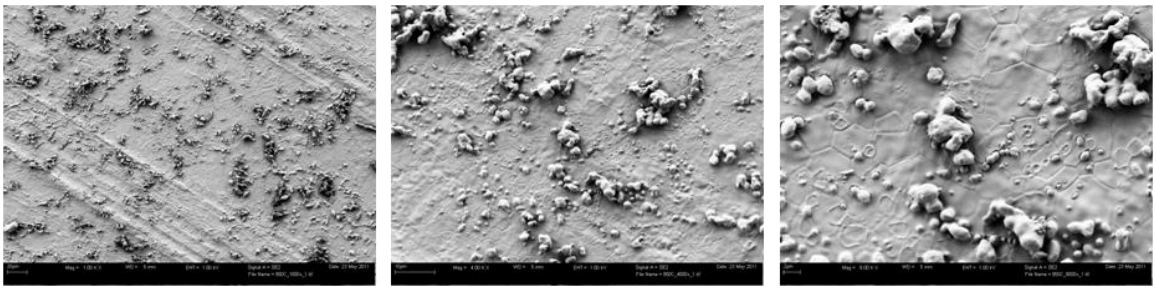

Figure D.13: YSZ baseline sample with nickel coating after being held at 850^{o}C for 100 hours in 5%H_2/95%N_2 at 1000x (left), 4000x (center), and 8000x (right) magnification.

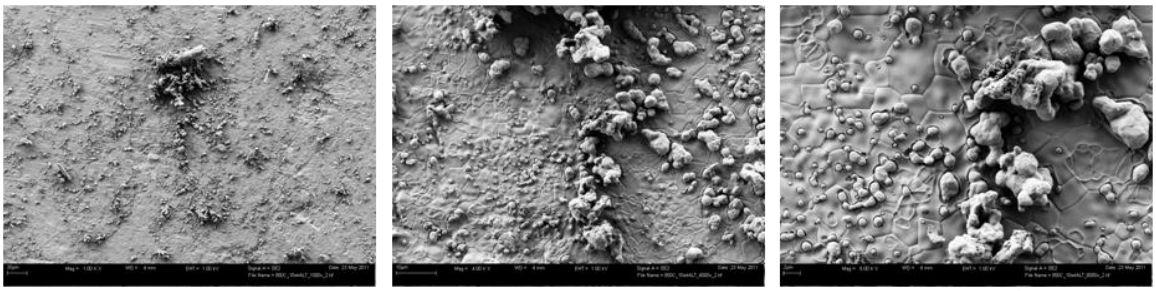

Figure D.14: YSZ and 10 wt% ALT with nickel coating after being held at 850^{o}C for 100 hours in 5%H_2/95%N_2 at 1000x (left), 4000x (center), and 8000x (right) magnification.

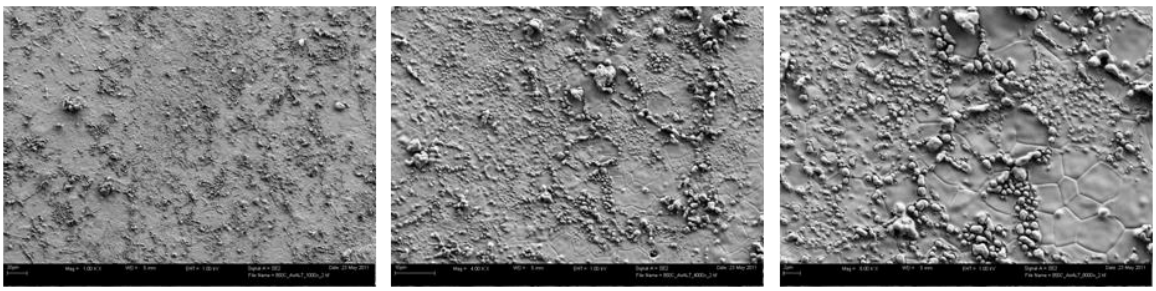

Figure D.15: YSZ and aerosol applied ALT with nickel coating after being held at 850^{o}C for 100 hours in 5%H_2/95%N_2 at 1000x (left), 4000x (center), and 8000x (right) magnification.

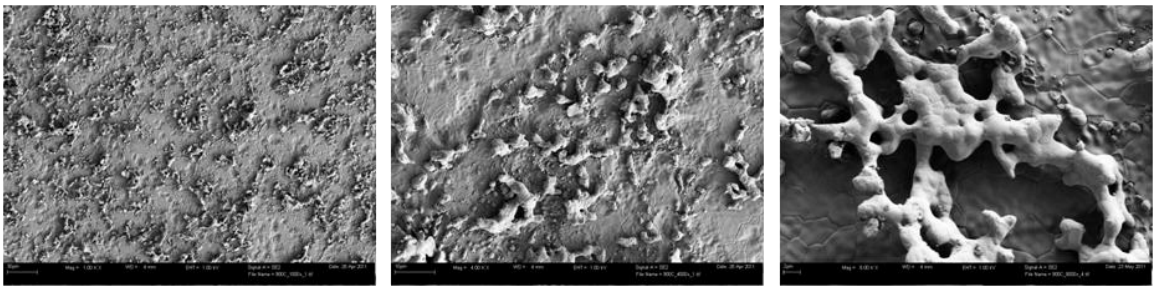

Figure D.16: YSZ baseline sample with nickel coating after being held at 900°C for 100 hours in 5%H_2/95%N_2 at 1000x (left), 4000x (center), and 8000x (right) magnification.

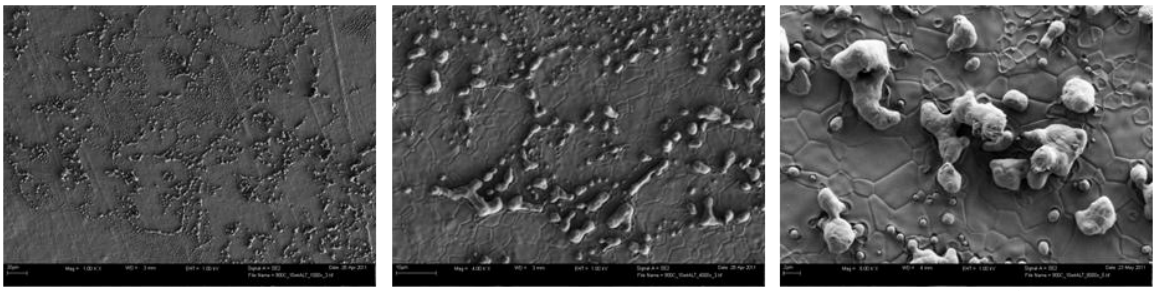

Figure D.17: YSZ and 10 wt% ALT with nickel coating after being held at 900°C for 100 hours in 5%H_2/95%N_2 at 1000x (left), 4000x (center), and 8000x (right) magnification.

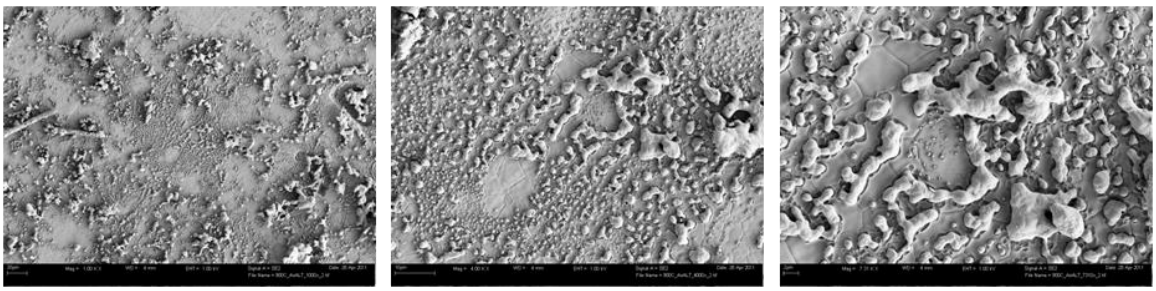

Figure D.18: YSZ and aerosol applied ALT with nickel coating after being held at 900°C for 100 hours in 5%H_2/95%N_2 at 1000x (left), 4000x (center), and 8000x (right) magnification.

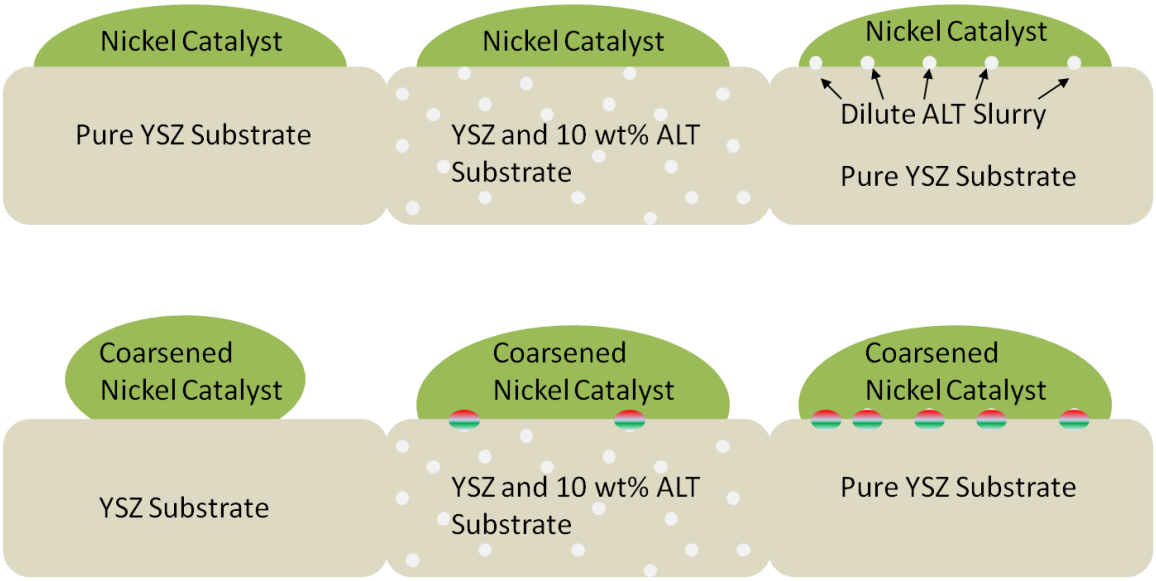

Figure D.19: Illustration of anchoring methods and effects on coarsening.